AN INVESTIGATION OF THE RHEOLOGY AND INDENTATION RESPONSE OF VEGETABLE SHORTENING USING FINITE ELEMENT ANALYSIS

by

Joamin Gonzalez-Gutierrez

A Thesis Submitted to the Faculty of Graduate Studies of
The University of Manitoba
in Partial Fulfillment of the Requirements for the degree of

MASTER OF SCIENCE

Department of Food Science
University of Manitoba
Winnipeg, Manitoba

Copyright © 2008 by Joamin Gonzalez-Gutierrez

ACKNOWLEDGEMENTS

My sincere appreciation is extended to Dr. Martin G. Scanlon for all his support during my time at the Food Science Department at The University of Manitoba. His guidance, advice and support had made a significant contribution to my academic, professional and personal development. I also would like to acknowledge Dr. Jung Han, Dr. Gary Fulcher, Department of Food Science and Dr. Stefan Cenkowski, Department of Biosystems Engineering for serving on my graduate committee.

I extend sincere thanks to Dr. Alejandro Marangoni, Guelph University for introducing me to the processes of lipid fractionation and sharing part of his research with me. My sincere thanks to the laboratory staff at the Richardson Centre for Functional Foods and Nutraceuticals, for allowing me to use their facilities during my research. Thank you to Mr. Grant Roy, Department of Physics and Astronomy for manufacturing the mould used during my preliminary experimentation. My sincere thanks go to Michael Stringer, Department of Food Science for lending his photographic skills and talent to this project. Thank you to David Treble, Faculty of Agriculture and Food Science, and Kim Majury, Department of Mechanical and Manufacturing Engineering for solving many of the computer problems I encountered during this research project. Also thank you to all the Staff and Graduate Students at the Food Science Department for your support and friendship which greatly contributed to the completion of this research project.

I am grateful to my mother Estela Gutierrez, my father Mario Gonzalez, the rest of family and friends for all their love, trust, inspiration and support through out the years. Last but not least, my appreciation goes to the Natural Sciences and Engineering Research Council (NSERC) of Canada for their financial support.

An Investigation of the Rheology and Indentation Response of Vegetable Shortening Using Finite Element Analysis

TABLE OF CONTENTS

LIST OF TABLES

CHAPTER 2: Literature Review

CHAPTER 3: Materials and Methods

CHAPTER 4: Results and Discussion

LIST OF FIGURES

CHAPTER 2: Literature Review

CHAPTER 3: Materials and Methodology

CHAPTER 4: Results and Discussion

LIST OF SYMBOLS

A	Current cross-sectional area of specimen
A_0	Initial cross-sectional area of specimen
A_c	Projected contact area
$A_{(e)}$	Cross-sectional area of element ‘e’
A_1	Cross-sectional area of element 1
A_2	Cross-sectional area of element 2
a	Displacement constant
α	Indentation constant
B	Creep bulk compliance
$B(t)$	Creep bulk compliance function
b	Radius of cylindrical indenter or specimen
$C(w)$	Indentation empirical function
c	Displacement constant
D_0	Instantaneous compressive compliance
D_b	Biaxial compressive compliance
D_f	Diameter after compression of cylindrical specimen
D_i	Compliance of springs of each Voigt element
$D(t)$	Compressive creep compliance function
D_o	Original diameter of cylindrical specimen
D_s	Steady state compressive compliance
d	Displacement
d_1	Displacement of node 1
d_2	Displacement of node 2
d_3	Displacement of node 3
$\vec{d}_{(e)}$	Displacement vector for element ‘e’
$\vec{d}^{\,T}$	Transpose of vector ‘d’
$d(x)$	Displacement function
$d_{i(e)}$	Displacement of node ‘i’ of element ‘e’

ΔD	Change in diameter
ΔH	Change in height
ΔL	Change in length
ΔV	Change in volume
$\Delta V/V$	Voluminal strain
$(\Delta V/V)_0$	Initial voluminal strain
δ	Penetration depth
E	Modulus of elasticity
$E_{(e)}$	Modulus of elasticity of element '*e*'
E_i	Stress relaxation constant for each Maxwell element
E_R	Compressive relaxation modulus
E_U	Unloading modulus
e	Exponential function
ε	True strain
ε_E	Engineering strain
ε_e	Elastic strain
$\varepsilon_{(e)}$	Strain of element '*e*'
ε_p	Non-elastic strain
ε_{y1}	First yield strain (onset of hardening)
ε_{y2}	Second yield strain (onset of perfect plasticity)
$\dot{\varepsilon}$	Strain-rate
$\dot{\varepsilon}_d$	Strain-rate of dashpot in Maxwell model
$\dot{\varepsilon}_s$	Strain-rate of spring in Maxwell model
$\dot{\varepsilon}_0$	Fluidity of a material
F	Reaction force
F_0	Static indentation response
Φ	Void fraction
G	Shear modulus
G_0	Instantaneous shear modulus
$G(t)$	Shear modulus function

G_R	Shear relaxation modulus
G'	Shear loss modulus
G''	Shear storage modulus
g_R	Normalized shear modulus
$g_R(\infty)$	Long term normalized shear modulus
$\bar{g}_i^P$	Constants of element 'i' in a Prony series
γ	Shear strain
γ_0	Constant shear strain
$\dot{\gamma}$	Shear strain-rate
H	Initial specimen height
h	Current specimen height
h_i	Indentation depth
$\dot{h}_i$	Indentation strain rate
η	Apparent viscosity
η_b	Biaxial viscosity
$\eta(\dot{\varepsilon})$	Viscosity as a function of strain rate
η_i	Viscous contribution of each Maxwell or Kevin-Voigt element
I	Potential energy
J	Shear creep compliance
$J(t)$	Shear creep compliance function
j_s	Normalized shear creep compliance
$j_s(\infty)$	Long term normalized shear creep compliance
K	Bulk modulus
$K(t)$	Bulk modulus function
$[K]$	Global stiffness matrix
$[K_{(e)}]$	Stiffness matrix of element 'e'
κ	Hardness
L	Original side length of cubic specimen
$L_{(e)}$	Length of element 'e'
L_1	Length of element 1

L_2	Length of element 2
M	Indentation modulus
m	Mass of conical indenter
μ	Coefficient of friction
N	Number of loading cycles
N'	Total number of elements in a Prony series
n	Number of Maxwell elements
ν	Poisson's ratio
P	Load or force
P_H	Hydrostatic pressure
P_i	Indentation force
P_{max}	Maximum indentation force
P_0	Constant applied pressure
P_1	Force at node 1
P_2	Force at node 2
P_3	Force at node 3
$\vec{P}_{(e)}$	Force vector of element '*e*'
θ	Relative hardness
R	Radius of cylindrical specimen before deformation
r	Radial distance from the center of cylindrical indenter or specimen
ρ	Density of vegetable shortening as sold
ρ_s	Density of solid degasified vegetable shortening
S	Slope of the initial part of unloading indentation curve
σ	True stress
σ_0	Constant compressive stress
σ_A	Average stress in a cylindrical specimen
σ_E	Engineering stress
σ_e	Equilibrium stress
$\sigma_{(e)}$	Stress at element '*e*'
σ_I	Initial stress during relaxation test

σ_{st}	Static stress
σ_{s0}	Constant shear stress
σ_y	Yield stress
σ_s	Shear stress
σ_z	Axial compressive stress
$\dot{\sigma}$	Stress rate
t	Time
τ	Retardation time
τ'	Relaxation time
τ_i	Retardation time for each Kelvin-Voigt element
τ'_i	Relaxation time for each Maxwell element
τ_i^G	Constant of element '*i*' of a Prony series
U1	Movement along axis 1
U2	Movement along axis 2
U3	Movement along axis 3
UR1	Rotation about axis 1
UR2	Rotation about axis 2
UR3	Rotation about axis 3
$u_{(e)}$	Strain energy of element '*e*'
V	Volume
W	Work done by external forces
w	Overstress power law constant
ω	Stress decaying factor
x	Longitudinal (horizontal) direction
ξ	Dimensionless constant: Indentation strain rate over fluidity
Y(t)	Relaxation function
z	Power law strain hardening constant

ABSTRACT

Many soft food materials, including vegetable shortening, exhibit complex rheological behaviour with properties that resemble those of a solid and a liquid simultaneously. The fundamental parameters used to describe the rheological response of vegetable shortening were obtained from uniaxial compression tests, including monotonic and cyclic compression, as well as creep and stress relaxation tests. The fundamental parameters obtained from the various compression tests were then used in two mechanical models (viscoelastic and elasto-visco-plastic) to predict the compression and conical indentation response of vegetable shortening. The accuracy of the two models was studied with the help of the commercially available finite element analysis software package Abaqus. It was determined that the viscoelastic model was not suitable for the prediction of the rheological response of shortening. On the other hand, the proposed elasto-visco-plastic model predicted with reasonable accuracy the uniaxial compression and indentation experimental response of vegetable shortening.

CHAPTER 1: GENERAL INTRODUCTION

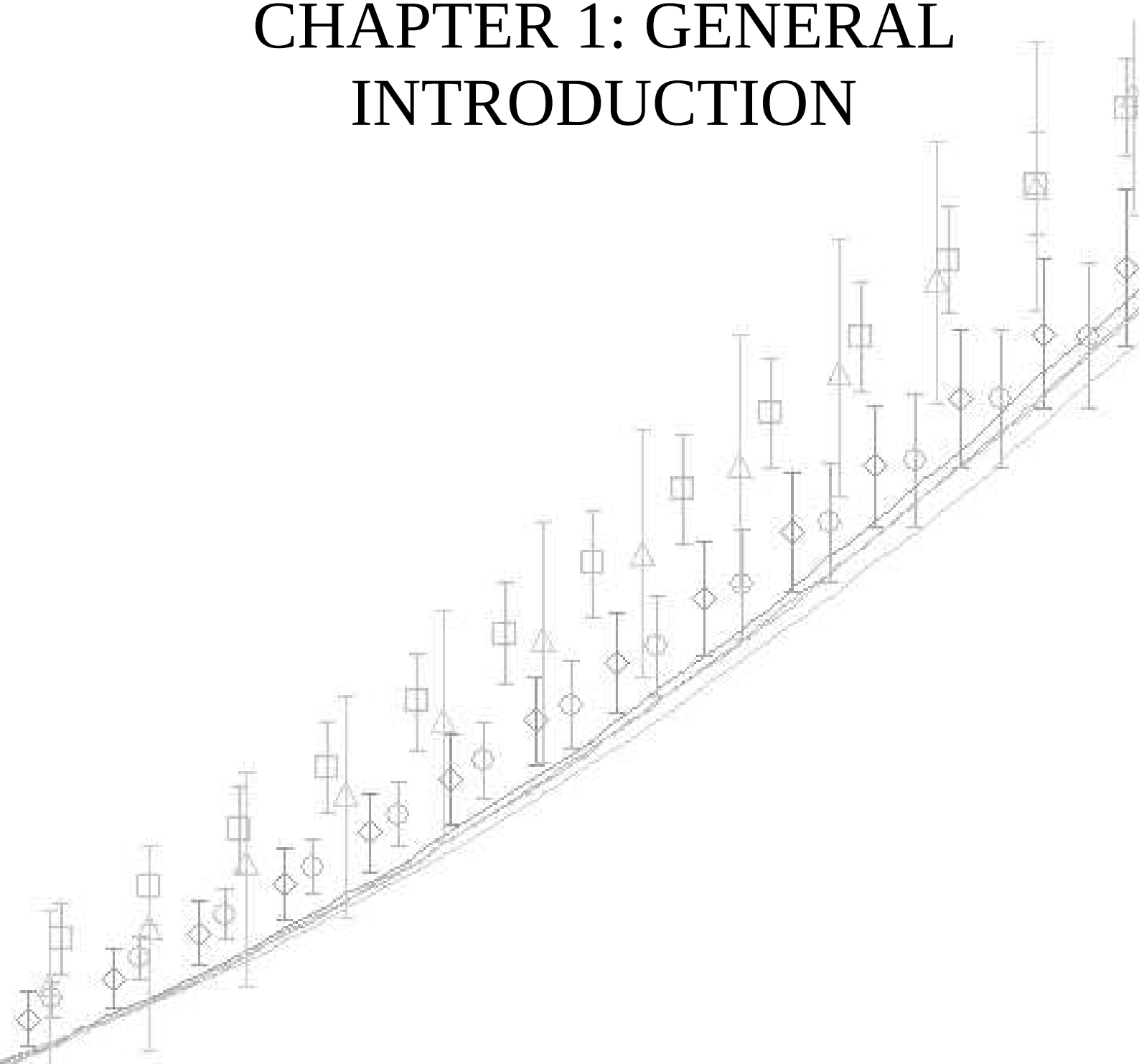

1.1.0 General Introduction

Vegetable shortening and many other semisolid foods can be classified as particle gels, since they consist of a network of weakly bonded particles comprised of solid lipid crystals suspended within a fluid (primarily liquid lipids) (Rzepiela et al, 2002; Kloek et al, 2005). Vegetable shortening is an important ingredient in the food industry; its uses include providing structure, lubrication, aeration, emulsification and moisture retention to a great variety of baked goods. In addition, it has beneficial heat transferring uses particularly when used as a frying agent (O'Brien, 1998). The main ingredients of vegetable shortening are liquid oils and solid fats from different sources. The choice of the type of oils and fats used, as well as their storage and processing conditions affect the structure of vegetable shortening and as a consequence its rheological properties and final applications (de Man et al, 1992; Schaink et al, 2007). Measuring the rheological properties of shortening is an important method of determining the quality and possible applications of the different types of vegetable shortening (Steffe, 1996; Afoakwa et al, 2008). The rheological response of shortening, as with other materials, can be measured by instrumental methods classified into two major categories: empirical and fundamental tests. Empirical tests are more commonly used in the food industry for the simplicity and economy that they provide. However, empirical methods do not provide rheological results in fundamental units and therefore they are difficult to compare with other empirical tests (Anand, 2001).

Indentation is one of the preferred methods of measuring the rheological response of shortening because it is generally inexpensive, no standard specimen is required,

measurements can be done on highly localized regions and the results are less dependent on the geometry of the specimen (Anand, 2001; Huang et al, 2002). Quality control parameters for the shortening industry can be derived from indentation measurements; an example of a quality control parameter is the relative hardness obtained from cone penetration, which can be used to determine whether a specific shortening has the right quality for a particular application (Metzroth, 2005). Even though indentation tests are very simple to perform, the results are not easy to interpret due to the non-uniform application of forces to the specimen under the indenter. Because of the complexity of indentation results it is difficult to derive fundamental parameters from them and therefore indentation results are generally interpreted empirically (Huang et al, 2002; Goh et al, 2004a). So if indentation is to be used to determine mechanical properties in fundamental units, it is necessary to know the properties of rheologically complex materials such as shortening in fundamental parameters before an attempt can be made to measure such parameters from indentation.

The rheological response of vegetable shortening can be described by measuring fundamental material properties, which are independent of the measuring method (Steffe, 1996). Vegetable shortening is a very complex material showing a rheological response that combines the behaviour of a solid and a liquid. Therefore, the fundamental material properties used to describe the rheological behaviour of vegetable shortening include the modulus of elasticity, Poisson's ratio, yield stress, viscosity, relaxation time, creep compliance, retardation time and relaxation time. Since these fundamental parameters

are independent of the measuring method they can be used in mechanical models, such as the elasticity, plasticity and viscoplasticity equations (Menard, 1999).

Fundamental material properties can be obtained from a variety of mechanical tests; some examples include simple shear, triaxial tension and uniaxial compression (Steffe, 1996). The first part of the current research was dedicated to obtaining the fundamental material properties of vegetable shortening from a variety of uniaxial compression tests. Uniaxial compression tests were chosen because they are simple to perform, their results are relatively easy to interpret, and Universal Testing Machines are commonly available (Gunasekaran and Ak, 2003). Fundamental material parameters, such as the modulus of elasticity and yield point, can be extracted from monotonic and cyclic compression, while the remaining parameters, the time-dependent parameters, can be obtained by performing compressive creep and stress relaxation tests.

Ascertaining correct values for the fundamental mechanical properties of vegetable shortening can be affected by how the compression test is carried out. An example of artefactual effects is the presence of frictional effects (Charalambides et al, 2001). Also for many complex materials, the rate at which compression tests are performed can affect the values of the fundamental mechanical properties measured (Meyers and Chawla, 1999; Goh et al, 2005). Therefore it is important to quantify the frictional effects and the rate-dependent behaviour of materials, especially for complex materials, like vegetable shortening, which show rate-dependency in their rheological response (Goh and Scanlon, 2007). Once the fundamental properties of vegetable shortening are known and the rate-

dependency behaviour is characterized, this information can be used in mathematical models to predict the indentation response at different rates and so attempt to measure the fundamental parameters of vegetable shortening directly from indentation measurements, thereby turning indentation from an empirical tool into a means of providing measurements of mechanical properties in fundamental units.

One of the major objectives of this research was to develop and test the accuracy of the mathematical models developed. Due to the rheological complexity of the indentation response of vegetable shortening, testing the accuracy of the developed model requires the use of numerical solutions using the finite element method. The finite element method is used to solve complex problems by dividing the solution region into smaller sub-regions, called finite elements, for which the solution can be approximated (Rao, 1982). Many commercially available software packages are currently available in the market that can implement the finite element method for the solutions of complex mechanical problems; for this current research project Abaqus was selected due to its wide material capability and its ability to be customized (Abaqus, 2008).

In summary, the two main objectives of the current research project include the measuring of the fundamental material properties of vegetable shortening with a variety of uniaxial compression tests, and the development of a constitutive model for shortening that is able to predict the indentation response of shortening with the help of the commercially available finite element analysis software package, Abaqus.

CHAPTER 2: LITERATURE REVIEW

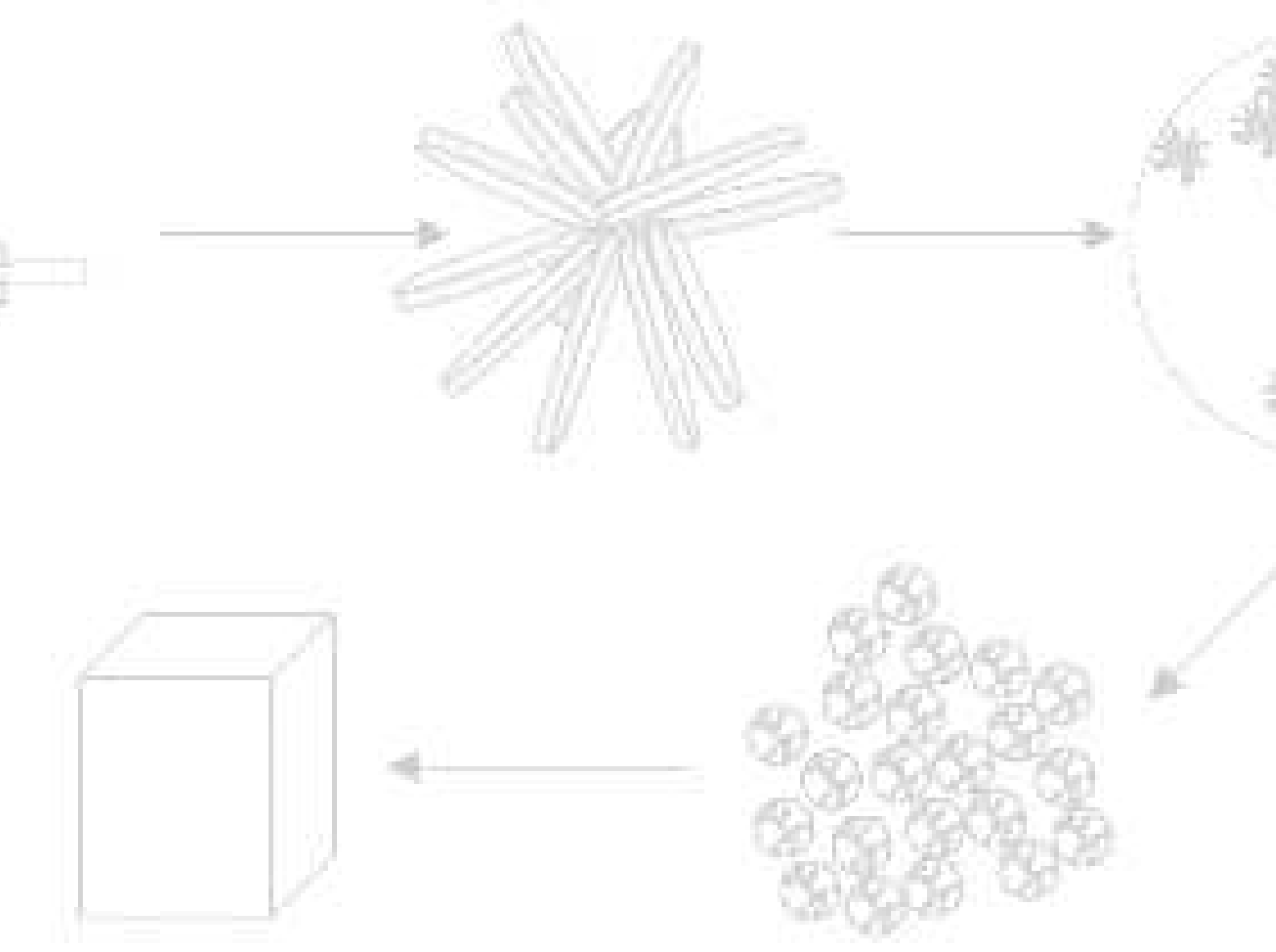

2.1.0 Introduction

Particle gels are formed by a network of weakly bonded particles surrounded by a fluid. The bonds between the particles are of several types and have different energy levels, but it is current thinking that the particles are bonded primarily with Van der Waals forces (Kloek et al, 2005). Many semisolid food products can be considered particle gels, including vegetable shortening. Vegetable shortening is a major ingredient in baked goods, and is also used as a frying agent. Its numerous applications in the food industry greatly depend on its rheological properties, which are a reflection of its composition and structure after processing. Understanding and predicting the rheological properties of vegetable shortening would be of great utility to the food industry because it could help in the development of new products with different functionality or improve the quality of existing products and the efficiency of the manufacturing process. A powerful tool in understanding and simulating the rheological response of complex materials, such as vegetable shortening, is the finite element method. The purpose of this literature review is to provide the background information necessary to define a model to simulate the rheological response of vegetable shortening using the finite element method.

2.2.0 Lipid-based Particle Gels

In particle gels weak forces maintain the solidity of the solid network and the network is interpenetrated by a suspended fluid (Rzepiela et al, 2002). The solid matrix in gels holds water, lipids, sugars, flavours and other ingredients useful in a great number of applications (Xiong et al, 1991). Many materials of great industrial importance are particle gels including paints, drilling muds, colloidal ceramics, some personal care

products, and many food products (Yanez et al, 1999; Goh and Scanlon, 2007). Of special importance to the food industry are lipid-containing particle gels which include a great number of semisolid foods such as chocolate, butter, yogurt, margarine and shortening (Lucey, 2002; Goh and Scanlon, 2007; Tang and Marangoni, 2007).

2.2.1 Structure of Lipid-based Particle Gels

The structure and the functional properties of foods and materials are determined by the physical state of their components. For example, the texture of chocolate and margarine are determined by the physical phase of their lipid components. At a given temperature the lipid components of lipid-based particle gels are present in either liquid or solid phase; a balance between the liquid and the solid state is what controls the crystalline structure of lipid-based particle gels (Duval et al, 2006). Lipid-based particle gels possess a network consisting of weakly bonded fat crystals arranged into different shapes that provide solid-like behaviour to the mixture of solid and liquid components (Awad et al, 2004).

Structurally, lipid-based particle gels are similar to crystallized colloidal gels; in both types of gels, crystals of different sizes (2 to 200 μm) aggregate and grow into clusters, these clusters aggregate forming microstructures called flocs and finally the flocs arrange themselves in a three dimensional network (Tang and Marangoni, 2006); a schematic representation is shown in Figure 2.1 (Tang and Marangoni, 2007).

The manner in which flocs bind to each other by van der Waals forces to form a three-dimensional network is very important in determining the rheological properties of particle gels. Current thinking suggests that the interfloc links carry most of the stress load and the failure of such bonds limits the elastic region of particle gels (Awad et al, 2004; Goh and Scanlon, 2007).

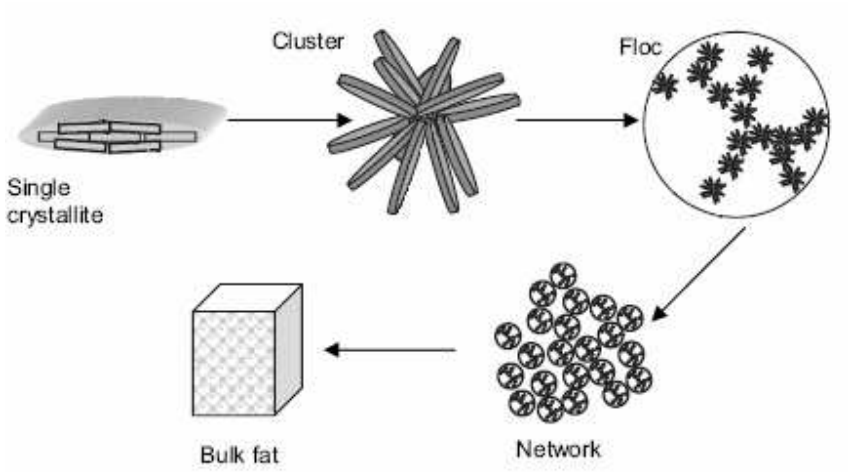

Figure 2. 1 Structural hierarchy of lipid gels (adapted from Tang and Marangoni, 2007)

Flocs forming the fat crystal network have different shape, size and strengths; as a result the network cannot be considered homogeneous. The weakest flocs will act as stress concentrators when the crystal network is subject to deformation (Tang and Marangoni, 2007), and the area around these weak flocs in the crystal network is probably the place where fractures can originate after large deformations (Kloek et al, 2005).

2.3.0 Shortening

The term shortening was originally used to describe the function performed by solid fats such as butter and lard on baked foods (Senanayake and Shahidi, 2005). Shortenings inhibit the formation of long gluten strands in wheat-based doughs and possess a high level of stability at elevated baking temperatures (Litwinenko et al, 2002). Shortenings are important industrial food ingredients because of their low cost of production, no need of refrigeration for storage, and desirable functional characteristics. These almost 100% fat products offer special functional utility to baking, confectionary and cooking applications (Ghotra et al, 2002) because they provide structure, improve shelf life and texture in baked goods and confectionary and when used as frying agents they offer a stable heat transfer medium.

Shortenings are a very important ingredient for the baking industry; they comprise from 10 to 50% of many baked goods (O'Brien, 1998). Shortenings are commonly used in dough and batter formulations where the fats need to be mixed with other ingredients at room temperature. The texture of breads, pastries and other baked goods is greatly affected when using shortening; breads, pastries and cookies become tender, flaky and fluffier when shortening is used in their formulation (Tecstra Systems, 2007). Shortening affects the properties of cake batters by improving aeration since shortening contains evenly distributed air or nitrogen cells, so that the cake batter will rise more. Staling can be retarded by using shortening in baked goods because shortening separates starch from coagulating protein that otherwise will stick together to give the sensation of hardness and toughness when chewed (Dogan et al, 2007). Shortening has also a lubricating effect

that provides moisture retention for shelf life improvement and smoother mouthfeel (Dogan et al, 2007).

Besides their use in baked goods, shortenings are used as frying or cooking agents because they allow for quick, uniform heat transfer during cooking and help in the formation of a moisture barrier on the fried food (Ghotra et al, 2002). Shortenings have a higher frying stability due to their lower content of unsaturated fatty acids, so that the oxidation rate of the frying oil is decreased (Choe and Min, 2007). Frying shortenings differ from all-purpose shortenings because they contain a higher amount of additives to increase stability such as antifoam (silicones) and antioxidant (BHA, BHT, PG, and TBHQ) agents; therefore frying shortenings have different functionality and can have adverse quality effects when used in food products such as baked goods (O'Brien, 1998; Choe and Min, 2007).

In this literature review the term shortening refers to processed vegetable fats and oil products that affect the stability, flavour, storage quality, and texture of food, as well as its visual appearance by providing structure, lubrication, aeration, emulsification, and moisture retention. Shortening also refers to the oil-base heat transfer medium used in cooking and frying (O'Brien, 1998).

2.3.1 Composition of Vegetable Shortening

The main ingredients in shortenings are vegetable oils and solid fats. The composition of such oils and fats plays an important role determining the physical properties of

shortening, such as its structural and thermal behaviour. At the same time the structural behaviour depends on the fatty acid composition and distribution on the glycerol of each single lipid (Schaink et al, 2007).

Vegetable edible oils, like the ones extracted from corn, soybean, cottonseed, sunflower, canola and palm, are the main ingredient in vegetable shortenings. These oils are mainly (95-96%) composed of triglycerides. Minor amounts of mono- and diglycerides from incomplete triglyceride biosynthesis or products of hydrolysis are also present in vegetable oils. Other minor lipid constituents comprise tocopherols, phytosterols and their fatty acid esters phospholipids, free fatty acids, fatty alcohols, waxes and long chain hydrocarbons (Andrikopoulos, 2002). Processing and blending several vegetable oils is necessary to obtain shortenings with the required functionality and quality. The simplest shortening consists of a fully hydrogenated fat blended with liquid oils; these products are marketed as “all-purpose” shortening and are generally suitable for pan frying and baking operations at home. Other shortenings with creamier qualities and greater resistance to oxidation generally include emulsifiers and other ingredients such as antioxidants (Martini and Herrera, 2008).

In the USA, the main liquid vegetable oil used for the manufacturing of shortenings is soybean oil due to its high availability. A fully hydrogenated fat is added (5 to 10%), which in the past used to be made mainly from palm oil. However due to the bad image of palm oil in the USA, shortening manufacturers have been forced to replace hard palm fat with cottonseed hard fat, even though hard palm fat produces a more stable crystal

network and replacing palm with cottonseed fat does not decrease the total saturates plus *trans* fatty acid content (deMan et al, 1992), components that are associated with cardiovascular disease.

In Canada, the most abundant vegetable oil is canola oil and after hydrogenation it is widely incorporated into shortenings as the main solid ingredient. However, it is generally mixed with hydrogenated soybean or palm oil because hydrogenated canola oil alone tends to form a coarser crystal structure that is undesirable for many applications (deMan et al, 1991).

The fatty acid composition of shortenings is highly variable due to the differences in the sources of fat, processes and desired final applications such as bakery, ice cream, and chocolate coating (Alonso et al, 2002). Table 2.1 shows the composition of major fatty acids in some vegetable shortenings produced in Canada and the USA.

Table 2. 1. Composition of major fatty acids in some North-American vegetable shortenings (deMan et al, 1992)

Oils in shortening	Major Fatty Acids (%)					
	16:0	18:0	18:1	18:2	Trans	Saturates + trans
Soy-palm	14.0–16.1	10.9–11.2	42.8–46.9	25.9–26.7	13.4–19.4	40.6–44.3
Soy-cottonseed	13.2–13.6	7.1–11.5	42.2–45.6	30.0-30.2	20.3–21.0	41.0–45.7
Canola-soy- palm	11.1–11.3	10.5–10.8	64.5–66.2	8.2-9.5	18.5-37.3	40.6–41.7

By looking at Table 2.1 one can see that, depending on the type of vegetable oil used in the formulation of vegetable shortening, the percentages of major fatty acids vary considerably.

In some cases emulsifier agents, such as saturated diacylglycerols, unsaturated diacylglycerols, and sorbitan tristearate are added to the vegetable oil and fat blends during the manufacturing of shortenings. The addition of emulsifier agents greatly affects the rheological properties of vegetable shortening because emulsifiers affect the crystallization behaviour of fat blends by changing the type of crystals formed and by changing the amount of crystals formed. It has been shown that the use of emulsifiers in vegetable shortening creates a “softer” texture as measured by cone penetrometer following AOCS official method Cc 16-60 (Martini and Herrera, 2008).

2.3.2 Manufacturing of Vegetable Shortening

Shortenings are manufactured from a mixture of oils from different sources commonly soybean, palm, sunflower, corn, cottonseed, and canola. The choice of oils used in a blend to manufacture shortening is more a function of empirical experience than scientific knowledge, but this choice affects the macroscopic physical functional properties of the final product (Dogan et al, 2007). Other factors that affect the macroscopic behaviour of shortenings include processing conditions, such as rate and degree of cooling, mechanical working and final product temperature (Ghotra et al, 2002).

During the manufacturing of vegetable shortenings, vegetable oil blends are solidified in various ways, such as by using hydrogenation and interesterification, and mixed with emulsifiers and other additives to produce a solid fat at room temperature with predetermined functionality and quality (Narine and Humphrey, 2004). The most common solidification techniques used with vegetable oils, as well as the processing steps involved during the manufacturing of vegetable shortening will be discussed in the following three subsections.

2.3.2.1 Hydrogenation of Vegetable Oils

Vegetable oils can be solidified by converting some of the double bonds present in triglycerides into single bonds. This process is achieved by adding hydrogen atoms across the unsaturated double bonds of specific triglycerides with the help of a catalyst, typically a nickel compound; this saturation process is called hydrogenation. Hydrogenation increases the solidity of a vegetable oil by increasing the percentage of saturated fatty acids (LaBell, 1997). Hydrogenation has been used since the beginning of the 20th century to produce solid fats from mainly liquid oils. Depending on the starting point of saturation of liquid oils and the degree of hydrogenation, solid and semi-solid fats can be produced. Hydrogenated oils impart firmness to margarines, and plasticity and emulsion stability to shortenings (Wassell and Young, 2007). During hydrogenation not all of the double bonds are converted into single bonds, instead some are converted from the *cis* orientation with both hydrogen atoms on the same side of the plane to the *trans* orientation with hydrogen atoms on both sides of the plane (Ledux et al, 2007); this isomerization gives rise to the formation of *trans* fatty acids which have been linked to

cardiovascular disease (Mensik and Catan, 1990; Han et al, 2002; Kummerow et al, 2004).

2.3.2.2 Interesterification of Vegetable Oils

The formation of *trans* fatty acids during hydrogenations has encouraged research for developing alternative methods to produce solid vegetable oils. One of these alternative methods is interesterification. During interesterification the distribution of fatty acids is rearranged on the glycerol backbone in a random or controlled manner without changing the chemical composition of fatty acids, and this rearrangement can be done chemically or enzymatically. Interesterification is an effective technique that can be used to produce fat products that are soft and spreadable as well as free of *trans* fatty acids (Wassel and Young, 2007). However, interesterification is harder to control and therefore is less efficient and more expensive than hydrogenation (Grün, 2004); also, interesterification does not improve the oxidative stability of fat and oils in the same way that hydrogenation does (Basturk et al, 2007).

2.3.2.3 Processing of Vegetable Shortening

Processing steps, such as mechanical working and super-cooling during the manufacturing process of shortening, are equally important in determining the physical properties and performance of shortening as are the design of the oil blend and the solidification process of such oil blends (Ghotra et al, 2002).

The basic industrial shortening manufacturing procedure starts by weighing hard and liquid oils as well as other ingredients though a series of scale tanks or mass flow meters. Once all the ingredients are measured they are introduced into a feed tank where they are thoroughly blended. Nitrogen is injected in precise controlled quantities, normally 12 to 14% by volume, into most shortenings to increase workability and provide a creamy and white appearance (O'Brien, 2005). Then the mixture is introduced to a scraped surface heat exchanger, typically called Unit A, where it is quickly cooled down so that a super-cooled oil is formed. Super-cooling is important in order to start crystal nucleation for the formation of fine crystals or the β' polymorphs. The super-cooled mixture then passes through a working unit consisting of a number of projecting fingers on a rotating shaft commonly known as Unit B. Unit B is used to plasticize and control the crystallization process of the product. Later the plasticized material is homogenized by passing through an extrusion valve and the product is packaged in bulk or into smaller consumer packages. After packaging many producers temper shortening for 1 to 10 days at temperatures slightly higher than the packaging temperature. During tempering the crystals transform to the preferred and more stable polymorphic form; lack of tempering produces shortening with undesirable functional properties (Ghotra et al, 2002). The quality of shortenings strongly depends on the storage and handling conditions from the moment the product leaves the manufacturing facility until it reaches the consumer (Martini and Herrera, 2008), and for this reason shortenings are generally stored and shipped at controlled temperatures between 21 and 27 °C to avoid crystal change and loss of plastic properties. Figure 2.2 summarizes the shortening manufacturing procedure (Anderson, 2005).

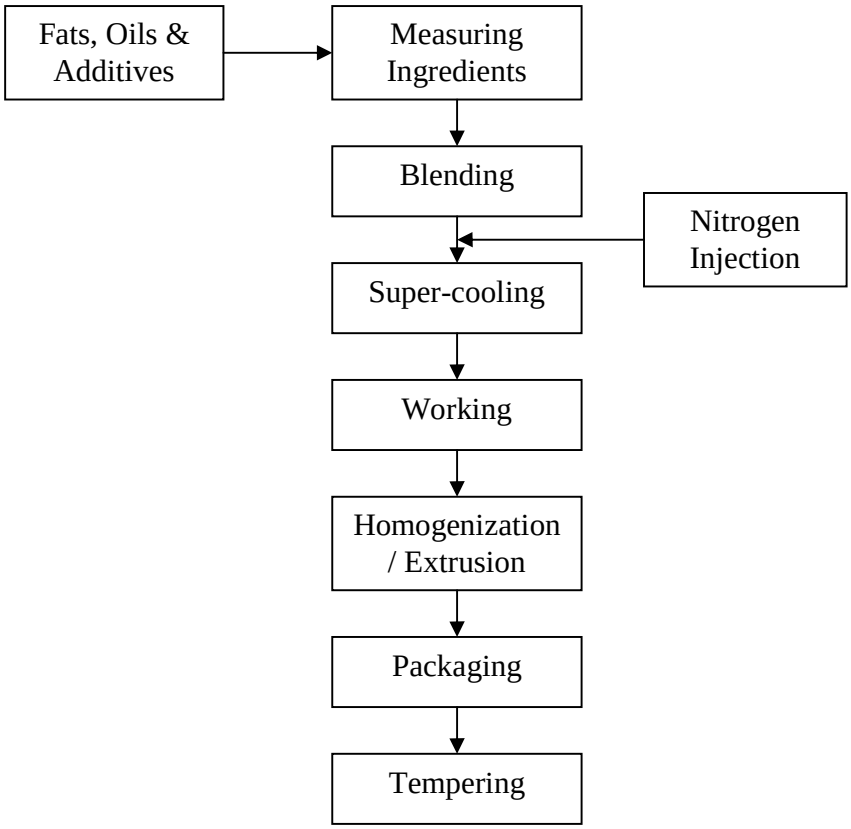

Figure 2. 2. Industrial manufacturing of shortening (adapted from Anderson, 2005)

2.3.3 Structure of Vegetable Shortening after Processing

Edible fat products, such as shortenings appear to be soft homogeneous solids, but microscopically they are a network of very small crystals (2 to 200 μm) in which liquid oil is enmeshed (O'Brien, 2005; Tang and Marangoni, 2006). Crystal structure is very important in shortenings because it will determine functionality and quality (deMan et al, 1991). Product attributes like spreadability, hardness and work softening are at least partially determined by the shape and size of individual fat crystals and also by the way these crystals interact to form clusters, flocs and networks (Heertje and Leunis, 1997).

Shortenings are polymorphic because their major components, triglycerides, occur in three crystal forms (Podmore, 2002). The three crystal forms present in shortenings are designated as α, β and β'. The α crystalline form is very fine and needle shaped, and forms a loosely packed and unstable network (Carden and Basilio, 2004); this crystal form has the lowest melting point (Podmore, 2002). During tempering α crystals remelt and slowly recrystalize into the β' form (Reigel and McMichael, 1966), which is the most desirable crystal structure for all-purpose shortenings (Senanayake and Shahidi, 2005). β' crystals are small, uniform and tightly knit and therefore produce smooth textured shortenings with good plasticity, heat resistance and creaming properties that can be use to make cakes and icing (Thomas, 1978). β crystals are larger than β' crystals and can produce shortenings with sandy and brittle consistency that results in poor baking performance. However, β crystals are desirable in some applications such as in pie crusts or when used as a frying agent (O'Brien, 2005).

The source of the fat used for the manufacturing of shortening plays a very important role in determining the structure of the final product because the crystalline habit and polymorphic form is determined by the triglyceride composition. In a mixture of triglycerides the individual triglycerides do not behave independently but take a totally new character in terms of crystallization behaviour (Podmore, 2002). For this reason, in order to attain the appropriate crystalline form, vegetable shortening is produced by blending base stocks of different origin. For example, when the solid portion of a shortening is comprised of glycerides that are stable in the β' form, the rest of the glycerides present in fat system will tend to crystallize in a β' form; thus producing

shortening with desirable characteristics. Hydrogenated fat from butter oil, cottonseed, modified lard, palm, rapeseed, and tallow tends to crystallize in a β' structure, while hydrogenated fats from cocoa butter, coconut, corn, olive, palm kernel, safflower, and soybean tend to form β crystals (Thomas, 1978).

2.4.0 Quality Attributes of Vegetable Shortening

The acceptability of shortenings, like any other food, is dependent on a number of criteria, in particular sensory impact; perceived qualities such as aroma, taste, visual appearance and texture are the reflection of the chemical and physical properties of their components and how these components interact during processing, preparation and consumption (Kinsella, 1987). During the production of vegetable shortening many analytical measurements are taken in order to determine the quality of the final product.

2.4.1 Conventional Industry Quality Indices for Vegetable Shortening

In order to obtain consistent shortenings and have good quality control during manufacturing, it is important to understand the principles, and apply the processes that influence cooling, texturizing and crystallizing (Metzroth, 2005). In order to understand and investigate the efficacy of manufacturing process analytical methods are required. In the shortening industry analytical methods are conducted to measure crystal size, colour, solid fat content, iodine value, refractive index, thermal properties, rancidity, viscosity, hardness, consistency and texture (Metzroth, 2005).

Crystal size and distribution is currently measured using light or x-ray scattering. Information on the crystal structure and distribution can be obtained using a revolving laser beam coupled with a computer. Crystal size distribution affects the rheological properties and texture of lipid-based soft products. For example, a soft material with a great amount of large crystals will have a larger viscosity and coarser texture, as compared with a material with small crystals, limiting its applications (Do et al, 2007). Nuclear magnetic resonance can be used to measure the solid fat index (Metzroth, 2005), which is the ratio of solids to liquids present in a fat at a given temperature, and this parameter is regularly used to determine quality and functionality of shortenings. For example, an all-purpose shortening is considered to have an acceptable plasticity if the solid fat index at room temperature is between 10 and 25 (Carden and Basilio, 2004). High performance liquid chromatography and gas chromatography can both be used to determine triglyceride and fatty acid analysis (Metzroth, 2005). Differential scanning calorimetry (DSC) can be used to determine the melting behaviour of shortenings. Crystal form can be correlated to DSC measurements but these results are not absolute indicators of the crystalline structure (deMan et al, 1991).

Hardness and plasticity of shortenings is measured using compression devices; from these devices a force-deformation curve is obtained. Initially the curve is straight, followed by flat sections and finally a break (Figure 2.3). Shortenings that are hard and brittle have a narrow flat section which is related to the plasticity, and the breaking point occurs after little deformation. Shortenings with larger viscous behaviour and plasticity show a curve that round off with long flat sections (Metzroth, 2005).

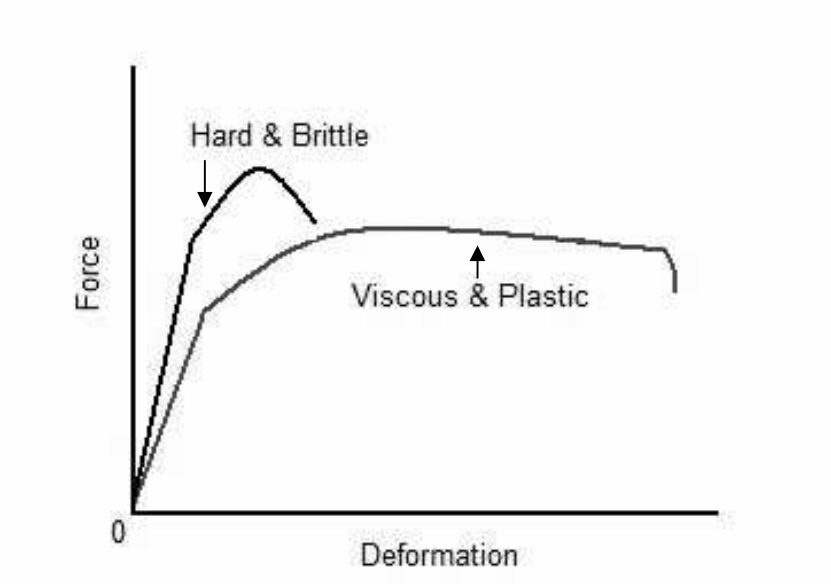

Figure 2. 3. Schematic force-deformation curve for two types of vegetable shortenings

Another common method of determining hardness is by using cone penetration; a cone of specified mass and dimensions is dropped into a sample, the penetration depth is measured and the relative hardness (θ) of the material is determined by dividing the mass of the cone (m) by the penetration depth (δ) (Metzroth, 2005).

$$\theta = \frac{m}{\delta} \qquad [2.1]$$

A soft shortening will have a smaller relative hardness because the cone will penetrate further than in a hard shortening. A shortening with a narrow difference in relative hardness values at low and high temperatures indicates that the shortening possesses a wide plastic range while very large differences indicate a narrow plastic range. Shortenings with different applications can be obtained by changing the formulation and processing conditions, and these shortenings will have different hardness values (Metzroth, 2005).

Many of the conventional quality indices used by the shortening industry are empirical in nature and depend on the utilization of a particular measuring device; this is the case, for example, of hardness as measured by cone penetration. Alternatively, the quality of shortening can also be quantified by measuring fundamental rheological properties. In theory, fundamental rheological properties are independent of the instrument which is used to measured them so different instruments will produce the same results for the same product (Steffe, 1996). Parameters such as the modulus of elasticity, Poisson's ratio, and yield stress are considered to be fundamental rheological properties that apply to all solid materials. These and other rheological properties will be discussed in detail in the following section.

2.5.0 Rheological Properties of Materials

Rheology is a part of mechanics that studies the deformation and flow of matter that occurs as a response to an applied stress or strain. All materials have rheological properties and therefore rheology is relevant in many fields of study, including Food Science (Steffe, 1996). In lipid-rich food products, including vegetable shortening, rheological properties are a direct result of the composition and structure of the product and the processing and storage conditions that it has been subjected to. Therefore, understanding and measuring rheological properties can be used to improve the quality of final products and improve the efficiency of the manufacturing process (Afoakwa et al, 2008).

The type of rheological response that is observed depends on the physical state of the material (liquid or solid). If the material is viewed as a solid then rheological properties such as the modulus of elasticity, Poisson's ratio and plasticity can be used to describe its deformation behaviour. If the material is viewed as a liquid, properties such as viscosity will be very important in describing its rheological behaviour. However if the material shows characteristics of a liquid and solid at the same time, viscoelastic parameters such as creep compliance, relaxation modulus, relaxation and retardation time, as well as loss and storage moduli become the parameters used to describe its rheological response (Steffe, 1996).

2.5.1 Modulus of Elasticity

The elasticity of a material can be quantified using the modulus of elasticity or Young's modulus. The force required to deform a material can be measured during rheological tests. From the measured force and deformation, stress and strain can be calculated. If the deformation is small and within the elastic region of the material, stress and strain can be approximated by the engineering stress (σ_E) and strain (ε_E) using the following equations:

$$\sigma_E = \frac{F}{A_0} \qquad [2.2]$$

$$\varepsilon_E = \frac{|h - H|}{H} = \frac{\Delta h}{H} \qquad [2.3]$$

where F is the reaction force exerted by the specimen on the measuring device, A_0 is the initial cross-sectional area of the specimen, H is the initial specimen height, and h is the

current height which is equal to the initial height (H) minus the current deformation of the specimen (Δh).

If the specimen is subject to a large deformation then true, or Hencky, strain (ε) and stress (σ) should be used to calculate the modulus of elasticity rather than the engineering stress and strain. Equations [2.4] and [2.5] show how Hencky stress and strain can be calculated respectively for a specimen (Charalambides et al, 2001),

$$\sigma = \frac{F}{A} \qquad [2.4]$$

$$\varepsilon = \left| \ln \frac{h}{H} \right| \qquad [2.5]$$

where A is the cross-sectional area of the specimen after a force (F) has been applied to it and h is the current height which is equal to the original height (H) minus the current deformation of the specimen (or plus the deformation if subject to tension). Measuring the actual value of A is not an easy task; therefore true stress is hard to calculate. An approximation of the true stress can be obtained if the material is assumed to have no change in volume when deformed by stresses, i.e., the material is incompressible; this assumption has been used for food materials like cheese, dough, shortening, butter, and margarine (Charalambides et al, 1995; Charalambides et al, 2001; Charalambides et al, 2006; Goh and Scanlon, 2007). Assuming incompressibility, stress at large deformations of a cubic specimen can be calculated using equation [2.6]:

$$\sigma = \frac{Fh}{L^2 H} \qquad [2.6]$$

where L is the original side length of the cubic specimen and other parameters are as previously defined.

Once the stress and strain are calculated, they can be used to determine the modulus of elasticity (E) as shown in equation [2.7] (Steffe, 1996; Ribeiro et al, 2004):

$$E = \frac{\sigma}{\varepsilon} \qquad [2.7]$$

The modulus of elasticity is an important parameter that describes the deformability of a food material, and is related to the sensory attributes of such a material when one deforms it in the mouth (Narine and Marangoni, 2000). The Young's modulus is a measure of the resistance to strain of a material. A small value of E means that a small stress produces a large deformation in a material, while a higher value of the modulus of elasticity corresponds to a higher material stiffness (White, 1999). The Young's modulus is usually calculated from the initial linear part of a stress-strain diagram (Figure 2.4a), but for highly non-linear stress-strain diagrams it can be expressed as the 5% strain secant modulus (Figure 2.4b) as done by Charalambides et al (1995).

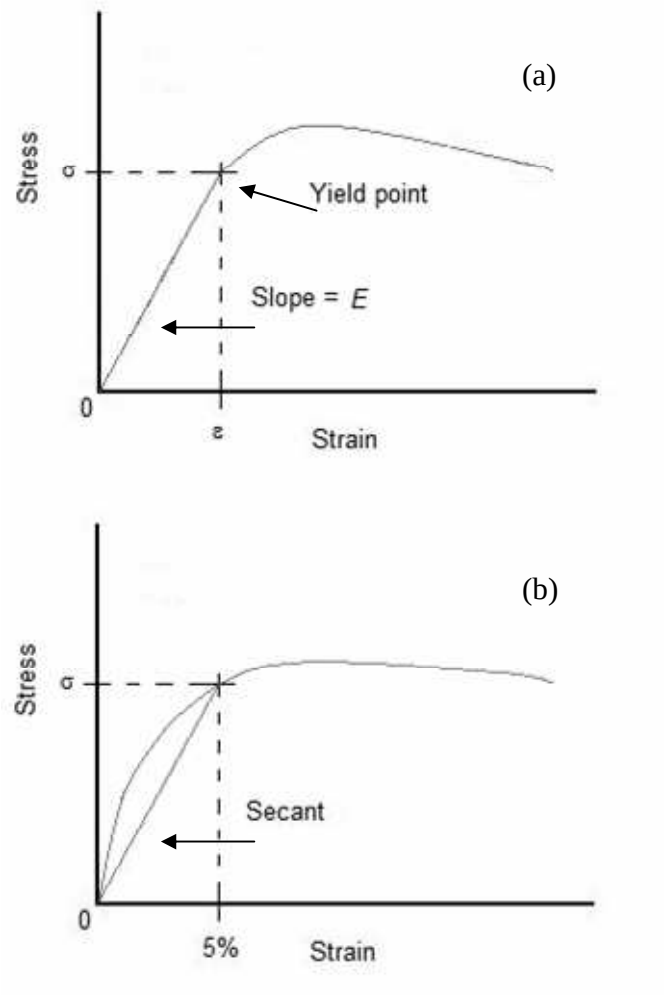

Figure 2. 4. Schematic stress-strain curve showing how to calculate (a) the Young's modulus and (b) the secant modulus at 5% strain

2.5.2 Yield Stress and Plasticity

The linear proportionality of stress and strain remains only if the stress is less than a certain value, a value that is referred to as the yield stress (Narine and Marangoni, 2000). The yield stress (σ_y) represents the amount of stress required to cause permanent deformation in a given material. In other words, the yield stress marks the end of the elastic region of a material (Figure 2.4a). When dealing with a perfectly elastic material no yield stress will ever be reached because any deformation is reversible in this type of

theoretical material. However most real materials have a yield point that, once exceeded, causes a permanent strain, and when the stress is removed the material remains deformed (White, 1999).

The yield stress is one of the most important macroscopic properties of economically important food products like chocolate, butter and shortening, since it strongly correlates to the sensory attributes of hardness and spreadability, as well as to material stability (Marangoni and Rogers, 2003). However, the determination of the yield stress for a soft food material is a difficult task, since many food materials show rate-dependency. Rate-dependency is observed when a high loading rate produces a different value of the apparent yield stress as compared to a lower loading rate (Marangoni and Rogers, 2003).

Many plastic materials also have an elastic region at low strains and for this reason they are called elasto-plastic materials. In the plastic region the total strain increment ($d\varepsilon$) is the sum of the elastic strain increment ($d\varepsilon_e$) and the plastic strain increment ($d\varepsilon_p$) (Yu et al, 2006):

$$d\varepsilon = d\varepsilon_e + d\varepsilon_p \qquad [2.8]$$

The initial yield point (σ_{y1}) differentiates the elastic and the plastic regions (Yu et al, 2006). After a material has been deformed beyond its initial yield point, the subsequent deformation is also affected by a behaviour known as strain-hardening (Dasgupta and Hu, 1992). So it can be seen that the fundamental elements of plastic deformation include initial yielding of the material, strain-hardening and subsequent yielding (Bulatov et al, 2006; Yu et al, 2006).

Plasticity of crystalline materials, such as vegetable shortening can be explained on the basis of mechanisms at an atomic or molecular level. In crystalline materials, the primary units are organized in uniform planes. During large strain deformation, slip occurs which implies that one plane is sliding across a neighbouring plane. Once slip occurs the primary units cannot return to their original position causing the deformation to be irreversible, i.e., plastic deformation (de With, 2006).

Defects in a perfect crystal are called dislocations and during plastic deformation these dislocations can move (Gottstein, 2004). During the first stage of plasticity, right after the yield stress is reached (Figure 2.5 stage I), dislocations on primary slip planes can move long distances and even reach specimen boundaries. As the deformation continues secondary slip planes develop; these secondary slip planes also have dislocations, which can move along the secondary slip planes in different directions than the primary dislocations. Secondary and primary slip planes can overlap at certain points, so it is possible for the primary and secondary dislocations to interact with one another. The interaction between primary and secondary dislocations causes immobility of some of the dislocations. For each immobile dislocation another mobile dislocation has to be generated in order to maintain the applied strain rate (during uniaxial compression for example). In order to maintain the strain rate constant, the internal stress has to increase more rapidly to allow the development of new mobile dislocations; this behaviour is what causes strain hardening (Figure 2.5 stage II) in crystalline materials. During the third stage of plastic deformation (Figure 2.5 stage III), the rate of strain hardening starts to

decrease. The decrease in hardening rate is related to the formation of dislocations that do not have a defined sliding plane and can change their sliding plane; these dislocations are called screw dislocations. Screw dislocations tend to avoid interactions with other dislocations by changing sliding planes, so they can move long distances and eventually reach the specimen boundary. However, during stage III, the generation of dislocations occurring in stage II is still taking place; therefore strain hardening is still possible but to a lesser extent (Gottstein, 2004).

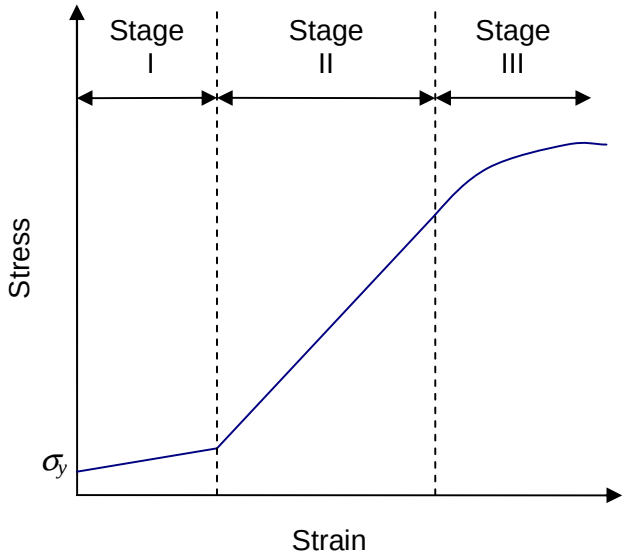

Figure 2. 5. Schematic stress-strain diagram showing three stages during plastic deformation (adapted from Gottstein, 2004)

2.5.3 Poisson's Ratio

When a material is compressed in one direction by a force (*F)* from original height (*H)* to a final height (*h*) it tends to get wider in the other two directions. In the case of the cylinder shown in Figure 2.6 the specimen goes from an original diameter (D_0) to a final diameter (D_f). The extent of this behaviour is characterized by the Poisson's ratio (v).

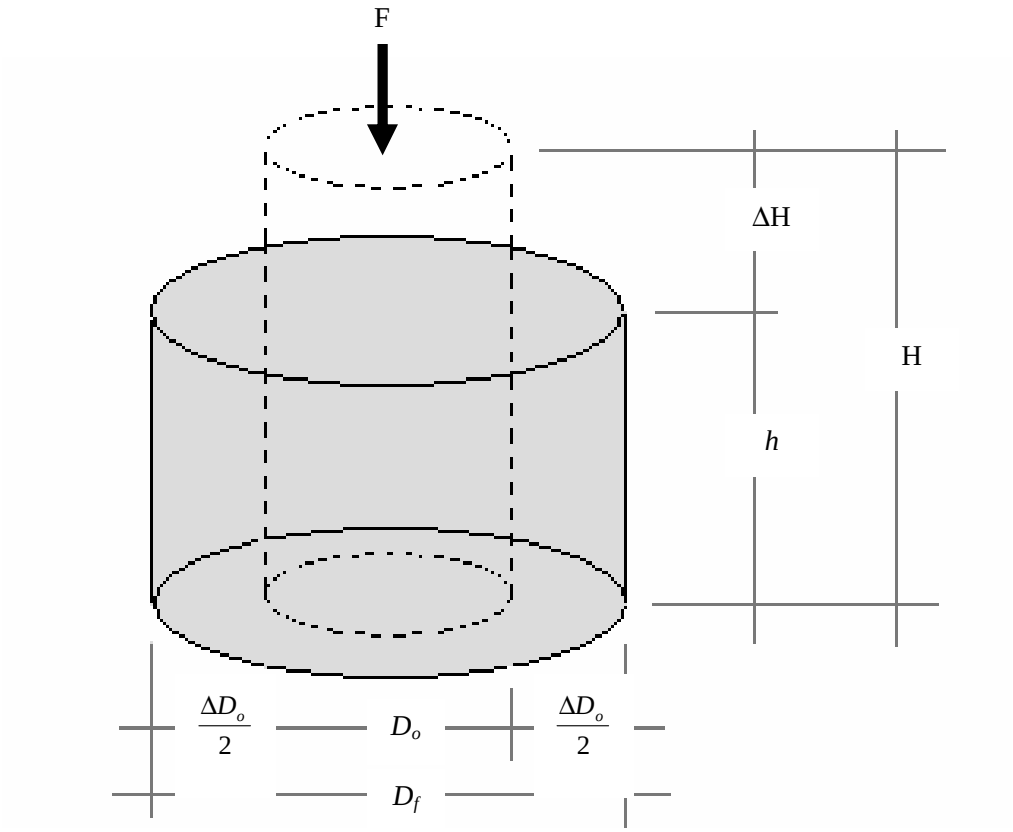

Figure 2. 6. Parameters used to calculate Poisson's ratio of a cylindrical specimen under compression (adapted from Gunasekaran and Ak, 2003)

Poisson's ratio is defined as the negative ratio between the strain normal to the applied load (transverse strain) and the strain in the direction of the applied load (axial strain) (Hjelmstad, 2005). The negative sign indicates that the lateral dimension increases as the axial dimension decreases under compression and vice versa during tension. The following equation summarizes the concept of Poisson's ratio for the cylindrical specimen shown in Figure 2.6 (Gunasekaran and Ak, 2003):

$$\nu = -\frac{\varepsilon_{lateral}}{\varepsilon_{axial}} = -\frac{\left[\frac{D_f - D_o}{D_o}\right]}{\left[\frac{h - H}{H}\right]} \qquad [2.9]$$

Most materials have a Poisson's ratio between 0.0 and 0.5, but there are materials with negative values and even with values higher than 0.5. A perfectly incompressible material will have a Poisson's ratio of 0.5; rubber is an example of a material that approximates to an incompressible solid, while cork is a common example of a compressible solid with a Poisson's ratio close to zero. Based on energy arguments, the theoretical allowable range of Poisson's ratio for isotropic three dimensional materials is -1 to 0.5 (Lee and Lakes, 1997). However until 1987 it was believed that materials with a negative Poisson's ratio were non-existent. Negative values for Poisson's ratio have been reported in specially-constructed polymeric and metallic foam structures (Lakes, 1987; Friis et al, 1988; Choi and Lakes, 1992) and Poisson's ratio greater than 0.5 were reported for specially-manufactured open-cell polyurethane foams (Lee and Lakes, 1997). Most biological materials including food have a Poisson's ratio between 0.2 and 0.5 (Steffe, 1996).

The Poisson's ratio is one of the four common elastic constants and can be used to relate the modulus of elasticity (E) to the shear modulus (G) and to the bulk modulus (K). The latter two moduli describe the change in dimensions of materials under shear stress and hydrostatic pressure respectively, by the following equations (Ferry, 1970):

$$E = 2G(1+\nu) \qquad [2.10]$$

$$E = 3K(1-2\nu) \qquad [2.11]$$

and for a perfectly incompressible solid (Ferry, 1970):

$$E = 3G \qquad [2.12]$$

2.5.4 Liquid Parameters

In previous sections the material parameters that are used to describe the rheological response of solid materials have been discussed. Other parameters are used to describe the rheological response of liquids. When a force is applied to a liquid, flow starts to occur. The Newtonian model is used to characterize the flow of many liquids. Flow of a liquid material is dependent on the rate at which strain is applied to it; therefore liquids are rate-dependent materials. Newton defined the stress-strain rate relationship using the dashpot as a model, which consists of a plunger with small holes through which a fluid is forced through; an example of a dashpot is a French coffee pot (Bodum) or an automobile's shock absorber. As the stress is applied the material starts to slowly flow through the holes and the speed at which the fluid flows through the holes (i.e., strain rate) increases with stress. For a Newtonian fluid this increase is linear and is summarised by the following equation (Menard, 1999):

$$\sigma = \eta\dot{\varepsilon} \qquad [2.13]$$

where the stress (σ) is related to strain rate ($\dot{\varepsilon}$) through viscosity (η). For a Newtonian fluid the viscosity is independent of the strain rate and is the slope of the stress-strain rate curve (Figure 2.7 curve (a)). Examples of Newtonian fluids include water, tea, coffee, beer, carbonated beverages, filtered juices, edible oils, sugar syrups, most honeys and milk (Bourne, 2002). However, most food materials are non-Newtonian; therefore their

stress-strain rate diagrams are not straight lines and their viscosity is not a constant independent of the strain rate (Menard, 1999); so that equation [2.13] becomes:

$$\sigma = \eta(\dot{\varepsilon})\dot{\varepsilon} \qquad [2.14]$$

For many non-Newtonian fluids, as the strain rate increases their apparent viscosity decreases; liquids that behave in this manner are called pseudoplastic or shear thinning fluids (Figure 2.7 curve (b)). Common examples of pseudoplastic fluids include ketchup, whipped cream, latex paint and polymer melts. In contrast, liquids for which the viscosity increases with increasing strain rate are called dilatant or shear thickening (Figure 2.7 curve (c)) (Böhme, 1987). At low to moderate strain rates, it is more common to encounter liquids showing pseudoplastic behaviour, but at very high rates it is more common to observe shear thickening behaviour as shown Figure 2.8 (Faber, 1996).

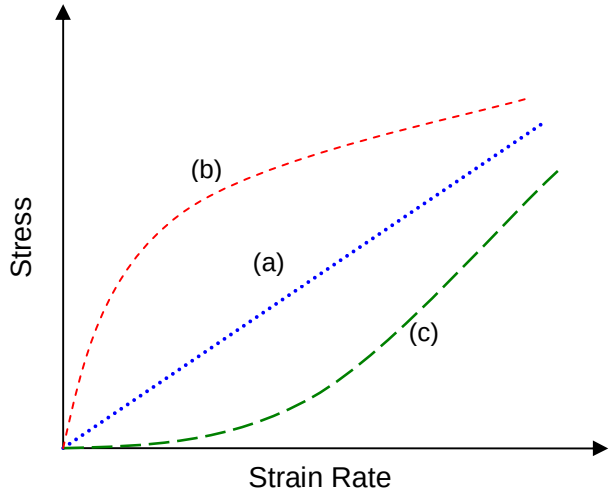

Figure 2. 7. Stress-strain rate curves for (a) Newtonian fluid, (b) pseudoplastic fluid and (c) dilatant fluid (Adapted from Böhme, 1987)

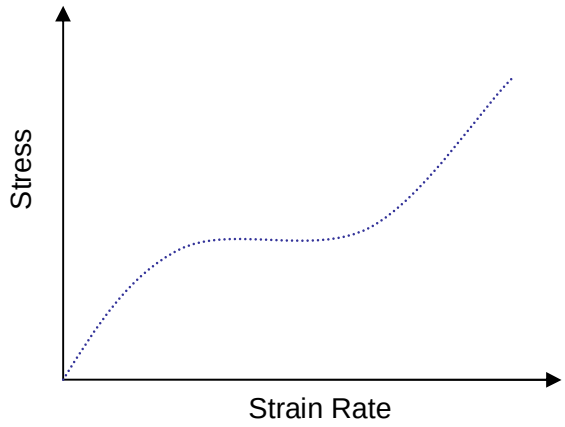

Figure 2. 8. Stress-strain rate curves for a fluid showing pseudoplastic and dilatant behaviour at different strain rates (Adapted from Faber, 1996)

2.5.5 Viscoelastic Parameters

Most food materials are not ideal and are strain-rate dependent because of their liquid and solid components, making them viscoelastic materials (Kinsella, 1987). The viscoelastic behaviour of materials can be modelled by a system of connected springs and dashpots (visualized as pistons moving in oil). When a spring is connected in series to a dashpot a Maxwell model is formed (Figure 2.9a), and when the spring is connected in parallel to the dashpot, the model is called the Kevin-Voigt model (Figure 2.9b). The spring represents the elastic component of the response that instantaneously deforms upon the application of a load and immediately relaxes upon the release of the load. The dashpot represents the viscous component that increases with time as long as the load is applied. In the case of the Maxwell model; the dashpot is permanently displaced by the applied load.

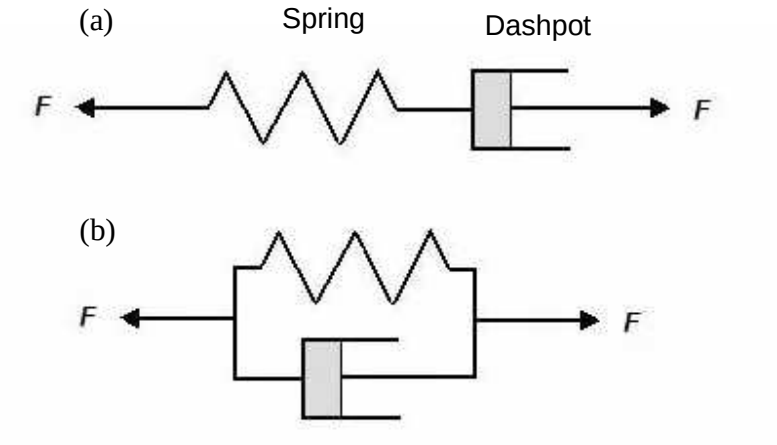

Figure 2. 9. Basic (a) Maxwell and (b) Kelvin-Voigt elements consisting of a spring and a dashpot

For a Maxwell element the total stress is the same as the stress acting concurrently on the spring and on the dashpot, but the total strain (ε) is a summation of the strain on the spring (ε_s) plus the strain on the dashpot (ε_d) (Hiemenz, 1984):

$$\varepsilon = \varepsilon_s + \varepsilon_d \qquad [2.15]$$

The strain in the elastic component (spring) is given by Hooke's law (equation [2.7]). However, there is no direct expression for the strain in the viscous component (dashpot), only for the way the strain varies with time, which is given by Newton and shown in equation [2.13]; therefore it is not possible to develop equation [2.15] any further as an explicit equation, but only as a differential equation (Hiemenz, 1984). Expressing equation [2.15] as a differential equation with respect to time (t) leads to the equation of motion for a Maxwell element of the following form (Cowie, 1991; Roylance, 1996):

$$\frac{d\varepsilon}{dt} = \frac{1}{E}\frac{d\sigma}{dt} + \frac{\sigma}{\eta} = \dot{\varepsilon}_s + \dot{\varepsilon}_d = \frac{\dot{\sigma}}{E} + \frac{\sigma}{\eta} \qquad [2.16]$$

where E is the elasticity constant of the spring and η is the viscosity of the dashpot, $\dot{\varepsilon}_s$ and $\dot{\varepsilon}_d$ are the strain-rates of the spring and dashpot respectively, and $\dot{\sigma}$ is the change in stress with respect to time (Findley et al, 1989; Steffe, 1996). For a Kelvin-Voigt element the total stress is the summation of the stress on the spring and the stress on the dashpot, but the strain is identical in both components; therefore, for a Kelvin-Voigt model the stress is related to strain and strain rate by the following equation (Meyers and Chawla, 1999):

$$\sigma = E\varepsilon + \eta\dot{\varepsilon} \qquad [2.17]$$

Other parameters related to the viscoelasticity of materials include the relaxation modulus, creep compliance, relaxation time and retardation time. The relaxation modulus is a measurement of how much the stress will decay in time when a constant strain is applied, while the relaxation time is the time needed for the stress to fall to e^{-1} of its initial value when the material is subject to constant strain, both of which can be measured during stress relaxation tests (Roylance, 1996). Creep compliance is a measurement of how much the strain will change with time when a constant stress is applied and retardation time is the time needed to strain a sample specimen by $1\text{-}e^{-1}$, both of which can be obtained after performing creep tests (Menard, 1999; Rao, 2007). Stress relaxation tests and creep tests can be performed under shear, bulk compression and uniaxial compression. These types of mechanical testing will be discussed further in the following section.

2.6.0 Measuring Rheological Properties

Experimental measurements of the rheological properties of materials are usually made by observing external forces and changes in external dimensions of a specimen of a given shape (Ferry, 1970). Lipid-based particle gels, and food in general, exhibit a broad range of rheological characteristics; for this reason a variety of measuring techniques have been developed to characterize their rheological properties. These measuring techniques can be classified according to the type of deformation they apply to the sample either as shear, uniaxial compression or tension, triaxial tests or a combination of these (McClements, 2003; Körstgens et al, 2001).

2.6.1 Shear-based Tests

Most of the techniques used to measure the rheological properties of particle gels have been shear-based (Shukla and Rizvi, 1995) because of the fluid-like behaviour of these gels. Shear-based test are generally performed to very small strain (<5%) because small strains do not greatly modify the original structure of materials; therefore these measurements can be related to the structure and structure development of materials (Gunasekaran and Ak, 2003). Simple shear deformation occurs when two opposite faces of an element of length L are displaced by a distance ΔL after opposite forces are applied on the faces of this element (Figure 2.9). During simple shear a change in shape is not accompanied by any change in volume and this can be useful when interpreting the mechanical behaviour of materials in molecular terms (Ferry, 1970)

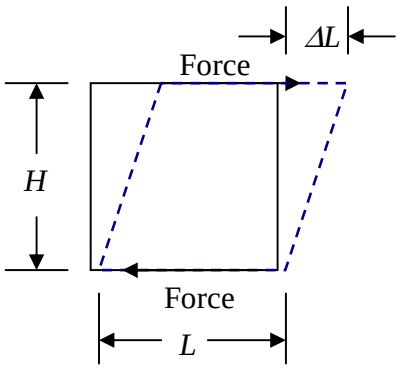

Figure 2. 10. Schematic representation of simple shear deformation

Shear can be generated by drag flow and pressure-driven flow. In drag flow a sample is placed between a sliding or rotating surface and a fixed solid surface (tractive displacement), so that the movement of a rigid surface causes the shearing of the sample, like in Figure 2.10. In pressure driven flow, pressure is used to force a sample to flow through a straight channel which may be a capillary or a slit in which a sample is sheared as it passes through the channel (Ouriev and Windhab, 2002; Gunasekaran and Ak, 2003). Shear tests are generally performed in machines called rheometers. Rheometers that rely on drag flow can be used to determine a variety of material functions including the shear loss (G') and storage (G'') moduli, the shear creep compliance (J) as a function of time, and the viscosity (η) as a function of shear-rate. Pressure-driven rheometers are primarily used for the measurement of viscosity at high-shear rates (Hatzikiriakos and Migler, 2004).

2.6.1.1 Dynamic shear tests

Since particle gels have a viscoelastic nature most shear-based rheological tests are dynamic in order to measure the frequency-dependency effects. Some dynamic tests consist of applying a sinusoidal simple shear, sometimes called an oscillatory test, although more often pure shear rotational displacements are applied in oscillatory tests. In a simple shear test a sample is placed between two parallel plates; one is fixed while the other one moves back and forth (Figure 2.11a), and by measuring the amplitude ratio (stress amplitude divided by strain amplitude) and the phase shift between stress and strain during the harmonic deformation (Figure 2.11b), rheological parameters such as the storage (*G'*) and loss (*G"*) moduli can be obtained (Ferry, 1970; Higaki et al, 2004; Rao and Quintero, 2003). The storage modulus is a parameter that directly relates to the elasticity of a material under shear, while the loss modulus relates to the viscous behaviour after shear is applied (Rao and Quintero, 2003).

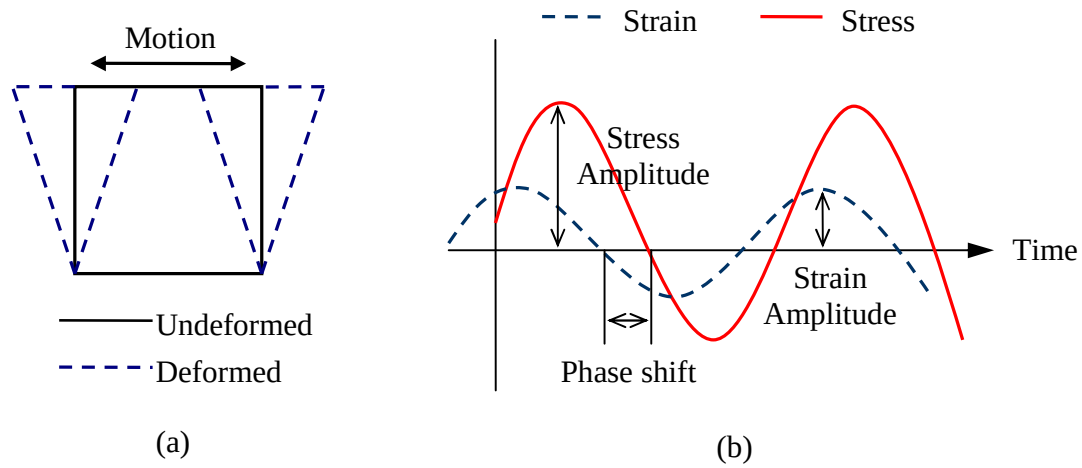

Figure 2. 11. Schematic representation (a) and time profile (b) of dynamic shear test with sinusoidally varying shear (adapted from Ferry, 1970)

2.6.1.2 Shear Tests to Measure Viscoelastic Properties

There are two types of experiment that can be used to study the time-dependent viscoelastic behaviour of materials; these experiments are stress relaxation and creep tests, and both can be performed under shear generated by drag-flow. During stress relaxation tests a constant shear strain (γ_0) is imposed in a short period of time into a sample material and the shear stress (σ_s) is monitored for a given amount of time (t). The shear stress and the shear strain are related by the relaxation modulus ($G(t)$) in the following manner (Ferry, 1970):

$$\sigma_s(t) = \gamma_0 G(t) \qquad [2.18]$$

During a creep test, a shear stress (σ_{s0}) is applied within a brief period of time and is maintained constant for a given amount of time while the shear strain (γ) is monitored. Similar to the stress relaxation test, the shear strain and the shear stress in the creep test are related by the shear creep compliance ($J(t)$) using the following equation (Ferry, 1970):

$$\gamma(t) = \sigma_{s0} J(t) \qquad [2.19]$$

Apparent viscosity (η) of a viscoelastic solid is commonly measured using a rotational viscometer. The sample is placed between two symmetrical rotating bodies (plates, cylinders or cones); the force that deforms the sample material is defined by the applied torque. The material exerts a resistance to the applied torque which is related to its viscosity; from the resistance force the shear stress can be obtained, while the shear rate is calculated from the rotational frequency and the geometry of the measuring device.

The viscosity of the material is then calculated as the ratio of the shear stress (σ_s) to the shear rate ($\dot{\gamma}$) (Brummer, 2006).

$$\eta = \frac{\sigma_s}{\dot{\gamma}} \qquad [2.20]$$

2.6.2 Triaxial Tests

Other methods used to characterize the stress-strain-strength behaviour of materials are triaxial tests, also known as bulk or volumetric tests. Triaxial tests consist of subjecting a sample of material to a pressure on all of its axes. By doing this the shape of the specimen is conserved and the volume increases or decreases depending on the direction of the pressure. The pressure is generally achieved by submerging the sample material into a surrounding fluid and it is controlled by an electrohydraulic loading piston and a pressure cell (Richter-Menge et al, 1986; Linton et al, 1988).

The relative change in volume of the specimen under triaxial tests is called the voluminal strain ($\Delta V/V$). Assuming that the hydrostatic pressure, P_H, surrounding the specimen is the same on all of the axes and that the initial voluminal strain, $(\Delta V/V)_0$, is accomplished in a very small time interval, a bulk relaxation test can be performed. During bulk relaxation tests the hydrostatic pressure is related to the initial voluminal strain by the following equation (Ferry, 1970):

$$P_H(t) = -\left(\frac{\Delta V}{V}\right)_0 K(t) \qquad [2.21]$$

where *K(t)* is called the bulk relaxation modulus, which is analogous to the shear relaxation modulus, *G(t),* from shear-based tests.

Also as with shear measurements, if a pressure P_0 is applied suddenly and held constant on all of the axes of the specimen, while the volume change as a function of time is followed, a bulk creep experiment can be performed. During bulk creep tests the relative volume change is related to the applied pressure by the creep bulk compliance function, *B(t),* as shown by the following equation (Ferry, 1970):

$$\frac{\Delta V}{V}(t) = -P_0 B(t) \qquad [2.22]$$

2.6.3 Uniaxial Compression-based Tests

Uniaxial compression tests can provide valuable information that relates the mechanical characteristics of food materials with data obtained from sensory analysis (Di Monaco et al, 2008); compression methods are used routinely in the shortening industry to measure quality parameters such as hardness and plasticity (Metzroth, 2005).

Uniaxial compression tests can be carried out using the versatile instrument commonly known as a Universal Testing Machine; this machine provides precise control of deformation while accurately measuring force. A universal testing machine has this name because it can also be used to perform tension, bending and shear tests by using different attachments (Gunasekaran and Ak, 2003).

During compression tests a sample is prepared typically in the shape of a cylinder or a prism and it is placed between two parallel rigid flat platens on the universal testing machine. Using this set-up produces a uniform stress at the top and bottom of the specimen, if frictionless conditions can be achieved and the specimen contact surfaces are completely parallel to the compression platens (Charalambides et al, 2001).

Compression-based tests include monotonic compression, cyclic compression, creep tests, and stress relaxation tests. During monotonic compression tests the top platen moves down on the top sample surface at a constant rate of travel until a certain distance is reached (Wright et al, 2001). Cyclic compression is similar to monotonic compression with the added difference that the same specimen is subject to loading and unloading several times. The deformation and the force as a function of time are recorded during these two tests. Creep tests are performed by applying a constant compressive load to the top platen and the deformation over time is recorded. And, during stress relaxation tests the top platen is moved to a fixed distance and the force is recorded as a function of time.

2.6.3.1 Uniaxial monotonic compression

Uniaxial monotonic compression tests have been widely used to study the mechanical properties of materials and are one of the most popular tests for determining rheological properties of foods; the main reason for their popularity is cost, since compression specimens are cheaper to prepare than tensile specimens and there is no need for sample gripping and therefore they are very easy to perform (Gunasekaran and Ak, 2003). Also for soft and brittle materials, it is very hard to prepare and grip tensile specimens; for this

reason compression tests are a better option for soft materials such as food products (Riviere and Castaing, 1997). However, compression tests are affected by the friction between fixtures and material samples (Charalambides et al, 1995). The presence of friction leads to inhomogeneous deformation; if the material adjacent to the compression platens is restrained from radial movement then the material appears to be stiffer than it truly is (Charalambides et al, 2006). The use of lubricants, such as low viscosity oils, can help reduce frictional effects. An alternative to deal with friction is to bond the samples to the compression platens using adhesives such as cyanoacrylate (Casiraghi et al, 1985), but for soft food materials such as shortening it would be very difficult to bond the specimens without damaging them.

2.6.3.2 Uniaxial cyclic compression tests

Cyclic compression consists in loading and unloading a single specimen more than one time. This type of compression test can be used to study the fatigue of materials, especially metals for which this type of loading is very common during their applications (Hakamada et al, 2007). For soft materials like food, cyclic loading tests can be used to study the onset of plastic behaviour and the amount of elasticity remaining after compression has occurred (Goh and Scanlon, 2007).

Fatigue is defined as the progressive damage to the structure of materials when subjected to cyclic loading. When measuring the fatigue of materials it is common to plot the cyclic loading results as a diagram of the strain (ε) versus number of loading cycles (N). An important feature of ε-N diagrams (Figure 2.12) is the point where the strain starts to

increase at a faster rate, a phenomenon called “strain jumping”. Strain jumping marks the point where fatigue of materials starts to occur (Hakamada et al, 2007).

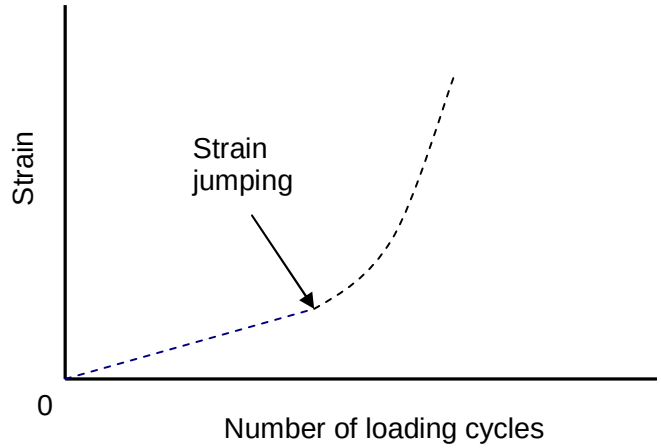

Figure 2. 12. Strain versus number of loading cycles for theoretical material showing strain jumping (adapted from Hakamada et al, 2007)

The amount of elasticity exhibited by a material after it has been subject to a specific amount of compression can be estimated by calculating the unloading modulus (E_U) (Goh and Scanlon, 2007). The unloading modulus is the slope of the tangent to the unloading stress-strain curve right after the load is removed (Figure 2.13). If the deformation is completely within the elastic region of a material the unloading modulus (E_U) and the Young’s modulus (E) will have the same values. On the other hand if the strain is large, causing the material to suffer permanent deformation during compression, the unloading modulus will be different from the modulus of elasticity, since the overall structure of the solid is modified by the onset of plasticity (de With, 2006).

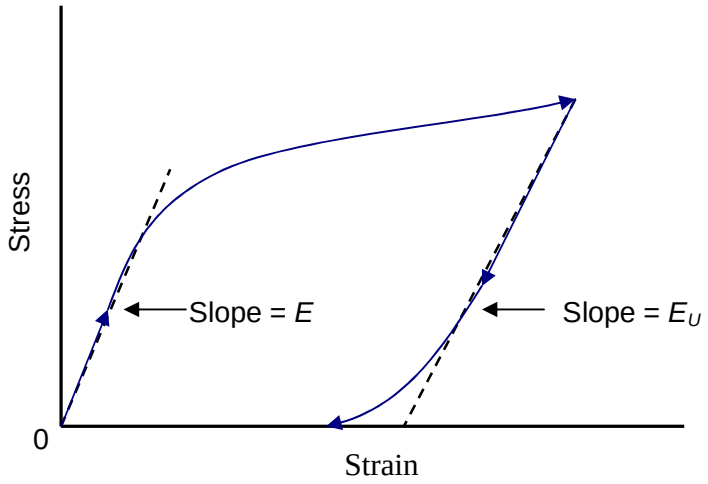

Figure 2. 13. Schematic loading-unloading curve showing the modulus of elasticity (E) and the unloading modulus (E_U) (adapted from Goh and Scanlon, 2007)

2.6.3.3 Compressive Stress Relaxation Tests

Stress relaxation is one of the most important tests to determine the viscoelastic properties of materials (Cenkowski et al, 1992). The ability of a material to alleviate stress under conditions of constant strain as a function of time is called stress relaxation (Hassan et al, 2005). Depending on the material being tested, different behaviours can be observed during stress relaxation; an ideal elastic material (Figure 2.14 curve (a)) will reach a finite and constant stress with no stress relaxation over time (Del Nobile et al, 2007). A perfect elastic solid material will store all the energy input during straining and use this energy to return the specimen to its original shape and size after the strain is removed (Gunasekaran and Ak, 2003). In contrast, an ideal viscous liquid material (Figure 2.14 curve (b)) will instantaneously show stress decay to zero, since viscous liquids do not store energy or have a memory of their initial state (Del Nobile et al, 2007; Gunasekaran and Ak, 2003). Viscoelastic solid materials (Figure 2.14 curve (c))

subjected to stress relaxation tests will gradually relax and reach an equilibrium stress (σ_e) greater than zero, a behaviour that can be observed in permanent gels with covalent crosslinks (Steffe, 1996). In contrast, viscoelastic liquids (Figure 2.14 curve (d)) will show a residual stress vanishing to zero, and this can be observed in gels with non-permanent crosslinks. This total dissipation of strain energy is generally very hard to observe since the relaxation to zero occurs within times far beyond experimental time scales (Steffe, 1996).

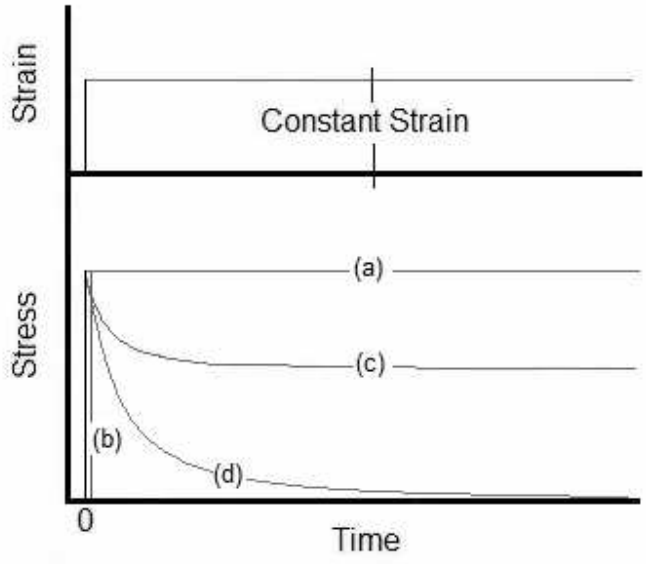

Figure 2. 14. Stress relaxation curve for (a) elastic solid, (b) viscous liquid, (c) viscoelastic solid, and (d) viscoelastic liquid (adapted from Gunasekaran and Ak, 2003)

The stress relaxation experiment can be viewed as consisting of two parts: the straining stage when the material is being squeezed up to a set displacement or strain, and the relaxation stage. Ideally the straining stage should be instantaneous but in reality it takes time, and since stress relaxation of materials is affected by the history of deformation, the time it takes for the material to be deformed to the specified strain will affect the stress relaxation results (Gunasekaran and Ak, 2003).

During compressive stress relaxation tests, the stress (σ) and the strain (ε_0) are related in the following manner:

$$\sigma(t) = E_R(t)\varepsilon_0 \qquad [2.23]$$

where $E_R(t)$ is the compressive relaxation modulus. It is important to note that if the material is an elastic solid $E_R(t)$ is a constant and is called the Young's modulus (E) or modulus of elasticity (Ferry, 1970).

If the material can be considered an incompressible solid, which is the case for many food materials and polymeric systems, the compressive relaxation modulus ($E_R(t)$) can be converted into a shear relaxation modulus ($G_R(t)$) using the following equation (Ferry, 1970):

$$G_R(t) = \frac{E_R(t)}{3} \qquad [2.24]$$

Stress relaxation behaviour for viscoelastic solids is generally described using equations that were derived from the generalized or discrete Maxwell model, using a combination of basic Maxwell elements that are shown in Figure 2.9a. The mathematical representation of the generalized Maxwell model is (Peleg and Pollak, 1982; Nussinovitch et al, 1989; Hassan et al, 2005):

$$\sigma(t) = \sigma_e + \sum_{i=1}^{n} E_i e^{-(t/\tau_i')} \qquad [2.25]$$

where σ is the stress as a function of time; σ_e is the equilibrium stress; n is the number of Maxwell elements; E_i is the stress relaxation constant for each Maxwell element; t is time;

and τ_i' is the relaxation time for each Maxwell element. The stress relaxation constant E_i represents the contribution of each of the Maxwell elements to the overall stiffness of the material and the relaxation time τ_i' is related to the viscous contribution of each Maxwell element to the overall viscous behaviour of the material. The relaxation time, τ_i', is related to the viscous contribution of each Maxwell element, η_i, through the relaxation constant, E_i, in the following manner (Ferry, 1970):

$$\tau_i' = \frac{\eta_i}{E_i} \qquad [2.26]$$

The generalized Maxwell model for viscoelastic behaviour of solids can be visualized as a spring connected in series to a dashpot and these two elements connected in parallel to other Maxwell elements (Figure 2.15).

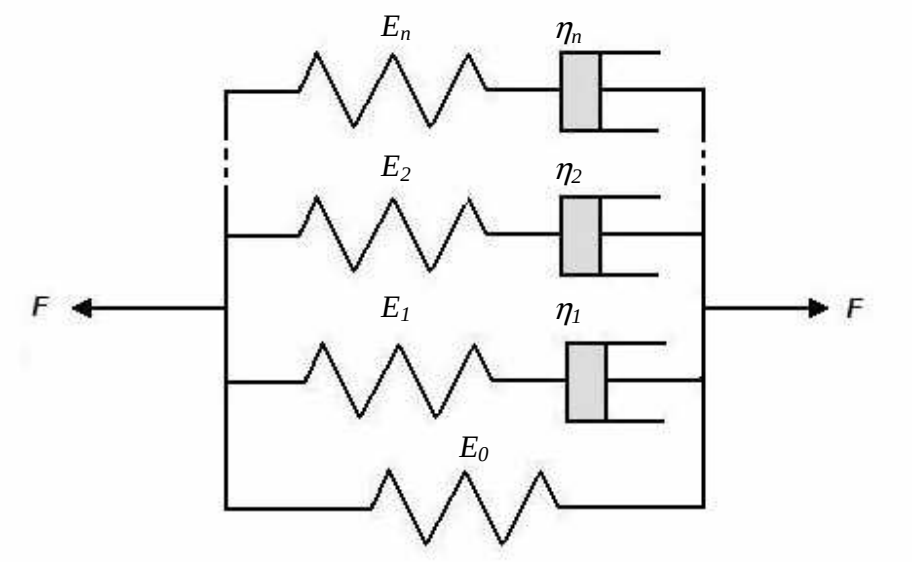

Figure 2. 15. Generalized Maxwell model for viscoelastic behaviour of solids (adapted from Ferry, 1970; Gunasekaran and Ak, 2003)

2.6.3.4 Compressive Creep Tests

In general the mechanical properties and performance of materials change with time and environmental conditions; even hard metals show time-dependent deformations especially when heated to temperatures beyond about half way to their melting temperature (Illston and Domone, 2001). For softer materials like food, time-dependent behaviours like creep can be observed at ambient temperatures. In a compressive creep experiment an undeformed sample is suddenly compressed to a constant stress while the strain is monitored within a given time frame (Rao, 2007).

Materials can be classified according to their creep behaviour; for example, an ideal elastic solid material (Figure 2.16 curve (a)) will have a constant strain as time passes due to its inability to flow and a complete recovery of the strain will occur after the load is removed. On the other hand an ideal viscous liquid material (Figure 2.16 curve (b)) will show a linear change of the strain as time passes due to its steady flow and will exhibit zero recovery after unloading (Steffe, 1996). Most food material will show simultaneous viscous and elastic behaviour, and for this reason they are called viscoelastic materials. Therefore the creep test can provide valuable information on the viscoelastic behaviour of food materials. In a viscoelastic liquid material (Figure 2.16 curve (c)) strain will increase with time until it approaches a steady state where the strain-rate is constant, in other words, there is a linearly increasing deformation with time. A viscoelastic solid material (Figure 2.16 curve (d)) will eventually reach an equilibrium strain, this equilibrium strain remains constant in time; therefore the strain rate is equal to zero (Ferry, 1970). Viscoelastic solids and liquids will show a certain amount of recovery

after the load is removed due to their ability to store energy (Gunasekaran and Ak, 2003; Rao, 2007).

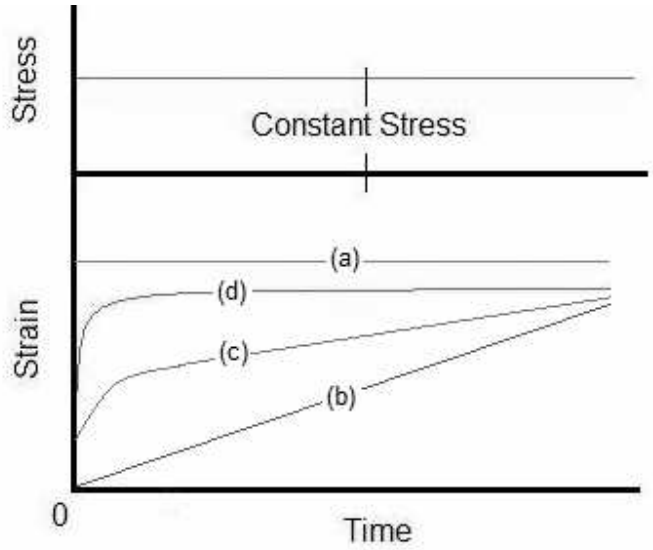

Figure 2. 16. Creep curve for (a) elastic solid, (b) viscous liquid, (c) viscoelastic liquid, and (d) viscoelastic solid (adapted from Gunasekaran and Ak, 2003)

Performing creep tests on soft solids like lipid-based particle gels using a universal testing machine is a very simple and convenient procedure. The response during compressive creep tests can be related to shear and bulk creep tests and this is important since most of the theory of creep was developed after shear or bulk studies on polymers and other non-food materials. During a compression-based creep test a sudden compressive constant stress (σ_0) produces time-dependent strains which are related in the following manner (Ferry, 1970):

$$\varepsilon(t) = \sigma_0 D(t) \qquad [2.27]$$

where *D(t)* is the compressive creep compliance which is defined as the compressive strain divided by the initial compressive stress (Rao, 2007). During uniaxial compression of materials a simultaneous change in volume and shape occurs and for this reason *D(t)* is

related to the bulk creep compliance (*B*), which is related to the change in volume, and also to the shear creep compliance (*J*), which is related to the change in shape. Since during uniaxaial compression there is no lateral stress, the following equation summarizes the relationship between the bulk and shear results and the uniaxial compression results (Ferry, 1970):

$$D(t) = \frac{J(t)}{3} + \frac{B(t)}{9} \qquad [2.28]$$

For viscoelastic materials such as food materials and polymers in a certain broad range of time scale, the volumetric creep compliance *B(t)* is very small compared to the shear creep compliance *J(t)*; therefore equation [2.28] can be simplified in the following manner:

$$D(t) = \frac{J(t)}{3} \qquad [2.29]$$

Therefore it can be said that shear and compression creep tests give results that are interconvertible by virtue of equation [2.29]. It is important to remember that equation [2.29] is only valid for materials in which the change in volume during compression is negligible compared to the change in shape, in other words it is applicable to an incompressible material (Ferry, 1970).

Material parameters such as compressive creep compliance (*D(t)*), retardation time (τ) and biaxial viscosity (η_b) can be derived from creep tests and are useful in describing the viscoelastic behaviour of many materials and will be defined later in this section. The compressive creep compliance (*D(t)*) is defined as the ratio of the strain (that is changing with time) relative to the constant applied stress. The retardation time (τ) is the time

required to deform a material by approximately 63% ($1\text{-}e^{-1}$) of its total deformation during a creep test (Menard, 1999).

In certain occasions, the results of a creep test can be presented as a compliance-time curve (Figure 2.17). Several parameters can be obtained from the compliance-time diagram such as the instantaneous compliance D_0, which represents the region where the bonds between the different structural units are stretched elastically and is the inverse of the modulus of elasticity ($D_0 = E^{-1}$). Another parameter that can be obtained from the compliance-time curve is the biaxial compliance (D_b). In the long-time region the bonds between the structural components break and flow past one another. The biaxial compliance is related to biaxial viscosity (η_b) and time (t) through the following equation (Rao, 2007):

$$D_b = \frac{t}{\eta_b} \qquad [2.30]$$

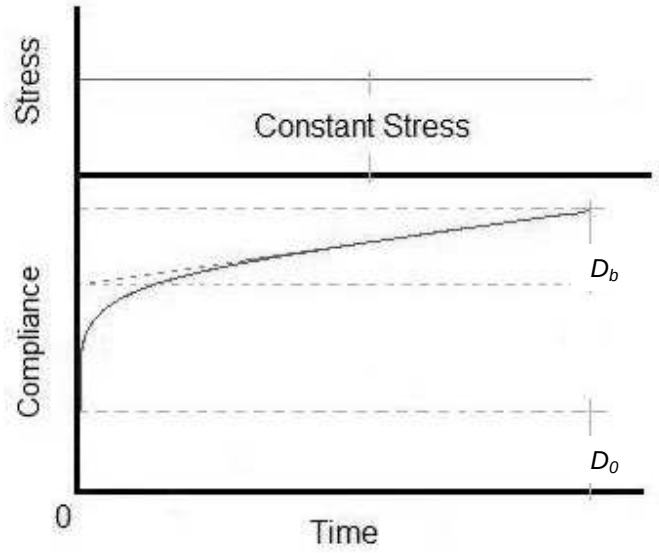

Figure 2. 17. Schematic compliance-time curve for a viscoelastic material (adapted from Rao, 2007)

From Figure 2.16 curve (d), one can see that if a creep test is done on a viscoelastic solid, the change in biaxial compliance will vanish to zero since the material would reach an equilibrium stress; therefore the biaxial viscosity will approach a value of zero. On the other hand, if the material is a viscoelastic liquid the change in biaxial compliance will have a value different than zero (Figure 2.17) since the strain would keep increasing with time (Figure 2.16 curve (c)) and the biaxial viscosity would also have a value different than zero.

The creep behaviour of materials can be visualized as a dashpot connected in parallel to a spring as shown in Figure 2.9b, this is called the Kelvin-Voigt model. However, most of the creep results cannot be accurately predicted using a single Kelvin-Voigt element, and for this reason several Kelvin-Voigt elements are connected in series to one another and to an individual spring and a dashpot to obtain a better approximation to the experimental creep test data of many viscoelastic materials; this model is called the generalized Kelvin-Voigt model and it is shown in Figure 2.18. Compliances (D_i) are assigned to each of the springs to describe their stiffnesses and viscosities (η_i) are assigned to each of the dashpots.

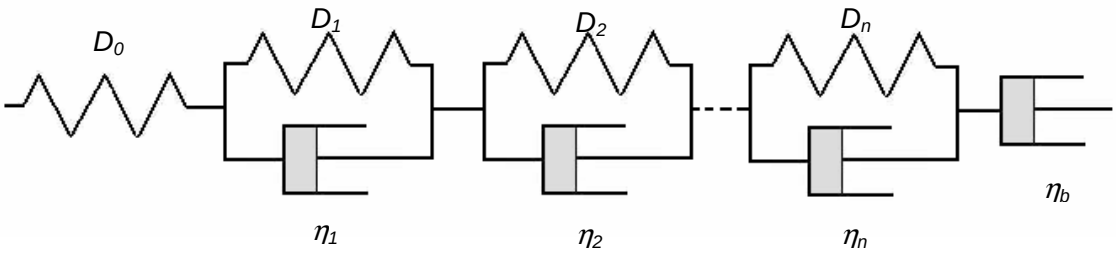

Figure 2. 18. Generalized Kelvin-Voigt model for creep behaviour (adapted from Gunasekaran and Ak, 2003)

The Kevin-Voigt model is summarized with the following mathematical expression:

$$D(t) = D_0 + \frac{t}{\eta_b} + \sum_{i=1}^{n} D_i \left(1 - e^{(-t/\tau_i)}\right) \qquad [2.31]$$

where D_0 is the instantaneous compliance, t the time, η_b the biaxial viscosity of the generalized Kevin-Voigt model and τ_i the retardation time of each Kelvin-Voigt element (Gunasekaran and Ak, 2003). The Generalized Kelvin-Voigt model can be used to simulate the creep response of both viscoelastic solids and liquids by assigning the appropriate values to the different parameters in equation [2.31]. For a viscoelastic solid the biaxial viscosity would have a value of zero, so Figure 2.18 would not have the last dashpot connected in series to the rest of the Kelvin-Voigt elements (Betten, 2005).

2.6.4 Indentation tests

Indentation tests are a convenient method of measuring the mechanical properties of solids; they are generally inexpensive (Huang et al, 2002; Ma et al, 2003) and no standard specimen preparation is required as with compression and tension measurements. Indentation is an ideal method for the evaluation of texture in localized areas of a given specimen and is less dependent on the geometry of the specimen (Anand, 2001). Indentation has proven to be a useful technique for assessing the mechanical properties of fragile materials such as food colloids and particle gels (Goh and Scanlon, 2007). Although indentation tests are easy to perform, interpretation of their results is not straightforward due to the complex strain field produced by the indentation process (Huang et al, 2002). For this reason many of the results are interpreted empirically (Goh et al, 2004). Depending on the material to be tested, indenters can be made of diamond,

hard carbon steel, tungsten carbide and even hard polymers. The geometry of indenters is also diverse, the most common ones include conical (Vandamme and Ulm, 2006), cylindrical (Liu and Scanlon, 2003), prismatic (Bae et al, 2006), pyramidal (Mencik, 2007), and spherical (Beghini et al, 2006).

During indentation tests the force required to push an indenter (in the food industry known as probe, punch or die) into a material is measured (Anand, 2001); therefore the most important quantities given by an indentation test are the indentation load, P_i, and penetration depth, h_i. The results of an indentation test are generally presented as a P_i-h_i curve and different sections of the curve are analyzed to obtain various mechanical properties (Anand, 2001). It is customary to condense the indentation results into two parameters: Hardness (κ) and the indentation modulus (M) (Vandamme and Ulm, 2006).

Hardness (κ) is defined as the maximum indentation force (P_{max}) divided by the projected contact area (A_c) (Vandamme and Ulm, 2006):

$$\kappa = \frac{P_{\max}}{A_c} \qquad [2.32]$$

while the indentation modulus (M) is the parameter that relates the slope of the initial part of the unloading curve (S) with the projected contact area (A_c). For a conical indenter M can be obtained with the following equation (Vandamme and Ulm, 2006):

$$M = \frac{\sqrt{\pi} S}{2\sqrt{A_C}} \qquad [2.33]$$

Many equations have been proposed to relate the indentation force and the indentation depth, but they are dependent on the geometry of the indenter and the type of material being tested. For example, in indentation tests done using sharp indenters, such as cones, the relationship between load (F) and penetration depth (h_i) is usually expressed as a parabolic relation known as Kick`s law:

$$F = \alpha h_i^{\,2} \qquad [2.34]$$

where α is a constant depending on the geometry of the indenter and the indented material properties (Ma et al, 2003). For rate-independent materials research has shown that the indentation response follows equation [2.34] (Ma et al, 2003). However, for rate dependent materials, such as viscoelastic materials, the force–deformation response can be better described with a model that includes the static response indentation and material constants that relate to the geometry of the specimen and rate dependent behaviours.

The static indentation response is assumed to be the non-rate dependent response of a material. In order to study the static response of a material, the deforming load is applied at very slow rates as done by Kajberg and Wikman (2007). Once the static response of a material is obtained, it can be modified to take into account the rate dependency of such material using a power law. An example of a power law is the overstress power law ($\sigma = k\dot{\varepsilon}^{w}$) in which the stress ($\sigma$) is related to the strain rate ($\dot{\varepsilon}$) by a multiplier constant (k) and an exponent constant (w). The two constants can be described as material constants (Ma et al, 2003; Beghini et al, 2006; Goh and Scanlon, 2007).

A model that appropriately describes the indentation response of a rate dependent material was given by Goh and Scanlon (2007) and it has the following equation form:

$$F = F_0(1 + C(w)(\xi)^w) \qquad [2.35]$$

where F_0 is the static indentation response, ξ is a dimensionless number which represents the ratio of the indentation strain rate ($\dot{h}_i$) over the fluidity of the material ($\dot{\varepsilon}_0$) and the height of the specimen (*H*), *w* is the overstress power law constant for a given material and *C(w)* is an empirical function (Goh and Scanlon, 2007). The fluidity ($\dot{\varepsilon}_0$) is a material property that relates the viscous behaviour to the plastic behaviour of solid materials, a concept that was introduced by Perzyna in 1963 (Adams et al, 1996; Tong and Tuan, 2007; Ubachs et al, 2007).

The force-depth curve produced during indentation tests is related to the stress-strain curve of the material being tested, just like in simple compression tests. However, this relation is not as simple as with compression tests due to the complexity of the deformation process in the indentation region. The indentation region of the material is subjected to multiaxial stresses with high gradients and large strains (Beghini et al, 2006). As an example, the stress distribution under a flat surface cylindrical indenter penetrating an elastic material has been approximated by the Boussinesq equation:

$$\sigma(r) = \frac{P_i}{2\pi b\sqrt{b^2 - r^2}} \qquad [2.36]$$

where $\sigma(r)$ is the stress at a distance *r* from the center of the indenter, *b* is the radius of the indenter and P_i is indentation load. Equation [2.36] predicts that the stress at the center of the indenter (*r=0*) has a finite value, while at the edge of the indenter (*r=b*) the stress is infinite (Anand, 2001).

2.7.0 Finite Element Method

The Finite Element Method (FEM) is used to find approximate solutions to complex problems by visualizing the solution region as being composed of many small, interconnected subregions called finite or discrete elements (Rao, 1982). FEM was developed as means of doing structural analysis in geometries that were different than rectangles and solving complex elasticity problems in civil and aeronautical engineering. In January 1954 Ray W. Clough presented the idea that a two-dimensional structure could be represented with discrete elements connected at more than two joints or nodes and that this representation could be used to solve problems in aeronautical engineering (Figure 2.19). Later Argyris (1954) and Turner et al (1956) published on the use of small discrete elements to describe the overall behaviour of simple elastic bars that could be used in components for the aeronautical industry (Pepper and Heinrich, 1992).

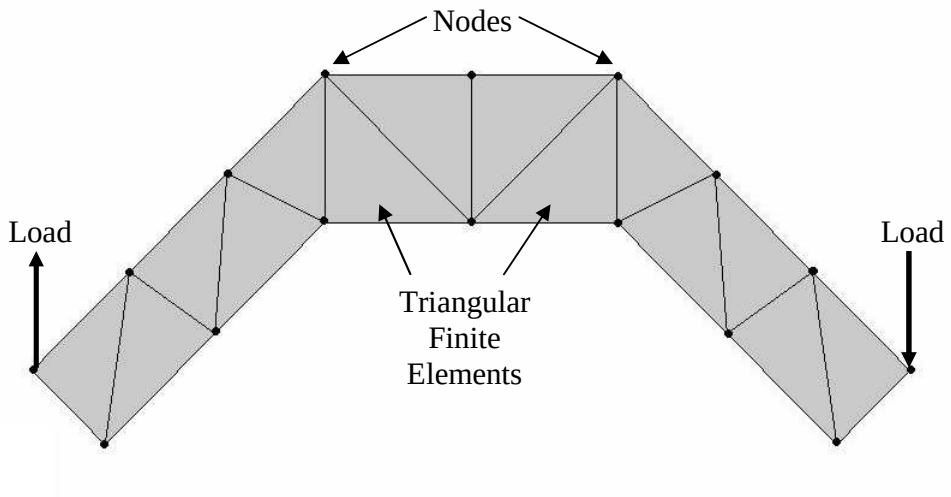

Figure 2. 19. Simplified airplane wing divided into triangular elements (adapted from Clough and Wilson, 1999)

In 1960 Clough coined the term Finite Element Method for any analysis done on models of both continuous structures and frame structures modeled as a system of elements

interconnected at nodes (Clough and Wilson, 1999). Nowadays, the finite element method has been generalized into a branch of applied mathematics for numerical modeling of physical systems and can be used to solve complex problems of solid mechanics, fluid dynamics, electromagnetism, and heat and mass transfer (Liu and Scanlon, 2003; Roduit et al, 2005; Bermudez et al, 2007; Farhloul and Zine, 2008).

The Finite Element Method has become an essential step in the design or modeling of physical phenomena occurring in a continuum of matter (solids or fluids) involving several field variables. Field variables are physical attributes that can change during the course of an experiment and according to position within a continuum of matter; some examples include stress, strain, pressure, temperature and chemical potential (Trigg et al, 1999). A continuum of matter is a continuous distribution of matter in space that can be subdivided into small elements with properties equal to the ones of the entire body (Fung, 1969); if a continuum has known boundaries then it is called a domain. A domain can be an entire physical object or a portion of it depending on the boundaries that are known. Within a domain there are an infinite number of solutions to the field variables since they change from point to point within the domain and the number of points within a domain can be infinite. The Finite Element Method relies on the decomposition of the domain into a finite number of elements for which an approximating function can be used to solve for a finite number of unknown field variables. The approximating functions are defined in terms of the values at specific points along the boundaries of elements, which are called nodes. Nodes also connect adjacent elements as seen in Figure 2.19 (Madenci and Guven, 2006).

2.7.1 Steps in FEM

The Finite Element Method can be divided into six major steps (Madenci and Guven, 2006):

1. Discretization of the domain into a finite number of elements
2. Selection of interpolation functions
3. Development of the element matrices or element equations for individual elements
4. Assembly of the element matrices for each element to obtain the global equilibrium matrix of the entire domain, also known as overall equilibrium equations
5. Determination of the boundary conditions of the domain
6. Solution of the equations in the global matrix and global vectors. Note that the global matrix and the global vectors form a system of equations that describe the desired physical phenomena within the domain.

A simple mechanical problem consists of calculating the stress in a stepped bar that is axially loaded (Figure 2.20). This will be used to illustrate the steps of the finite element method. The bar is made of a material with a modulus of elasticity E, has cross-sectional areas of A_1 and A_2 over the lengths L_1 and L_2 and is subjected to a load P. A_1= 2m^2, A_2=1m^2, L_1= L_2=10m, E=2×10^6 Pa, and P= 1N (Rao, 1982).

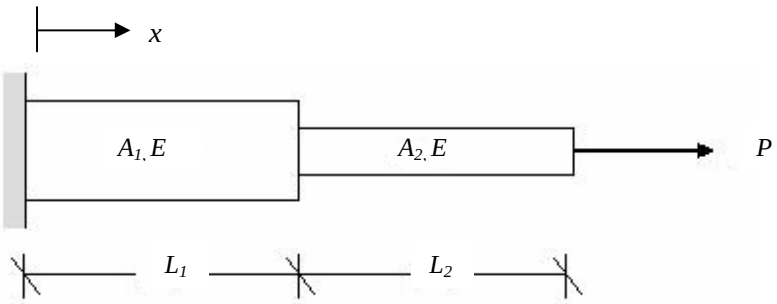

Figure 2. 20. Stepped bar axially loaded (adapted from Rao, 1982)

2.7.1.1 Discretization

The first step in the finite element method is the discretization of the domain, or the division of the solution region, into elements. During this step the domain that has an infinite number of degrees of freedom is replaced by a system that has a finite number of degrees of freedom. The shape, size, number and configuration of the basic elements that form the domain are selected during the discretization step; care must be taken while choosing these characteristics so that the original body is simulated as closely as possible without increasing calculation efforts needed to obtain the solution (Rao, 1982).

In the example shown in Figure 2.20 the domain is the bar and is going to be divided into two elements (element 1 and 2) with two nodes each (node 1, 2, and 3 because element 1 and 2 are connected at node 2; both elements use node 2 in their discretization). Since the load is axial the change of nodal position or displacement (*d*) will also be in the axial direction; therefore each element has only one degree of freedom which is displacement in the *x*-direction. Figure 2.21 shows the discretization for the stepped bar problem.

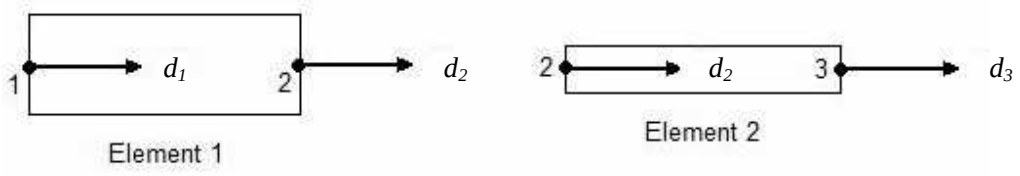

Figure 2. 21. Discretization of stepped bar into two one dimensional elements; dots 1, 2 and 3 are nodes while d_1, d_2 and d_3 are the potential-displacements of these nodes (adapted from Rao, 1982)

2.7.1.2 Selection of Interpolation Functions

Once the domain has been discretized, simple functions for the solution of each element must be selected. The functions used to simulate the behaviour of the solution within each element are called interpolation functions; such functions are formulated to act at the nodes of each element. The most common type of interpolation functions used in the finite element method are polynomials, because it is easier to perform differentiation and integration with polynomials and the accuracy of the results can be increased by increasing the order of the polynomial function. Several conditions must be met by the interpolating functions: these functions are expressed in terms of the nodal degrees of freedom (in mechanics the number of displacements and rotations that a node can have). The nodal degrees of freedom should not change with a change in the local coordinate system, should converge to the exact solution if the size of the element is reduced successively, and the number of unknown coefficients in the polynomial equation should be equal to the number of nodal degrees of freedom (Rao, 1982).

Since the interpolation functions do not change from element to element within a given domain, each of the elements shown in Figure 2.21 can be generalized as shown in Figure

2.22 and will be called element '*e*', the interpolation functions are assigned to each of the nodes.

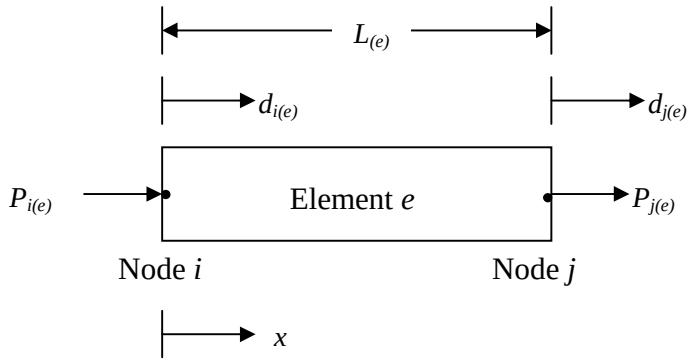

Figure 2. 22. Nodal positions (*d*) and loads (*P*) for generalized element '*e*' (Rao, 1982). Notice that nodes are labelled *i* and *j* but only in the element local coordinate system, since both elements of the entire domain have two nodes. So for element 1, *i* is equal to 1 and *j* is equal to 2, but for element 2, *i* is 2 and *j* is 3

In each of the elements of the stepped bar problem the position of each node (d_i and d_j) can be thought to vary in a linear fashion as the axial load is applied, such that a polynomial of first degree can be used to describe this behaviour:

$$d(x) = a + cx \qquad [2.37]$$

where *a* and *c* are constants. The nodal position at the left hand side of each element ($x=0$ in the element local coordinate system) is $d_{i(e)}$ and the nodal position at the far end of each element ($x=L_{(e)}$ in the element local coordinate system) is $d_{j(e)}$; therefore $a=d_{i(e)}$ and $c=(d_{j(e)}-d_{i(e)})/L$. The interpolation function [2.37] can be expressed in terms of the nodal positions at each element as follows:

$$d(x) = d_{i(e)} + \frac{d_{j(e)} - d_{i(e)}}{L_{(e)}} x \qquad [2.38]$$

Notice that equation [2.38] has only one unknown since each node has only one degree of freedom, which is the displacement in the horizontal direction (x), since the load is only applied in the x-direction.

2.7.1.3 Development of Matrix for Individual Elements

The third step in the finite element method involves the formulation of matrices and vectors characteristic of each element. Depending on the complexity of the problem the development of the matrix for each element can be accomplished by direct physical reasoning if the problem is very simple; by the variational approach if the problem can be stated in variational form involving calculations associated with maxima and minima (Mura and Koya, 1992); and, by a weighted residual approach which can be used to obtain approximate solutions to linear and nonlinear governing differential equations (Rao, 1982).

The sample problem presented in Figure 2.20 is simple and the element matrix can be derived directly from the principle of minimum potential energy. The potential energy of the stepped bar (I) is given by the difference between the strain energy in element ($u_{(e)}$) and the work done by external forces (W):

$$I = -W + \sum_{e=1}^{2} u_{(e)} \qquad [2.39]$$

The strain energy (u) of each element 'e' is related to the strain difference at each of the nodes and it can be calculated by the following equation:

$$u_{(e)} = \frac{1}{2} A_{(e)} E_{(e)} \int_0^{L_{(e)}} (\varepsilon_{(e)})^2 dx \qquad [2.40]$$

where $A_{(e)}$ is the cross-sectional area of each element, $L_{(e)}$ is the length of each element, $\varepsilon_{(e)}$ is the strain of each element and $E_{(e)}$ is the modulus of elasticity of each element. The strain of each element can be derived from the interpolating function [2.38] since

$$\varepsilon_{(e)} = \frac{\partial d}{\partial x} = \frac{d_{j(e)} - d_{i(e)}}{L_{(e)}} \qquad [2.41]$$

therefore $$u_{(e)} = \frac{A_{(e)} E_{(e)}}{2L_{(e)}} \left((d_{i(e)})^2 + (d_{j(e)})^2 - 2 d_{i(e)} d_{j(e)} \right) \qquad [2.42]$$

To apply this solution to the domain (i.e., all elements), it makes sense to express equation [2.42] in matrix notation. In order to follow the rules of matrix multiplication, it is necessary to transpose the displacement vector ($\vec{d}_{(e)}$) into a matrix ($(\vec{d}_{(e)})^T$). Equation [2.42] is then given as half the product of the element nodal position vector transpose times the element stiffness matrix times the element nodal position vector or:

$$u_{(e)} = \frac{1}{2} (\vec{d}_{(e)})^T [K_{(e)}] \vec{d}_{(e)} \qquad [2.43]$$

where $\vec{d}_{(e)} = \begin{Bmatrix} d_{i(e)} \\ d_{j(e)} \end{Bmatrix}$ is the vector of nodal position of each element, so for element 1, $\vec{d}_{(e)} = \begin{Bmatrix} d_1 \\ d_2 \end{Bmatrix}$ and for element 2, $\vec{d}_{(e)} = \begin{Bmatrix} d_2 \\ d_3 \end{Bmatrix}$, while $(\vec{d}_{(e)})^T = \begin{bmatrix} d_{i(e)} & d_{j(e)} \end{bmatrix}$ is the transpose of element nodal position (transposing means to exchange the rows of a matrix or vector for its columns, so that a 2×1 vector becomes a 1×2 matrix), and $[K_{(e)}] = \frac{A_{(e)} E_{(e)}}{L^{(e)}} \begin{bmatrix} 1 & -1 \\ -1 & 1 \end{bmatrix}$ which is called the stiffness matrix of each element.

The work done by external forces (*W*) on the whole stepped bar can be expressed as:

$$W = d_1 P_1 + d_2 P_2 + d_3 P_3 = \begin{bmatrix} d_1 & d_2 & d_3 \end{bmatrix} \begin{Bmatrix} P_1 \\ P_2 \\ P_3 \end{Bmatrix} \qquad [2.44]$$

If the system is in equilibrium then the summation of the forces must equal to zero; therefore P_1 is the reaction at the fixed node 1 in the global coordinate system, P_2 =0, since there is no external force applied at node 2, and P_3= P= 1N. Also due to equilibrium, the stepped bar shown in Figure 2.20 has a potential energy *I* equal to zero, since the work done by force *P* must be equal to the total strain energy of the system as per equation [2.39]. Therefore, the equilibrium equation ($I=u_{(e)}-W=0$) can be expressed in matrix notation as follows:

$$\sum_{e=1}^{2} \left([K_{(e)}] \vec{d}_{(e)} - \vec{P}_{(e)} \right) = \vec{0} \qquad [2.45]$$

Note that if one is adding and subtracting vectors, like in equation [2.45], the result has to be a vector, and even if the vector is full of zeroes it is appropriate to use the vector sign on top of a zero, in order to comply with matrix and vector notation.

2.7.1.4 Development of Global Matrix

After the characteristic matrices and vectors for each element have been defined in a common global coordinate system, the next step of the finite element method is the construction of the overall or system equations. This procedure is based on the requirement of compatibility at each of the element nodes, which means that the values of the variables are the same for all elements joined at that node (Rao, 1982).

In the stepped bar problem (Figure 2.20), the global stiffness matrix ([*K*]) is the summation of the stiffness matrices of two elements ($\sum_{e=1}^{2}[K_{(e)}]$). For the values assigned in this example ($A_1=2m^2$, $A_2=1m^2$, $L_1=L_2=10m$, $E= 2\times10^6 Pa$ *and* $P = 1N$) the element stiffness matrices are:

$$[K_{(1)}]=\frac{A_1E}{L_1}\begin{bmatrix}1 & -1\\ -1 & 1\end{bmatrix}=\begin{matrix}\text{1}\\ \text{2}\end{matrix}\overset{\begin{matrix}\text{1} & \text{2}\end{matrix}\quad\text{Global Nodes}}{\begin{bmatrix}4\times10^5 & -4\times10^5\\ -4\times10^5 & 4\times10^5\end{bmatrix}} \qquad [2.46]$$

$$[K_{(2)}]=\frac{A_2E}{L_2}\begin{bmatrix}1 & -1\\ -1 & 1\end{bmatrix}=\begin{matrix}\text{2}\\ \text{3}\end{matrix}\overset{\begin{matrix}\text{2} & \text{3}\end{matrix}\quad\text{Global Nodes}}{\begin{bmatrix}2\times10^5 & -2\times10^5\\ -2\times10^5 & 2\times10^5\end{bmatrix}} \qquad [2.47]$$

Each of the rows and columns in the element stiffness matrices are related to the displacement of each node (1, 2 and 3). These nodes can be used as coordinates for assembling the global stiffness matrix, and for this reason they are usually written around each row and column as shown in equations [2.46] and [2.47]. In the global stiffness matrix, the stiffness matrix of element 1 overlaps with the stiffness matrix of element 2 at node 2 of the global coordinate system, and so at node 2 the strain energy should have some contributions from both elements; therefore the global stiffness matrix becomes:

$$[K]=\begin{bmatrix} 4\times10^5 & -4\times10^5 & 0 \\ -4\times10^5 & 4\times10^5+2\times10^5 & -2\times10^5 \\ 0 & -2\times10^5 & 2\times10^5 \end{bmatrix}=2\times10^5\begin{bmatrix} 2 & -2 & 0 \\ -2 & 3 & -1 \\ 0 & -1 & 1 \end{bmatrix}\begin{matrix} 1 \\ 2 \\ 3 \end{matrix} \quad [2.48]$$

In the equilibrium equation [2.45], the stiffness matrix is multiplied by the summation of the displacement vectors of each element ($\sum_{e-1}^{2}\vec{d}_{(e)}$), which can be called the global displacement vector ($\vec{d}$), and finally subtracted by the summation of the applied load vector of each element ($\sum_{e=1}^{2}\vec{P}_{(e)}$), which can be called the global applied load vector ($\vec{P}$). Therefore the equilibrium equation [2.45] can be written in terms of the global matrix and the global vectors as $[K]\vec{d}=\vec{P}$, and substituting the given numerical values one obtains:

$$2\times10^5\begin{bmatrix} 2 & -2 & 0 \\ -2 & 3 & -1 \\ 0 & -1 & 1 \end{bmatrix}\begin{Bmatrix} d_1 \\ d_2 \\ d_3 \end{Bmatrix}=\begin{Bmatrix} P_1 \\ 0 \\ 1 \end{Bmatrix} \quad [2.49]$$

2.7.1.5 Determination of Boundary Conditions

Before solving the equations on the global matrix it is necessary to specify some restrictions so that the system does not have an infinite number of solutions. It is necessary to specify the value of at least one and sometimes more than one boundary condition, i.e., restrict the motion or degrees of freedom of certain nodes. The number of boundary conditions that need to be specified is dictated by the physics of the problem (Rao, 1982).

The overall equilibrium equations [2.49] cannot be solved since there are four unknowns and only three equations, so the equations would have an infinite number of solutions. However looking closely at Figure 2.20, one can see that the bar is fixed at global node 1; therefore the position of this node is fixed and d_1 =0. This is the only boundary condition needed to be specified in order to solve the overall equilibrium equations, since now there are three unknowns and three equations. The system of equations [2.49] then becomes:

$$2\times10^5\begin{bmatrix}0 & -2 & 0\\ 0 & 3 & -1\\ 0 & -1 & 1\end{bmatrix}\begin{Bmatrix}0\\ d_2\\ d_3\end{Bmatrix}=\begin{Bmatrix}P_1\\ 0\\ 1\end{Bmatrix} \qquad [2.50]$$

2.7.1.6 Solving Global Matrix

Once the global matrix has been constructed and the boundary conditions have been established, the equations in the global matrix can be solved. If the equations in the global matrix are linear they can be solved by the different variations of the Gaussian elimination method. If the problem is nonlinear then the global matrix will be formed of nonlinear equations and would have to be solved by some sort of iterative procedure, such as Newton-Raphson, continuation, minimization or perturbation methods (Rao, 1982). All of these numerical solving methods have been implemented in computer software packages, which greatly simplify the solution of complex problems.

The global equilibrium equations defined for the stepped bar problem (Figure 2.20) are linear so they can be solved by the Gaussian elimination method, which consists in eliminating unknowns by expressing them in terms of the remaining unknowns until only

one unknown appears in the system of equations. The system of equations [2.50] can be solved using the Gaussian elimination method in the following manner.

The first equation of the system is $2\times10^5(-2(d_2)) = P_1$; solving for d_2 one gets $d_2 = P_1/-4\times10^5$; substituting d_2 into the second equation of the system, one gets $2\times10^5(3(P_1/-4\times10^5) - d_3) = 0$; solving for d_3, the second equation becomes $d_3 = 3P_1/-4\times10^5$; substituting d_2 and d_3 into the last equation allow us to get $2\times10^5((P_1/4\times10^5) - 3(P_1/4\times10^5)) = 1$; therefore P_1=-1 N, $d_2=2.5\times10^{-6}$ m, and $d_3=7.5\times10^{-6}$ m. With these values the strains in each of the elements that form the stepped bar can be calculated using equation [2.41]:

$$\varepsilon_{(1)} = \frac{d_{j(1)} - d_{i(1)}}{L_{(1)}} = \frac{d_2 - d_1}{L_1} = \frac{2.5\times10^{-6} - 0}{10} = 0.25\times10^{-6}$$

$$\varepsilon_{(2)} = \frac{d_{j(2)} - d_{i(2)}}{L_{(2)}} = \frac{d_3 - d_2}{L_2} = \frac{7.5\times10^{-6} - 2.5\times10^{-6}}{10} = 0.50\times10^{-6}$$

And the stresses in each element are calculated with $\sigma_{(e)} = E\varepsilon_{(e)}$ to give the numerical results of $\sigma_{(1)} = 0.5Pa$ and $\sigma_{(2)} = 1.0Pa$.

2.7.2 Computer Implementation of Finite Element Method

Finite element methods are primarily used when hand calculations cannot provide sufficiently accurate and detailed results or when the problem to be solved is too complex for hand calculations to be appropriate (Baran, 1988). The utilization and popularity of the Finite Element Method has greatly increased with the improvement and increased

availability of general purpose digital computers (Cooke et al, 1976). Until approximately 1980 almost all the finite element analyses (FEA) were performed on mainframe computers which had a cost well over $1 million and required separate air-conditioned rooms and high level of maintenance and vendor support (Baran, 1988). Nowadays complex FEA can be performed using personal computers and the results can be expected in minutes, instead of hours or even days. As computers became more powerful and cheaper, finite element software has also become more powerful and more accessible.

FEA software first became commercially available in the early 1970's and it was primarily used in the nuclear and aerospace industries. Examples of commercially available finite element software that were available in the 1970's are ANSYS and MSC/NASTRAN (Baran, 1988). Table 2.2 shows a list of some of the finite element analysis software packages available today.

Nowadays FEA software is very much user friendly with the provision of graphic interfaces (that facilitate the setup of the problem) and drop down menus (where many choices can be selected to properly set up realistic situations eliminating the need to write lengthy codes which was the norm in the past). Today the finite element method has been integrated with other computer applications such as computer aided design to give rise to what is now called Computer Aided Engineering or CAE.

Table 2. 2. Examples of Finite Element Analysis software packages currently available

Software Name	Company	Website
Abaqus	Dessault Systemes S.A. Suresnes, France	www.simulia.com
ALGOR	ALGOR Incorporated Pittsburgh, PA, USA	www.algor.com
ANSYS	ANSYS Incorporated Canonsburg, PA, USA	www.ansys.com
CalculiX	Open source code started and maintained by Guido Dhondt and Klaus Wittig	www.calculix.de
COMSOL Multiphysics	COMSOL AB Stockholm, Sweden	www.comsol.com
Femap	Siemens PLM Software Plano, TX, USA	www.femap.com
LS-DYNA	Livermore Software Technology Corporation Livermore, CA, USA	www.lstc.com
MSC Nastran (Adams, Patran, Marc, Dytran, Easy5)	MSC Software Corporation Santa Ana, CA, USA	www.mscsoftware.com
Strand7	Strand7 Pty Limited Sidney, Australia	www.strand7.com

One of the most popular FEA software packages is Abaqus. Abaqus has been preferred by many academic and research institutions due to its wide material capability and its ability to be customized, but it is also used in the automotive, aerospace, and product manufacturing industries. One of the versions of Abaqus is called Abaqus/CAE and this provides a graphic interface that facilitates the visualization of the problem to be solved, as well as the results after the analysis has been completed. Abaqus/CAE prepares an input file from the parameters entered into the graphic interface, which is submitted into

analytical software packages which can be Abaqus-Standard or Abaqus-Explicit where the solutions are calculated (Abaqus, 2008).

2.7.3 Finite Element Method and Rheology of Food Materials

Food materials have a complex rheological response due to their complex composition and structure. Because of such complexity the finite element method is an appropriate tool in the study of the rheological properties of various food products. Early finite element analysis done on food materials arose from the need to try to predict the mechanical damage done to agricultural products during harvesting and processing (Puri and Anatheswaran, 1993), while current research has been focussed on obtaining models that accurately describe the rheological response of processed food such as butter, cheese, bread, dough, margarine and shortening.

Rumsey and Fridley (1977) used a viscoelastic finite element computer model developed by Herrmann and Peterson in 1968 at the Aerojet General Corporation to predict stresses resulting from contact loads on fruits and vegetables after harvesting. The fruits and vegetables were simulated as perfect spheres. It was concluded that the finite element model was in agreement with the analytical solutions formulated for viscoelastic materials as long as the deformation was small since the viscoelastic theory used during the experiment was developed for small strains only.

In 1991 two finite element elastic deformation models, axysimmetrical and three-dimensional, were implemented by Cardenas-Weber et al (1991) on the commercially

available FEA software ANSYS to analyze the compression of a melon by a robot gripper. The two models predicted lower stresses than the ultimate strength of the melon tissue for a v-shaped robot gripper and higher stresses for a flat gripper. It was concluded that the model could be used to predict the maximum force which could be applied to a melon before bruising by a gripping device, but a clear definition of bruising was needed to be established through research because it was not known what force magnitude produces damage to melons and other soft fruits that can be considered as bruising.

Frictional effects on the stress-strain data obtained during the uniaxial compression of gruyere and mozzarella cheeses and bread dough were studied by Charalambides et al (2001; 2006) using the commercial finite element software package Abaqus. Simulations of uniaxial compression tests on cylindrical cheese specimens of different heights were set up in Abaqus and, using an iterative method developed by Parteder and Bünten in 1998, Charalambides et al (2001) found a correction factor as a function of strain for the force measured during unlubricated compression tests. The analytical solution was based on equation [2.51] and its numerical approximation using a Maclaurin series expansion [2.52]:

$$\sigma_A = \frac{1}{\pi b^2}\int_0^b 2\pi\sigma_z r dr \qquad [2.51]$$

$$\sigma_A = \sigma_y\left(1+\frac{2\mu R}{3H}e^{\frac{3}{2}\varepsilon}\right) \qquad [2.52]$$

where σ_A is the average stress in the specimen, a is the radius of a cylindrical specimen, σ_z is the axial compressive stress, r is the radial distance, σ_y is the yield stress, μ is the

coefficient of friction, R is the radius of the cylindrical specimen before compression, H is the original height of the specimen and ε is the true strain. It was concluded that iterative finite element analysis can be used as a more accurate alternative to extrapolation of the analytical solution to very large specimen heights in order to convert the results of unlubricated compression into frictionless compression. The finite element method yielded values for the coefficient of friction (μ) of cheeses in agreement with values obtained from analytical method based on the assumption that the friction is a Coulomb friction that can be obtained from the slope of plots of the average stress (σ_A) versus the inverse of the initial height ($1/H$) of the specimen (see equation [2.52]).

Liu and Scanlon (2003) used finite element analysis to study the rheological properties of white bread crumb. Using the material model Abaqus HYPERFOAM, based on the Ogden (1972) strain energy function, Liu and Scanlon (2003) were able to correlate the modulus of elasticity and the critical stress of the experimental data to the predicted values obtained by finite element analysis. The Poisson's ratio for bread crumb was assumed to be 0 or 0.21 (highly compressive) during the simulations and it did not affect the prediction of the results at lower strains (<0.35). The Abaqus simulations were set up as axisymmetrical simplifications in which a two-dimensional drawing was used, where a similar shape and properties on both sides of the axis of symmetry were assumed. The use of an axisymmetric indentation finite element simulation allowed good prediction of the load-displacement curves produced by cylindrical indenters of various sizes, but under-predicted the measurements produced by spherical indenters. Liu and Scanlon (2003) concluded that finite element analysis is a robust tool useful in assisting

researchers to study the role of various factors contributing to the textural quality of food materials.

By using the Abaqus finite element software package and Microsoft Excel Solver function, Goh et al (2004b) were able to extract the parameters that define the viscoelastic response of materials after being subjected to a stress relaxation test with a finite initial loading rate. The analytical model used to describe the viscoelastic behaviour of materials subject to finite loading stress relaxation tests is a convolution integral that cannot be solved analytically. However, it is possible to solve the integral using an algorithm based on finite increments of time first suggested by Taylor et al in 1970. This algorithm can be implemented in the finite element method to extract the viscoelastic parameters of materials. Goh et al (2004b) indicated that the use of finite element analysis is a simple and quick method that facilitates the extraction of viscoelastic constitutive constants of materials to approximate experimental data under any arbitrary strain history.

In 2005, Goh et al studied the use of a model to predict the response of cheese wire cutting with the help of Abaqus finite element analysis software. The numerical model consisted of two parts: the first part dealt with indentation until crack formation caused by a cylindrical wire and the second part dealt with crack propagation as the indentation was continued to cut the specimen. Goh et al (2005) were able to accurately predict the indentation part of the wire cutting procedure of cheddar and gruyere cheese. This model showed reasonable success in predicting the cutting force, especially for cuts made with

small diameter wires. The numerical method was able to incorporate strain-rate dependent effects into the wire cutting simulation that closely matched experimental results. The numerical model was simpler, computationally cheaper to use, and more successful in predicting the cutting force than current analytical methods. However it was not successful in predicting the fracture toughness of cheese during wire cutting, a parameter which can be calculated analytically.

A two dimensional finite element model was developed by Ressing et al (2007) to simulate the puffing of a dough ball during vacuum microwave drying. The finite element model was written in Matlab and implemented in ANSYS. This model enabled the coupling of heat and mass transfer effects with solid mechanics effects. The combination of thermodynamic and mechanic effects provided an insight into the two puffing mechanisms of food products during vacuum microwave dehydration: the pressure difference between the inside of the dough and the drying chamber and the pressure created by formation of vapour due to the temperature rise of the dough.

Using Abaqus finite element analysis software, Goh and Scanlon (2007) were able to develop a viscoplastic model to simulate the compression and conical indentation response of three lipid-based particle gel systems (margarine, butter and shortening). In general the viscoplastic model predicted reasonably well the indentation response, but the load at a given displacement was underpredicted for shortening and butter while it was overpredicted for margarine. Using the viscoplastic model Goh and Scanlon (2007) were able to back predict the stress-strain properties from the conical indentation response, and

these stress-strain properties were consistent with results from other studies performed on these three particle gels. There were some discrepancies between the results predicted from the finite element model and the experimental data due to the lack of knowledge of the large strain compression and time-dependent behaviours of the lipid gels; Goh and Scanlon (2007) suggested that large strain, stress relaxation and creep tests should be performed to better understand the rheological response of lipid-based particle gels and to develop a more accurate model.

The use of finite element analysis software packages can be of great help in understanding the complex rheological response of food materials due to the ability of finite element analysis to add complex features to simple mechanical models without the need to solve complex mathematical equations. Understanding the rheological response in turn can be used to predict the quality of foods as the composition and structure is changed to provide better nutrition or functionality. Also the finite element method can be used to combine thermal, mass transfer and mechanical effects to realistically simulate processing of raw materials into food products.

CHAPTER 3: MATERIALS & METHODOLOGY

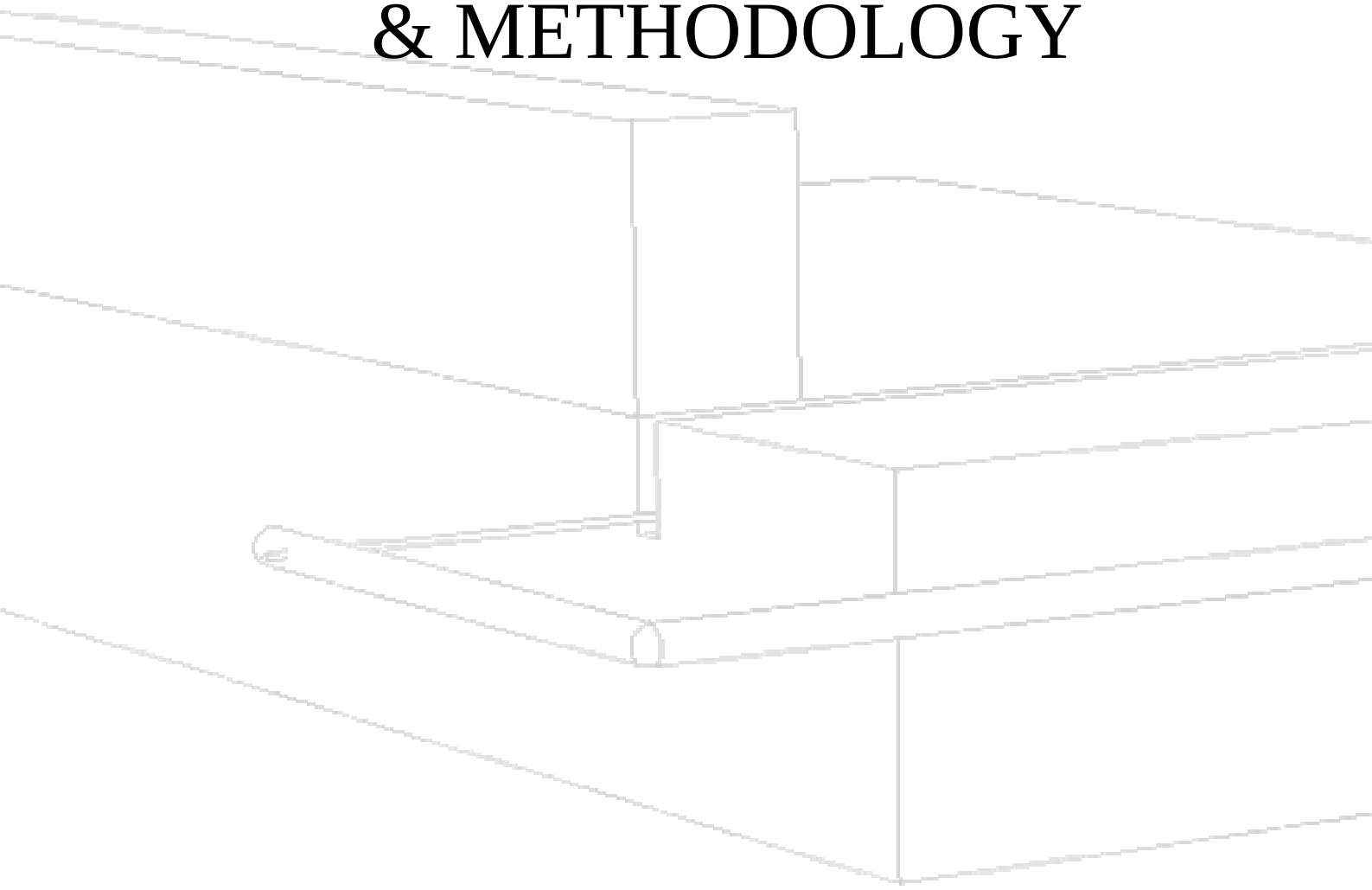

3.1.0 Materials

All purpose vegetable shortening (Crisco® Smucker Foods of Canada Co., Markham ON, Canada) was selected as the material to be tested due to its homogeneity and stability at room temperature as compared with other lipid-based particle gels, like margarine and butter. Vegetable shortening appears to be very homogeneous to the naked eye and is one of the simplest fat systems being composed of nitrogen gas dispersed throughout a semi-solid triacylglycerol matrix (Goh and Scanlon, 2007). Ingredients listed in the package of this shortening were soybean oil, hydrogenated cottonseed and soybean oils.

Preliminary mechanical testing was performed on two other lipid-based particle gels: an experimental shortening manufactured by blending the high melting fraction of Ghee butter (extracted as per Marangoni and Lencki, 1998) with canola oil, and a commercially available shortening (No Name® all-vegetable shortening Loblaws Inc., Calgary, AB, Canada), whose ingredients were listed as hydrogenated vegetable oils (canola and/or soybean and/or palm), mono- and diglycerides, BHA, BHT and citric acid. The mechanical properties derived from compression testing of both these sample materials varied substantially and so further testing was discontinued.

3.2.0 Physical Characteristics of Shortening

From the literature review it has been learned that all purpose vegetable shortening maintains its solid state within the temperature range at which the laboratory can be maintained (deMan et al, 1991). Also the literature suggests that all-purpose vegetable shortening contains approximately 13% of nitrogen gas per volume uniformly distributed

in bubbles (Shahidi, 2005). It is important to determine these two physical characteristics for the particular shortening studied (Crisco®), since they could affect the results obtained during the mechanical testing and the finite element modelling of the results.

3.2.1 Solid Stability of Shortening

According to deMan et al (1991), North American vegetable shortenings have melting points that range from 49.0 to 50.2 °C, which are much higher than room temperature (19 to 23 °C); therefore it can be assumed that the vegetable shortening chosen in this study is stable at room temperature. However since the formulations of vegetable shortenings of different brands is very diverse it was necessary to confirm this assumption. The Differential Scanning Calorimetry (DSC) thermogram can provide valuable information on the melting profile of fats and can be correlated to how they melt in the mouth during mastication (Dian et al, 2006). DSC was performed using a micro-calorimeter (Micro DSC III high sensitivity DSC and isothermal calorimeter, SETARAM Inc., Pennsauken, NJ, USA), in order to investigate the solid stability of the selected vegetable shortening at room temperature (19 to 23 °C). Vegetable shortening blocks were stored at 4 °C until tested. Three sequences were set up for the calorimeter, first the calorimeter internal temperature was dropped from room temperature to 4 °C at 3 °C min^{-1}, then the calorimeter was run isothermally for 60 min at 4 °C, and finally the calorimeter was ramped from 4 to 40 °C at 1 °C min^{-1}. The test was performed on triplicate, from three different blocks of the same lot (Crisco® Lot# 7232 420 1936 1). The mass of the specimens placed on the DSC machine was 118±4 mg. The measurements were repeated on the same shortening blocks nine weeks later (time it took to finish all mechanical

testing) to observe whether time and storage conditions affected the melting characteristics of shortening.

3.2.2 Void Fraction of Shortening

The void fraction of vegetable shortening was estimated by calculating the density of solid shortening as sold at room temperature (20.5 °C), this density was then compared to the solid shortening density after de-gasification had occurred. Three 30x30x30 mm cubes were cut and their respective masses were measured. The three replicates were melted (50±2 °C) and agitated under vacuum to release the nitrogen gas from the liquid shortening. The liquid shortening was transferred into a graduated cylinder so that the volume could be measured. The liquid shortening was allowed to cool down to room temperature (20.7 °C) inside the graduated cylinder and its volume and its mass were measured once again. The void fraction, Φ, was calculated using the following equation:

$$\Phi = 1 - \frac{\rho}{\rho_s} \qquad [3.1]$$

where ρ is the density of vegetable shortening as sold and ρ_s is the density of solid vegetable shortening after de-gasification.

3.3.0 Mechanical Testing of Shortening

In order to obtain the constitutive parameters used to define a material's rheological behaviour a series of mechanical test were performed on standardized cubic shortening

specimens using a Universal Testing Machine. Specimen preparation and mechanical testing set-up are described in the following sections.

3.3.1 Sample Preparation for Mechanical Testing

Blocks of vegetable shortening (Crisco® Lot# 7080 420 0702 2) weighing 454 g each were bought from a local supermarket and were stored at 4±2°C until testing. A minimum storage time of 10 hours after purchase was given to the shortening blocks so they hardened, making cutting of specimens easier. Specimens were cut into rectangular prisms of three different sizes to investigate the effects of friction between the compression set-up and vegetable shortening. Three different sizes were used to investigate the frictional effects. By increasing the dimensions of the specimens parallel to the compression plates (contact area), the stress results during compression should increase due to the presence of friction or should remain the same within experimental error if there is an absence of friction (Gunasekaran and Ak, 2003).

Sizes used were 15x15x15, 22.5x22.5x15, and 30x30x15 mm. These were nominal dimensions; the exact dimensions of each specimen were recorded to an accuracy of ±0.5 mm prior to testing. The cutting was done using a modified wire cheese cutter, consisting of a marble base, a wooden stopper, and a metallic arm that stretched a steel wire (Figure 3.1). The block of shortening was placed on the marble base and rested against the wooden stopper to form a 90° angle, while the metallic arm swivelled up and down cutting the shortening that was not resting on the wooden stopper.

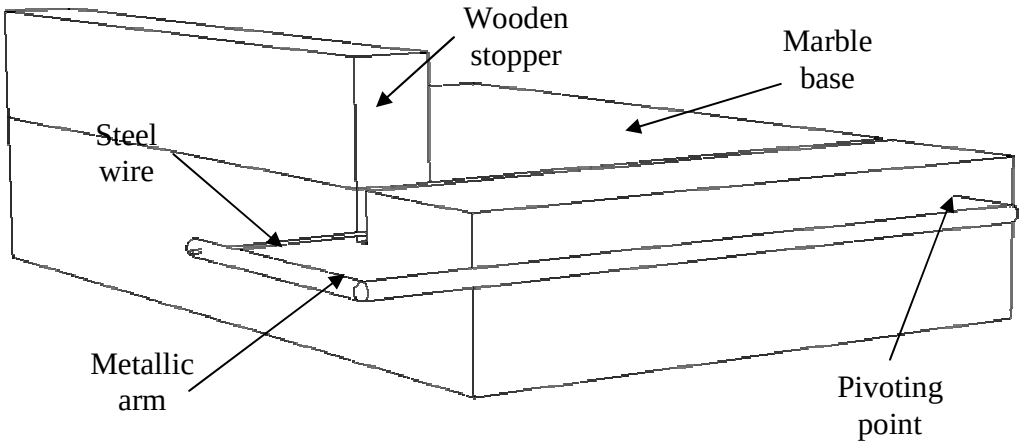

Figure 3. 1. Modified cheese wire cutter used during specimen preparation

The shortening blocks were cut immediately after they were removed from the refrigerator. Mineral oil (Light white oil EEC No 232-455-8, Sigma Chemical Co., St. Louis, MO, USA) was used on the steel wire to facilitate specimen preparation. About seven 30x30, seven 22.5x22.5 and twenty one 15x15 mm by mm specimens were prepared from each block of shortening. Specimens were rejected if large air bubbles or damage at the edges were observed. The specimens were carefully placed on square sheets of weighing paper (Fisher Scientific Corporation, Ottawa ON) for easy transport and to reduce further handling of specimens. Specimens were covered with a second sheet of weighing paper and allowed to equilibrate to room temperature (19 to 23°C) for a minimum of 3 h. The temperature equilibration time of 3 h was selected on the basis that it took approximately 1 h for the core of a 30x30x15 mm specimen to reach room temperature; the extra 2 h was chosen in order to allow all the cut specimens to reach room temperature, since specimens were randomly selected for testing.

3.3.2 Temperature Measurements during Mechanical Testing

The ambient temperature was measured using a digital thermometer (TEGAM 871A, Tegam Inc., Geneva, OH, USA) with an insulated thermocouple (Chromega®-Alomega®, Omega Engineering Inc., Laval, PQ, Canada). Temperature readings were taken at the beginning and at the end of each set of mechanical tests. Mechanical tests were not performed if the room temperature was below 19 °C or above 23 °C, to minimize variation in the results due to temperature.

3.3.3 Mechanical Testing Set-up

All mechanical tests were performed on a Zwick materials testing machine (Zwick USA, Kennesaw, GA, USA) with a 100 N load cell (resolution of 0.0002 N). Tests were controlled and data were compiled using the software TextXpert II (Zwick GmbH, Ulm, Germany). For compression based tests (simple compression, cyclic compression, creep test and stress relaxation) a layer of mineral oil was applied to both compression platens, sheets of overhead transparency were placed on top of the mineral oil and more mineral oil was applied to the upper face of both transparencies. Specimens were carefully taken from their weighing paper and placed on top of the mineral oil, as shown in Figure 3.2. Application of mineral oil and the use of stiff transparency sheets in between platens and specimen were utilized to reduce the frictional effects during testing. For indentation tests, a conical indenter with a half angle of 45° was used. The indentation set-up was similar to the compression one with the exception that no transparency was placed on top of the specimen, but the indenter surface was lubricated with mineral oil to reduce friction between indenter and specimen.

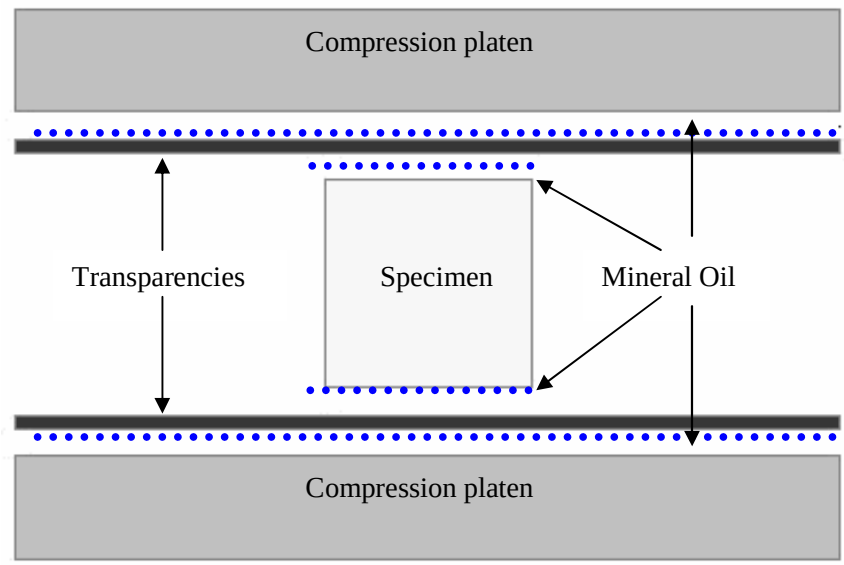

Figure 3. 2. Specimen set-up for compression testing of vegetable shortening

3.3.3.1 Treatments per Mechanical Test Type

In order to observe the rate dependent behaviour of shortening four monotonic loading rates were used during simple compression tests (0.4, 4, 40, and 400 mm min^{-1}) and three during cycling loading (4, 40 and 400 mm min^{-1}). The initial compression in cyclic loading was 1 mm and in the next cycles the compression distance was increased by 2 mm until a maximum compression distance of 7 mm was reached. An additional cyclic compression test was done with smaller compression distances (minimum compression 0.3mm, increments of 0.3 mm up to a maximum of 1.2 mm) at a crosshead speed of 4 mm min^{-1}. During the creep tests, specimens were subjected to three loads (0.5, 2.5 and 5 N) for a period of 30 min. For stress relaxation tests, specimens were subjected to three different compression displacements (0.5, 2.0 and 5.0 mm) that were reached by crosshead movement either at 4 or 40 mm min^{-1}, and the displacements were held for 20

min. In the indentation tests, monotonic loading at 0.4, 4, 40, and 400 mm min^{-1} up to a depth of 2.5 mm were performed. All the tests were done in triplicate. For compression-based tests specimens of three different contact areas were used (225, 506.25 and 900 mm^2) while for indentation, specimens with two different contact areas (225 and 900 mm^2) were used. Table 3.1 summarizes the treatments done for each type of test.

Table 3. 1. Summary of tests and treatments for vegetable shortening

Test	Monotonic Compression	Cyclic Compression	Creep test	Stress Relaxation	Monotonic Indentation
Treatments	Four constant compression rates: 0.4, 4, 40, 400 mm min^{-1}	Three constant compression rates: 4, 40, 400 mm min^{-1}	Three fixed loads: 0.5, 2.5, and 5.0 N	Three fixed displacements: 0.5, 2.0, and 5.0 mm Two crosshead speeds: 4 and 40 mm min^{-1}	Four constant indentation rates: 0.4, 4, 40, and 400 mm min^{-1}
Limit conditions	Maximum compression: 9.75 mm	Maximum compression: 1.2* or 7 mm	Holding time: 30 min	Holding time: 20 min	Indentation depth: 2.5 mm
Specimen Sizes (mm)	15x15x15 22.5x22.5x15 30x30x15	15x15x15 22.5x22.5x15 30x30x15	15x15x15 22.5x22.5x15 30x30x15	15x15x15 22.5x22.5x15 30x30x15	15x15x15 30x30x15
Replicates per treatment	3	3	3	3	3
Replicates per test	36	30	27	54	24

* Maximum compression of 1.2 mm was performed on three specimens 15x15x15 at the compression rate of 4 mm min^{-1}, so that the total replicates for cyclic compression is only 30.

3.3.3.2 Universal Testing Machine Control Parameters

A master test program from TextXpert II called "Cyclic Tests" version 1.41 was used to control the test. The parameters needed for each type of test are specified in Table 3.2.

Table 3. 2. Test control parameters inputted into TextXpert II version 1.41

Parameter	Monotonic Compression	Cyclic Compression	Creep Test	Stress Relaxation	Monotonic Indentation
Tool separation at start position	60 mm	60 mm	60 mm	60 mm	20 mm
Speed to reach start position	200 mm min^{-1}	200 mm min^{-1}	200 mm min^{-1}	200 mm min^{-1}	200 mm min^{-1}
Approach travel to a initial tool separation	Specimen height plus 1.0 mm	Specimen height plus 1.0 mm	Specimen height plus 1.0 mm	Specimen height plus 1.0 mm	Specimen height plus 1.0 mm
Speed of approach	200 mm min^{-1}	200 mm min^{-1}	200 mm min^{-1}	200 mm Min^{-1}	200 mm min^{-1}
Type of measurement phase	Cyclic loading	Cyclic loading	Creep test / Creep	Creep test / Creep	Cyclic loading
Number of cycles	2	4	1	1	2
Cycles controlled by	Position	Position	Force	Position	Position
Speed of cycles	0.4, 4.0, 40.0, or 400 mm min^{-1}	4.0, 40.0, or 400.0 mm min^{-1}	400 N/s	4.0 or 40.0 mm min^{-1}	0.4, 4.0, 40.0, or 400 mm min^{-1}

Point marking the end of first cycle	Standard travel: 65% of the initial tool separation (mm)	Standard travel: 2.0 or 0.3 mm	Not applicable	Not applicable	Standard travel: 25% of the initial tool separation (mm)
Point marking the beginning of holding time	Not applicable	Not applicable	Standard force: 0.5, 2.5, or 5.0N	Standard travel: 1.5, 3.0, or 6.0 mm	Not applicable
Increase after each cycle	0.2 mm	2.0 or 0.3 mm	Not applicable	Not applicable	0.2 mm
End test	End of cycles or maximum extension of 14.0mm	End of cycles or maximum extension of 14.0mm	After 30 min of holding load	After 20 min of holding displacement	End of cycles or maximum extension of 14.0mm
Travel save interval standard extensometer	10.0 μm	10.0 μm	10.0 μm	10.0 μm	10.0 μm
Time save interval	0.1 s	0.1 s	0.1 s	0.1 s	0.1 s
Force shutdown threshold	80 N	80 N	80 N	80 N	80 N

3.3.3.3 Conversion of Force-Displacement to Stress-Strain

The force and displacement measurements obtained were converted to total true stress, σ, and total true strain, ε, by assuming incompressibility of the materials following

equations discussed in the last chapter (equations [2.5] and [2.6]) (Charalambides et al, 2001), rewritten here for convenience:

$$\varepsilon = \left| \ln \frac{(H-d)}{H} \right| \qquad [2.5]$$

$$\sigma = \frac{F(H-d)}{L^2 H} \qquad [2.6]$$

where F is the force measured by the load cell, H is the original height of the specimen (15 mm), d is the displacement measured by testing machine and L is the original side length of the specimen (15, 22.5, and 30 mm).

3.3.3.4 Replicates Selection after Mechanical Testing

The order in which the tests were performed was randomized using a random number generation function in MS Excel. All the compression-based tests were grouped together since no change of fixtures was needed to perform the tests; therefore indentation test's treatments were randomized separately from compression-based tests and were performed after all the compression-based tests were finished.

Once three replicates per treatment were performed it was determined if the replicates were significantly different from each other by calculating the coefficient of variance of the total true stress at the end of loading for stress relaxation, simple and cyclic compression. For the creep test, the coefficient of variance was calculated for the strain at the point where the load was removed. And for indentation the coefficient of variance was calculated for the maximum force at the point of unloading. If the coefficient of

variance was smaller than 8% then the replicates were deemed not to be significantly different. If the coefficient of variance was higher than 8%, new specimens were prepared and tested; the new coefficient of variance was calculated for the specified parameter using only three replicates but mixing the older replicates and the newly acquired replicates randomly until the coefficient of variance was below 8% for three of the replicates. It was observed that most of the variability in the results arose from the way the specimens were cut rather than from temperature differences in the testing environment.

3.4.0 Visual Analysis during Compression

It is important to relate the data collected during the compression tests to the visible response of the specimen. For this reason it was decided to continuously photograph two specimens during simple compression at 40mm min^{-1}. Two 15x15x15 shortening specimens were prepared as previously described. One specimen at a time was placed on the compression platen as shown in Figure 3.2 and a black piece of cardboard was placed behind the specimen to increase the contrast between sample and background. Two incandescent lamps with tissue paper diffusers were placed at both sides of the specimen to properly illuminate the specimen and reduce shadows when the compression platens were close to each other. A digital single-lens reflex camera (Nikon D80, Nikon Canada, Mississauga, ON, Canada) was placed directly in front of the specimen on a tripod. The continuous shooting option was selected in order to take three frames per second. As soon as the top compression platen was in contact with the specimen, photographs were taken until the compression test completed the loading cycle. The photographs were later

matched to specific points of the stress-strain curve by relating the time at which a picture was taken as recorded by the digital camera to the time the force was measured by the load cell and recorded by universal testing machine software.

3.5.0 Modelling Mechanical Tests by Finite Element Analysis

Finite element analysis has proven to be a useful tool for studying the complex mechanical behaviour of metals, polymers and even food materials. One of the advantages of finite element analysis is its capacity to carry out 'virtual' experiments that cannot be readily performed experimentally (Liu and Scanlon, 2003), but in order to check the validity of such virtual experiments they must be verified with simulations of standard experiments.

During this study the rheological response of vegetable shortening after compression and indentation was modelled using Abaqus/CAE finite element analysis package version 6.6 and 6.7 (Abaqus Inc., Providence, RI, USA). Abaqus/CAE provides a user-friendly and consistent interface for creating and interpreting finite element simulations (Abaqus Inc., 2007). Abaqus/CAE is divided into eight modules that are necessary to create a simulation; these modules are Part, Property, Assembly, Step, Interaction, Load, Mesh, and Job.

3.5.1 Part Module

The Abaqus Part module is used to define the geometry of the parts involved in the simulations. Three two-dimensional axisymmetric parts were used for the simulations in this study. According to Goh and Scanlon (2007) the difference between 2-D and 3-D analytical results shows little difference, while the computation time is significantly longer for 3-D models. A DEFORMABLE part represented the shortening specimen while two ANALYTICAL RIGID parts were the fixtures in contact with the shortening specimen during mechanical testing, a fixed support platen and a compression platen or conical indenter. The ANALYTICAL RIGID option was used due to the geometric simplicity of the fixtures, and because stainless steel and aluminium plates are perfectly rigid when compared to vegetable shortening. A reference node was assigned to the rigid parts where constraints were applied (Figure 3.3).

3.5.2 Property Module

The Abaqus Property module is used to define the material properties to be assigned to the parts drawn in the Part module. The material properties include physical properties such as density, and mechanical properties arranged into different models such as elastic, viscoelastic, and plastic. For this study several material models and different combinations of them were tried; a comparison of the different models is shown in the results section of this thesis (Sections 4.9.0 and 4.10.0).

3.5.3 Assembly Module

In Abaqus/CAE the parts drawn are independent from each other until they are put together in the Assembly module; the relative position to each other is assigned in the assembly module. Just like in the experimental tests, during simulations the shortening specimen was placed on top of the support platen and the indenter or compressor on top of the shortening specimen (Figure 3.3).

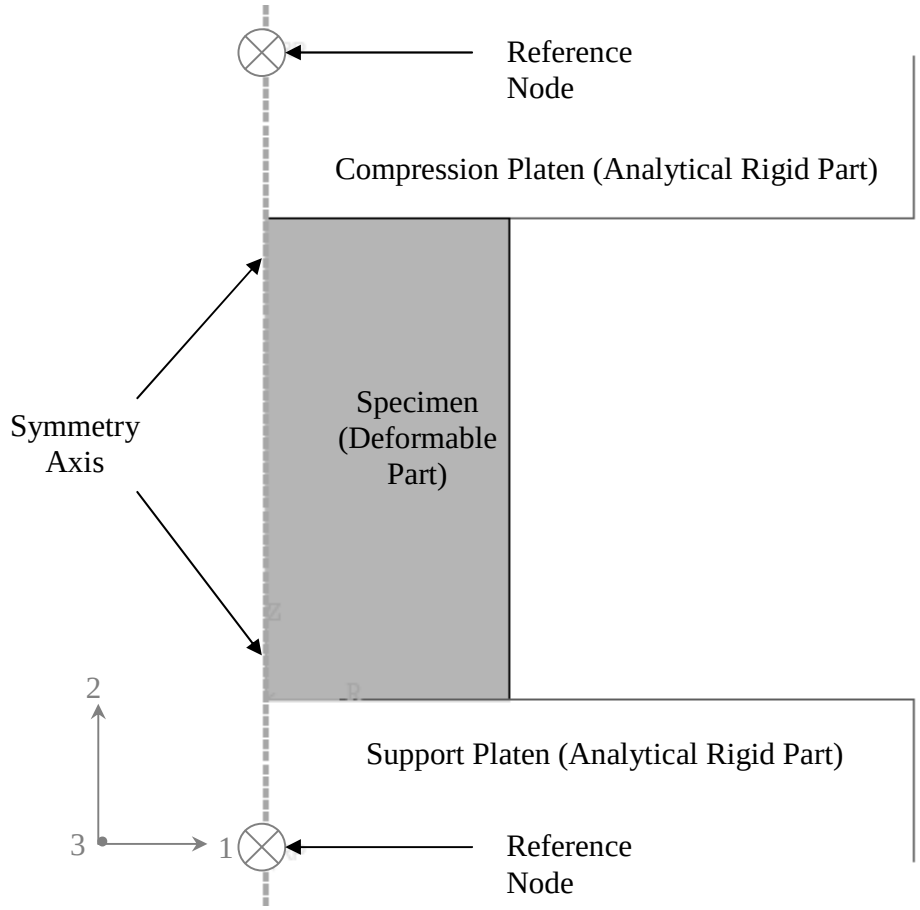

Figure 3. 3. Parts and assembly used during compression simulations

3.5.4 Step Module

The step module is used to define the type of analysis to be performed, the simulated time, the frequency and number of data points to be collected and the techniques used to solve the different constitutive equations. In this study a VISCO or STATIC type of analysis was selected in order to model viscoelastic or elastic, plastic and elastoplastic behaviours. The simulated time was adjusted according to the different compression rates used during experimental tests. One hundred data points at even intervals were collected throughout the step for most of the simulations.

3.5.5 Interaction Module

The interaction module is used to determine the type of interactions between the different parts in an assembly. For the test simulations a SURFACE TO SURFACE contact was selected between the fixtures and the specimen. A FRICTIONLESS contact was assigned between the fixtures and the specimen because no apparent frictional effects were observed experimentally; see results section of this thesis (Section 4.4.2).

3.5.6 Load module

The load module is used to apply direct loads and boundary conditions to the assembly used during simulations. No direct or point loads were used to cause the deformation of DEFORMABLE parts during compression or indentation simulations, but rather the RIGID parts movement onto the DEFORMABLE parts caused the deformation, so that all simulations mimicked actual experimental protocols. The support platen was

completely fixed by selecting the ENCASTRE (U1=U2=U3=UR1=UR2=UR3=0) boundary condition at the reference node, so that no movement along any of the axes (U1, U2, U3) and no rotation around any of the axes (UR1, UR2, UR3) was allowed for the reference node of the support platen. Rollers that allow only movement in the vertical direction (U1=UR3=0) were placed on the axis of symmetry of the sample and on the reference node of the compression platen. The vertical displacement (U2) of the compression platen was assigned in the load module accordingly to simulate the different treatments done during experimental compression and indentation (Figure 3.4).

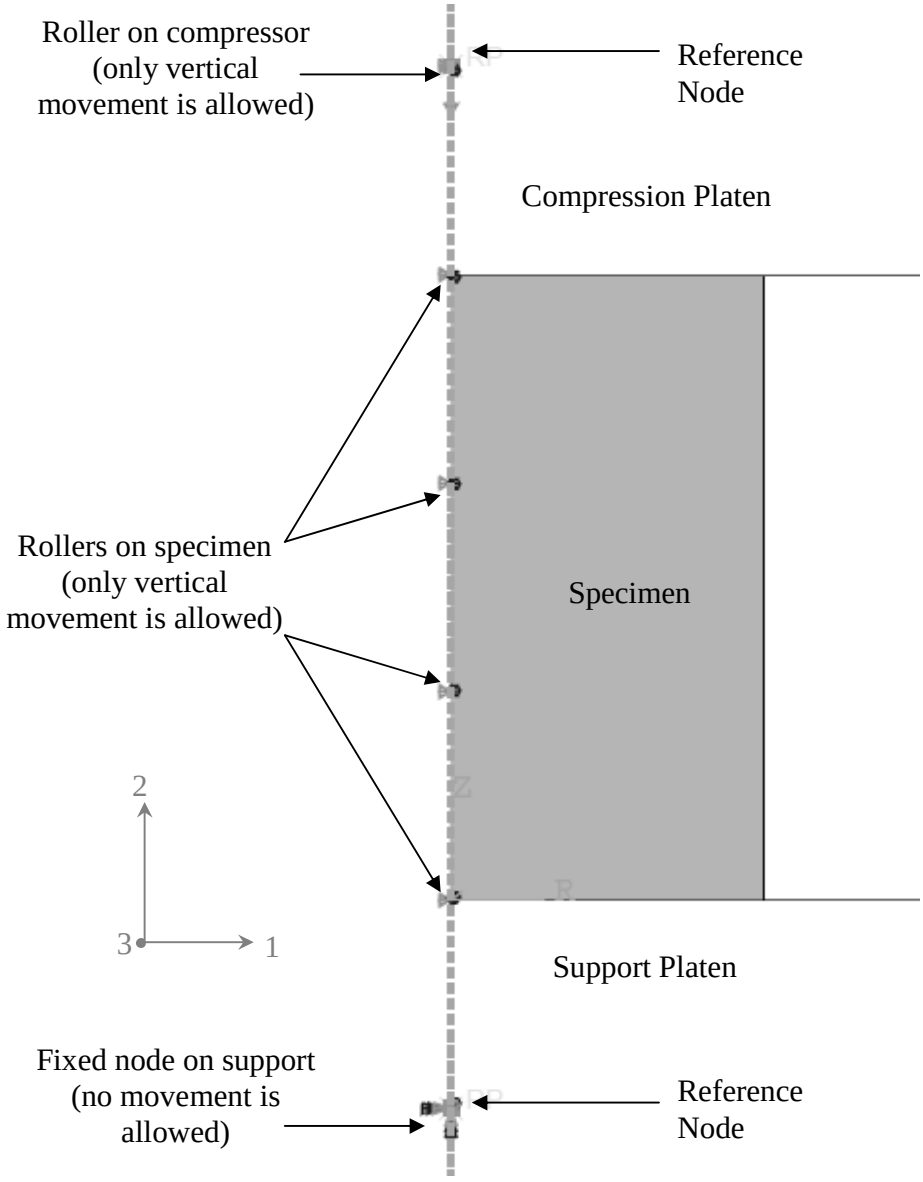

Figure 3. 4. Constraints used during compression and indentation simulations

3.5.7 Mesh module

The mesh module is used to assign the type and number of elements used to analyse the mechanical behaviour of a simulated material. The element type used during all the simulations was a 4-node bilinear axisymmetric quadrilateral, with reduced integration and hourglass control (CAX4R), which is the default when axisymmetric stress analysis

is selected. For frictionless compression simulations a uniform mesh with 120 elements of the same size was used, since the load is evenly distributed and there is no stress concentration as a result of the crosshead squeezing the specimen (Figure 3.5a). For frictionless indentation simulations a mesh with 315 elements of different sizes had to be used in order to increase accuracy of the results without greatly increasing the computational time. Smaller elements were used right underneath the indenter because this section is subjected to a greater deformation than any other part of the sample and more accuracy is required here than at other points in the mesh, this is in agreement to the simulations done by Bucaille and Felder in 2002 (Figure 3.5b).

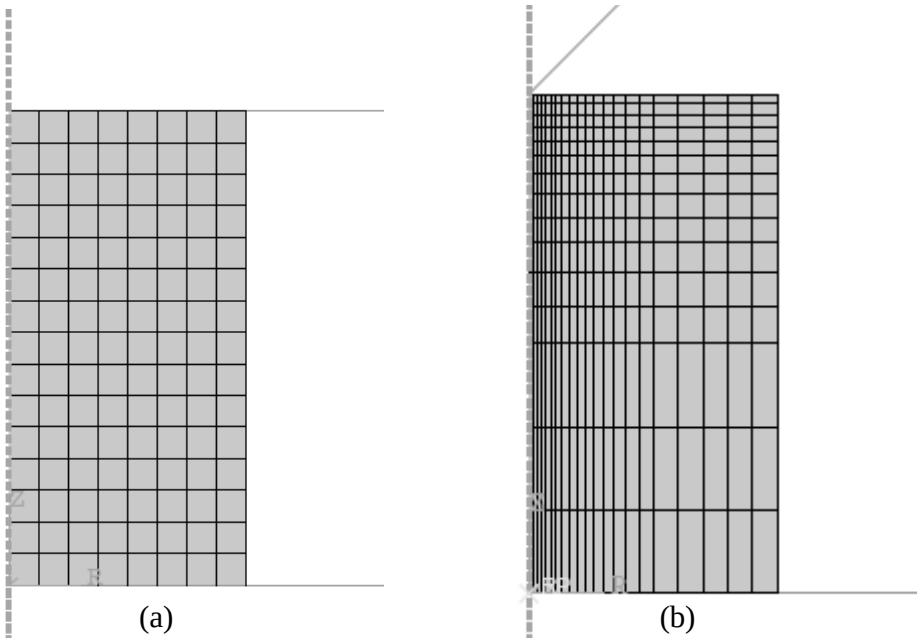

Figure 3. 5. Meshes used for compression (a) and indentation (b) simulations

3.5.8 Job module

Once the simulation has been set up in the previous modules it can be submitted for analysis and monitored using the Job module. An appropriate name was assigned to the

simulations and a general description was added before submitting a job for analysis. All jobs were assigned a DOUBLE Abaqus/Explicit precision and a FULL nodal output precision.

CHAPTER 4: RESULTS & DISCUSSION

4.1.0 Introduction

The two main objectives of the research project are the measurement of the fundamental material parameters of shortening and the development of a mechanical model that is able to accurately predict the indentation response of vegetable shortening. Since the rheological response of vegetable shortening is affected by its composition, differential scanning calorimetry and the void fraction of the selected vegetable shortening were performed to better characterize the material; the results of these two measurements are shown in sections 4.2.0 and 4.3.0 of this chapter. Sections 4.4.0 to 4.8.0 deal with the extraction of the fundamental material parameters of vegetable shortening from the different uniaxial compression tests, which include monotonic compression, cyclic compression, creep test and stress relaxation tests. The last two sections (4.9.0 and 4.10.0) of this chapter are devoted to an assessment of the suitability of two different mechanical models (viscoelastic and elasto-viscoploastic) that could be used to predict the rheological response of complex materials such as vegetable shortening, and its application to predicting the mechanical response in an indentation test.

4.2.0 Solid Stability of Shortening

Differential Scanning Calorimetry (DSC) was used to determine if phase changes were occurring in the shortening samples during mechanical testing due to fluctuations in room temperature. Since the mechanical properties of shortening are extremely sensitive to solid fat content (Carden and Basilio, 2004; Marangoni and Narine, 2002), it is important to ascertain potential variability in mechanical properties that might be brought about temperature variability. The results of a DSC test are generally presented in a curve that

shows the heat flow as a function of temperature. If an exothermic process such as crystallization occurs during the test, the curve will show a peak in the positive direction, and if an endothermic process such as melting occurs a peak in the negative direction will appear. If the heat flow remains constant as the temperature increases this means there is no change in phase. A DSC curve was produced for vegetable shortening between 4 and 40 °C (Figure 4.1).

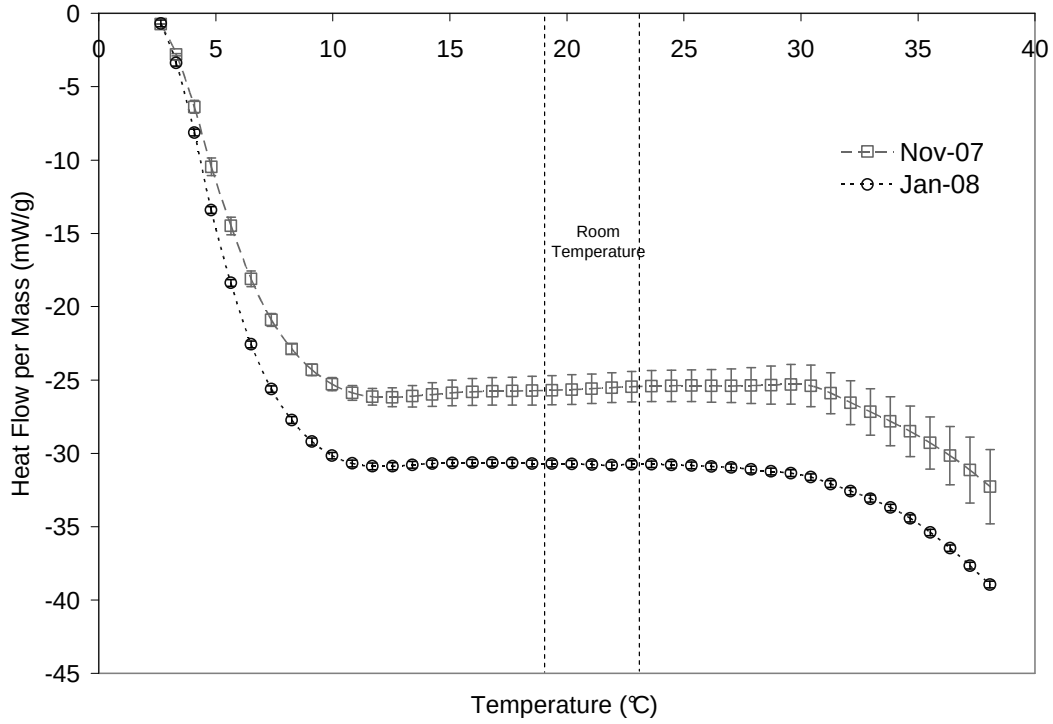

Figure 4. 1. Average DSC curves for vegetable shortening at two storage times. Error bars represent ± 1 standard deviation

As one can see in Figure 4.1 vegetable shortening remains in the same state at the temperatures in which the mechanical test were performed (19 to 23 °C) since the DSC curve is almost horizontal. Melting starts to occur beyond 30 °C and it appears that further crystallization occurs below 10 °C. The shape of the curve did not change as the

storage time progressed, however the heat flow increased with storage time. The increase in heat flow can be attributed to an increase in the solid fat content (Metzroth, 2005). Based on these results it can be assumed that the rheological properties of vegetable shortening were not changing as a result of ambient temperature fluctuations in the laboratory, but some of the variability between replicates can be attributed to the changes that occurred during refrigerated storage.

4.3.0 Void Fraction of Vegetable Shortening

Vegetable shortening as sold has a white and creamy appearance which can be attributed to the presence of evenly distributed nitrogen bubbles (Shahidi, 2005). Once the shortening was melted, agitated and re-solidified its appearance can be described as opaque and yellowish in colour; therefore one could partially explain this change in appearance to the removal of nitrogen bubbles from the shortening matrix. In order to calculate the void fraction (Φ) of vegetable shortening the density of solid shortening as sold (ρ) and the density of degasified solid shortening (ρ_s) were measured. The density of shortening as sold at 20.5°C was measured to be 0.834 ± 0.002 g cm^{-3} while the density of solid degasified shortening at 20.7°C was 0.895 ± 0.009 g cm^{-3}; therefore the void fraction was calculated as 0.068 ± 0.008 as per equation [3.1] in the methodology section:

$$\Phi = 1 - \frac{\rho}{\rho_s}.$$

This void fraction is smaller to what Shahidi (2005) records as the added nitrogen to most shortenings (12-14% by volume), but it is important to remember that there are many formulations for shortening and it is possible that during the manufacturing of Crisco®

all-purpose vegetable shortening only 7% of nitrogen is added to increase workability and to provide a white and creamy appearance.

4.4.0 Uniaxial Monotonic Compression

All purpose vegetable shortening was subjected to uniaxial monotonic compression in order to observe its rheological behaviour and try to classify the material as elastic, plastic, viscoelastic, or a combination of the above. In general, uniaxial compression tests are used to obtain some fundamental rheological properties of materials, such as the modulus of elasticity (E) and yield stresses (σ_y), which are necessary to create a model for the simulation of their rheological response.

4.4.1 Classification of Shortening from Monotonic Compression Response

Goh and Scanlon (2007) noted that the compression response of vegetable shortening can be divided into three sections, a linear elastic region at the beginning, followed by a plastic region with strain hardening and finally a perfectly plastic region. Because of this rheological response, vegetable shortening can be classified as an elasto-viscoplastic material. The experimental compression results shown in Figure 4.2 suggest that vegetable shortening has a perfectly elastic region at very small strains and it appears that at large strains a perfectly plastic region is present just as reported by Goh and Scanlon (2007). However in the intermediate region a stress-overshoot region develops which suggests strain hardening as well as strain softening, as opposed to just strain hardening.

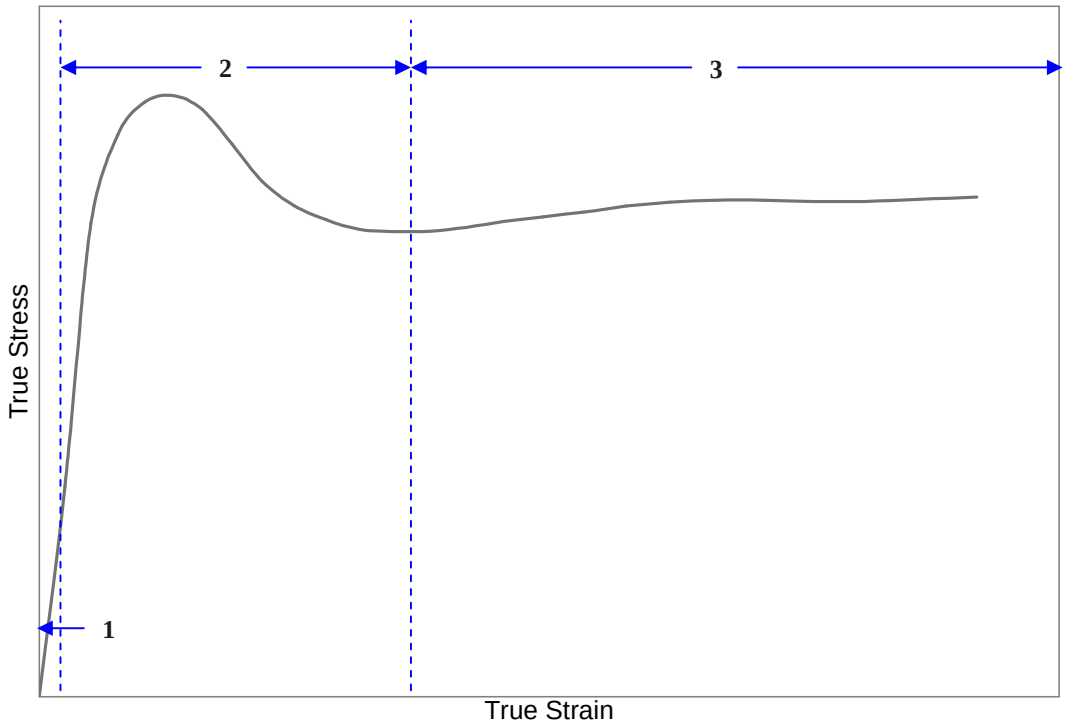

Figure 4. 2. Monotonic uniaxial compression true stress- true strain schematic curve for vegetable shortening; three different sections are visible: Linear elasticity (1), stress overshoot hardening/softening (2), and perfect plasticity (3)

An attempt to quantify the value for the modulus of elasticity was made by fitting a straight line through the stress-strain data at strains greater than 0.5% and below 5%. Using this technique the modulus of elasticity was found to be the values in Table 4.1.

Table 4. 1. Modulus of elasticity of shortening obtained after monotonic compression at different crosshead speeds.

Crosshead speed (mm min^{-1})	Average modulus of elasticity (kPa)
0.4	248.3 ± 9.7
4.0	360.3 ± 5.5
40.0	306.7 ± 105.4
400.0	246.3 ± 6.5

The variability in the modulus of elasticity (E) can be attributed to the variability in specimen shape, rather than being a true rate-dependent effect, because there is not a real pattern as the loading rate increases. This behaviour was expected since the modulus of

elasticity is a rate-independent parameter since it is used to describe purely elastic behaviour which is always non rate-dependent. The specimen shape variation was pretty hard to eliminate. Even though great care was taken during the cutting process to have flat contact areas there was a variation in height, maximum of ±0.5mm (or 3.3% of specimen height), between the different sides of the same cubic specimens. This uneven contact area affects the compression results by changing the initial slope of the stress-strain diagram as discussed by Gunasekaran and Ak (2003). If the specimen contact surface is uneven (Figure 4.3), the initial force value measured during compression would be smaller than if the compression platen was in contact with the entire face, this in turn leads to the underestimation of the modulus of elasticity.

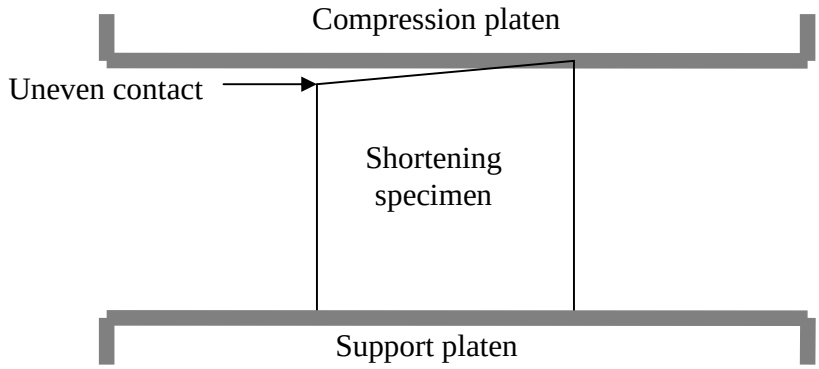

Figure 4. 3. Schematic representation of uneven contact between specimen and compression platen leading to underestimation of modulus of elasticity

4.4.2 Frictional Effects during Monotonic Compression

The frictional effects were also studied during uniaxial monotonic compression by varying the area of the specimens in contact with the compression and support platens. Altering the dimensions of specimens is a common method of studying the frictional

effects during compression (Charalambides et al, 2001). In order to study fictional effects during compression, Charalambides et al (2001) varied the specimen height and Gunasekaran and Ak (2003) suggested the variation of the contact area of the specimen. Charalambides et al (2001) observed that when no lubricant was used, shorter cheese cylindrical specimens appear stiffer than taller specimens due to the presence of friction. On the other hand Gunasekaran and Ak (2003) stated that if frictional effects are significant during compression tests, one could expect the stress at a given strain to increase as the contact area of specimens increases, because a larger contact area will contribute to more friction than a smaller contact area.

The compression results of shortening specimens with different contact areas are shown in Figure 4.4. One would expect the 30x30 mm^2 specimens to have larger stresses at a given strain independently of the compression rate, if there were significant frictional effects during compression. However, as seen in Figure 4.4 this trend is not visible in the experimental data especially at strains below 0.5. For example at a compression rate of 4 mm min^{-1} (Figure 4.4a) the 30x30 specimens appear to have the smaller true-stress values than the 15x15 and 22.5x22.5 specimens at true strains below 0.5, while at 40 mm min^{-1} the stress values for the three specimen sizes are close to each other and within the error bars at strains below 0.5 (Figure 4.4b). At strains larger than 0.5 there is a slight increase in the true-stress values as the size of the specimen increases but at strains larger than 0.5 the specimen shape starts to greatly deviate from its cubical shape and it appears that shear fractures start to appear as discussed in section 4.4 of this chapter, so the stress increase may not be attributed to friction alone.

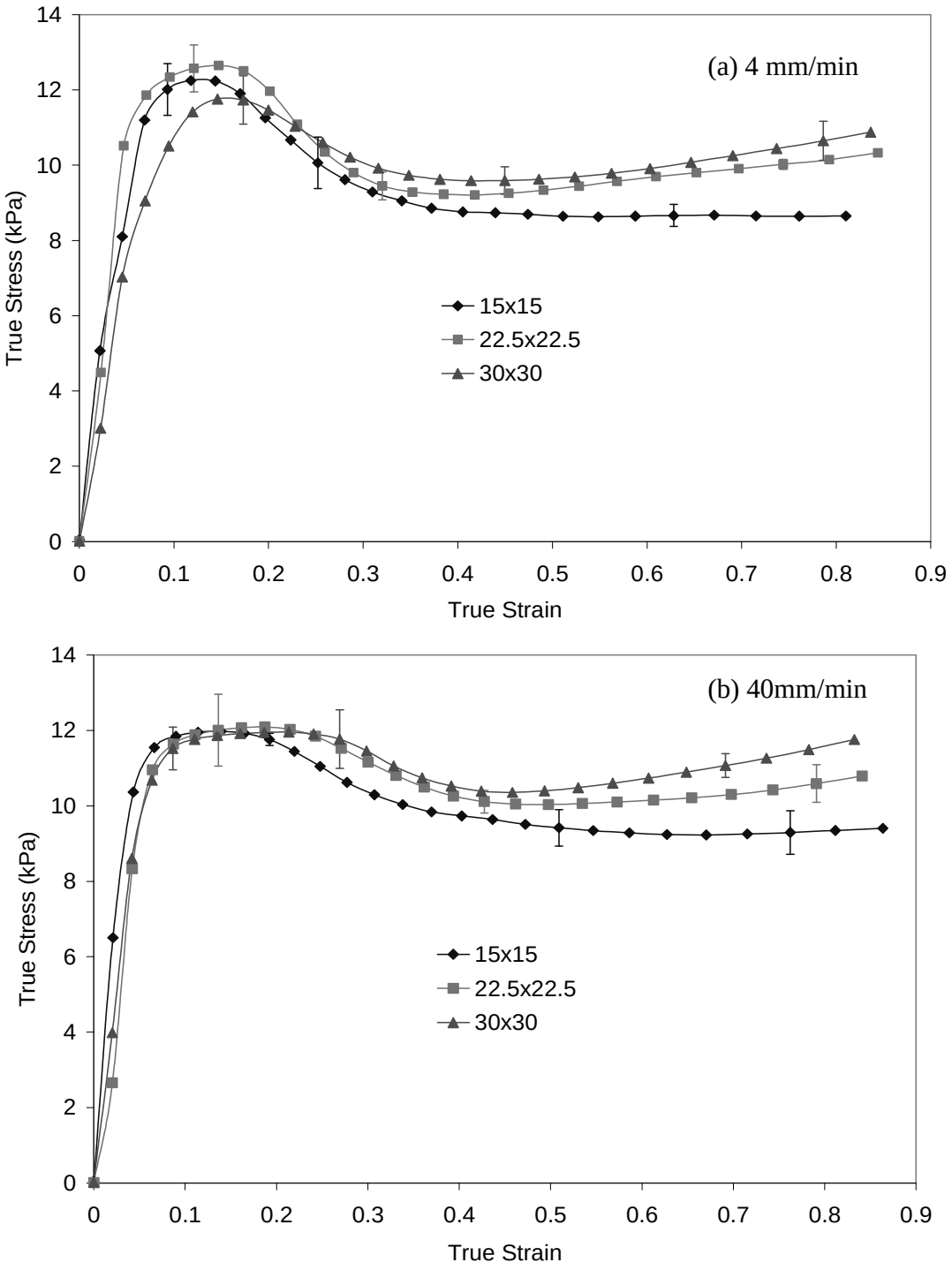

Figure 4. 4. True stress-true strain diagram from uniaxial monotonic compression of vegetable shortening cubic specimens with three different contact areas (dimensions in mm^2) and at two crosshead speeds (a) 4 and (b) 40 mm min^{-1}. Each curve is the average of three specimens with similar dimensions and error bars are the average standard deviation of three specimens

Specimens with different contact areas were not only used during monotonic compression but also during other uniaxial compression tests, which included cyclic compression. In order to observe if the stress measurements were affected by frictional effects, a student t-test (95% confidence, 2 tails) was performed using MS Excel between the true-stress results of specimens with different contact areas at different true strain values (at the end of the loading of each type of test) during monotonic and cyclic compression tests. The results of the t-tests are shown in Tables 4.2 and 4.3.

Table 4. 2. Student t-test comparison between stress values at strain values larger than 0.5 after monotonic compressions for specimens of different sizes.

Crosshead speed (mm min^{-1})	Specimen size comparison (mm)	t-test value (95% Confidence, 2 tail)	Significantly different (Yes/No)
0.4	15 vs. 22.5	0.0478	Yes
0.4	15 vs. 30	0.0263	Yes
0.4	22.5 vs. 30	0.2040	No
4.0	15 vs. 22.5	0.0006	Yes
4.0	15 vs. 30	0.0062	Yes
4.0	22.5 vs. 30	0.0492	Yes
40.0	15 vs. 22.5	0.0692	No
40.0	15 vs. 30	0.0012	Yes
40.0	22.5 vs. 30	0.1761	No
400.0	15 vs. 22.5	0.0996	No
400.0	15 vs. 30	0.1650	No
400.0	22.5 vs. 30	0.4584	No

The t-test comparisons for monotonic compression (Table 4.2) at strain values larger than 0.5 indicate that at low crosshead speeds (0.4 and 4 mm min^{-1}) there is a significant difference between the measured true stresses of specimens of different sizes. However at higher crosshead speeds (40 and 400 mm min^{-1}) there is no significant difference between specimens of different sizes. In order to conclude if the specimen size had an

effect on the measured stress cycling compression test results were subjected to t-test comparisons (Table 4.3).

Table 4. 3. Student t-test comparison between stress values at strain values larger than 0.5 after cyclic compressions for specimens of different sizes.

Crosshead speed (mm min^{-1})	Specimen size comparison (mm)	t-test value (95% Confidence, 2 tail)	Significantly different (Yes/No)
4.0	15 vs. 22.5	0.2308	No
4.0	15 vs. 30	0.0834	No
4.0	22.5 vs. 30	0.1125	No
40.0	15 vs. 22.5	0.2919	No
40.0	15 vs. 30	0.5479	No
40.0	22.5 vs. 30	0.9428	No
400.0	15 vs. 22.5	0.3539	No
400.0	15 vs. 30	0.3260	No
400.0	22.5 vs. 30	0.6132	No

By looking at Table 4.3 one can conclude that changing the specimen size during cycling compression test of vegetable shortening did not cause a significant difference in the measured stress at strains larger than 0.5.

The student t-test showed that 71% of all the comparisons were not significantly different; the t-test results indicate that there was more variability among specimens with similar dimensions than between specimens with different dimensions. Based on the observations done on Figure 4.4 and the statistical analysis (Table 4.2 and 4.3), one can conclude that at all strains, the measured stress is not significantly different as a result of compressing specimens of different sizes when the crosshead speed is either 40 or 400 mm min^{-1}. However if compression tests are carried out at either 0.4 or 4 mm min^{-1} there is a significant difference between the true stress values measured at strains larger than 0.5. Therefore it is only safe to neglect frictional effects during compression tests at

strains lower than 0.5; therefore one can assume frictionless behaviour at strains lower than 0.5 during finite element analysis simulations, which will be discussed later in this thesis.

4.4.3 Monotonic Compression Rate-Dependent Behaviour

The literature review revealed that most lipid-based particle gels are rate-dependent materials (Wright et al, 2001; Goh and Scanlon, 2007); therefore in order to investigate the rate-dependent behaviour of vegetable shortening, cubic specimens were compressed at four different crosshead speeds (0.4, 4.0, 40 and 400 mm min^{-1}). The results of uniaxial monotonic compression of shortening at different crosshead speeds are shown as a true stress-true strain diagram in Figure 4.5.

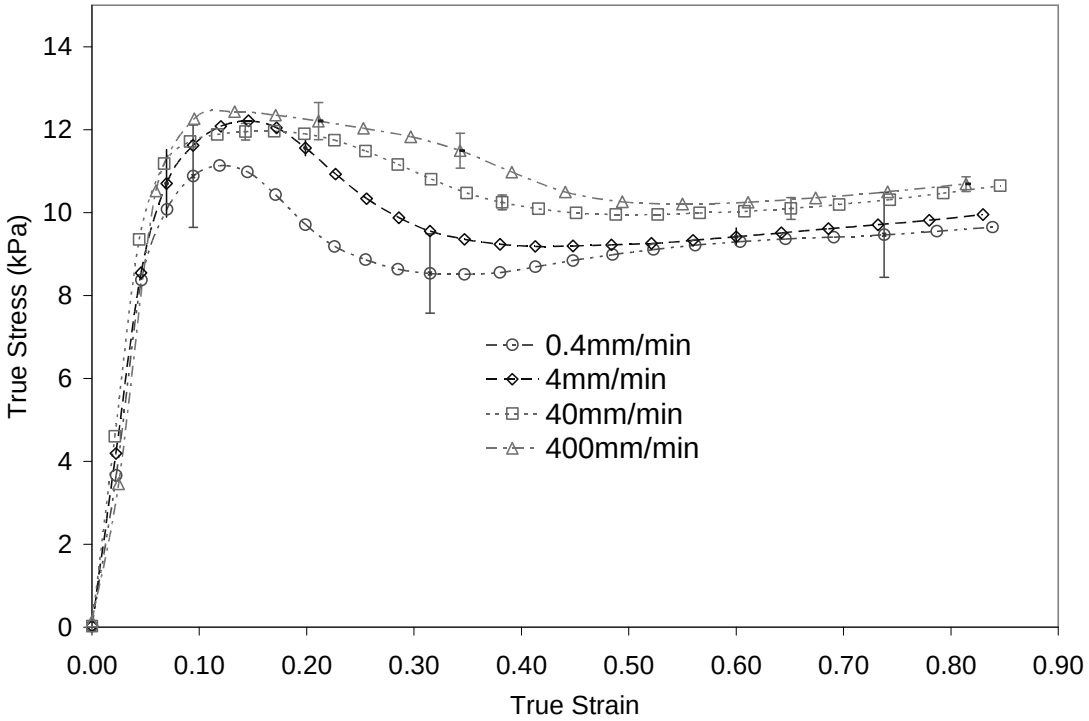

Figure 4. 5. True stress- true strain diagram from uniaxial monotonic compression of vegetable shortening at four different loading rates. Each curve is the average of 9 specimens with three different contact areas and error bars are 95% C.L from 9 specimens at each data point

Figure 4.5 suggests that vegetable shortening has a rate-dependent response to uniaxial compression; however it is not seen as an increase in the stress values as the compression rate increases as reported by Goh and Scanlon (2007), but a change in the shape of the stress-strain curve. As the compression rate increases the perfectly plastic region is only reached at greater strain values. In addition, the stress peak broadens significantly, the maximum stress appears to increase but the difference between different crosshead speeds is not significant due to the variability of the results (Figure 4.5). The increases in the value of the plateau stress with loading rate are not as pronounced as described by Goh and Scanlon (2007) and are within the error bars for each of the different crosshead speed compression tests, so they are also not significantly different.

4.4.4 Visual Analysis during Monotonic Compression

Continuous photographs were taken during uniaxial monotonic compression and then matched to specific points in the stress-strain curve. This was done in an attempt to understand the macroscopic effects of uniaxial compression and to try to understand what was causing the stress overshoot at intermediate strain seen in Figure 4.2. The results are summarized in Figure 4.6.

If a material is subject to predominantly compressive stresses, failure occurs on planes that are inclined to the planes of normal stress and more aligned with planes of maximum shear. Failure at the shear planes is common for brittle solid materials such as cast iron and concrete (Dowling, 2007). By looking at Figure 4.6 it appears that shortening undergoes failure along the planes of maximum shear, which is inclined to the

compressive plane. Many materials usually contain, or easily develop, small flaws or other geometric features that are equivalent to small cracks. In vegetable shortening these flaws might be the nitrogen bubbles in the solid matrix (O'Brien, 2005) that account for the void fraction discussed in section 4.3.0. Failure in materials generally occurs as a result of these flaws joining or growing, and such a process is often time dependent; therefore shear failure is dependent on the loading rate (Dowling, 2007).

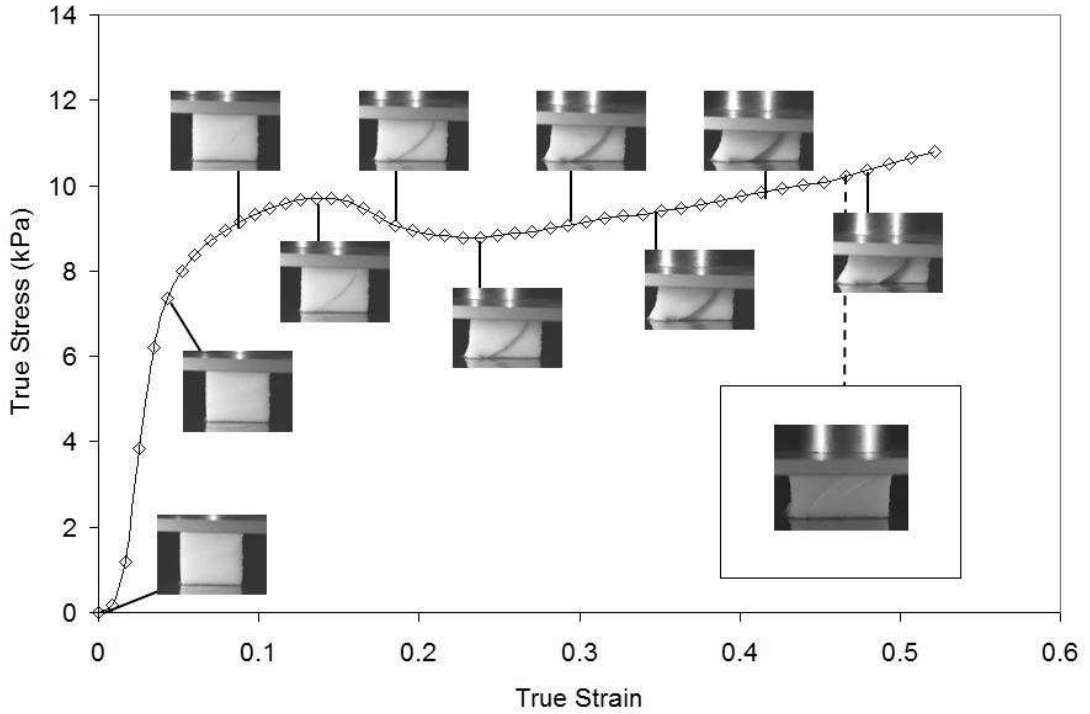

Figure 4. 6. Stress-strain curve from uniaxial monotonic compression of a 15 mm cubic shortening specimen at 40 mm min^{-1} and photographs of macroscopic behaviour of shortening specimens at a given strain. Inset shows another shortening specimen compressed to 0.46 strain

By looking at Figure 4.6, one can see that the stress overshoot region is related to the formation of a shear failure almost at the centre of the cubic specimen. At the maximum stress of the stress overshoot the shear-failure becomes visible and the failure becomes more pronounced as the stress decays. When stresses are applied to a material specimen

work must be done, and during purely elastic deformation all the work is stored as potential energy (Dowling, 2007). For materials that undergo plastic deformation (e.g., shortening) there is an expenditure of potential energy prior to failure (Liu, 2005). Materials that undergo plastic deformation are called ductile materials. Failure of ductile materials usually occurs by glide or slip, whereby one part of the body is sheared against the other (Liu, 2005). By looking at Figure 4.6 one can see that vegetable shortening seems to be failing by slip, so that the strain energy is converted into plastic work.

It is important to emphasise that ductile, not brittle failure, occurred in the cubic shortening specimens. In Figure 4.6 it appears that separation of parts of the specimen has occurred. This is actually an artefact associated with illumination of the specimen as a result of shadows forming due to displacement of one part of the specimen relative to another about the slip plane. In the inset to Figure 4.6 another specimen deformed to 0.46 strain is shown, and no separation of the specimen into two parts is observed. Further evidence of the absence of crack formation is apparent in the elastic recoil of the entire specimen in Figure 4.12.

Also from Figure 4.6 one can see that the final shape of the compressed specimen is no longer a cube since one of the sides is no longer at 90 degrees from the compression platen and the lower contact surface appears to be larger than the upper contact surface. The change in shape of the specimen suggests that the material's Poisson's ratio is no longer close to 0.5 when the strain is larger than 0.4 and from the photographs in Figure 4.6 it appears that there might be some frictional effects on the upper compression platen, since the specimen does not slide as much as in the bottom surface.

4.4.5 Conclusions from Monotonic Compression

From monotonic uniaxial compression of vegetable shortening it can be concluded that the rheological behaviour of shortening can be characterized by three distinct behaviours, purely linear-elastic at small strains, strain hardening and softening at intermediate strains and pure plasticity at large strains. The Young's modulus of vegetable shortening obtained from monotonic compression is in the range of 185 to 371 kPa. Rate-dependency effects were observed during the monotonic compression of vegetable shortening, and these effects were shown as a change in the shape of the stress-strain curve rather than just an increase in the stress values as the crosshead increases. Also the frictional effects of the experimental set-up can be considered negligible at strains below 0.5. It appears that the stress overshoot present in the compression stress-strain diagram is related to the formation and propagation of a shear failure at the center of the shortening specimen.

4.5.0 Cyclic Uniaxial Compression

Cyclic uniaxial compression tests can be used to determine the elasticity region of a material. If a material is truly elastic the loading and unloading curve would overlap, but if the material has already suffered permanent deformation and is therefore in the plastic region the unloading curve will not overlap the loading curve (i.e., hysteresis occurs) and the strain will not return to zero when the load is removed from the material (i.e., plastic deformation). The unloading modulus gives a purely elastic modulus whereas the loading modulus is comprised of the elastic and plastic compliance (de With, 2006; Goh and Scanlon, 2007). Furthermore the loading curve for subsequent cycles will start at

strains larger than zero and will run parallel to the other loading curves i.e., the loading curves will not overlap due to the permanent deformation.

4.5.1 Determination of Initial Yield Strain

Two types of cyclic compression were performed during this research project: with an initial compression of 0.3 mm and increments in compressive distance of 0.3 mm (Figure 4.7); initial compression of 1.0 mm with increments in compressive displacement of 2.0 mm (Figure 4.8 and Figure 4.9). It was observed that vegetable shortening exhibits permanent deformation even at the small strain of 2% (Figure 4.7a), since the loading and unloading paths do not overlap and there is a residual strain when the load is removed as shown in cycle 1 of Figure 4.7a; this is in agreement with the results of Goh and Scanlon (2007) who reported that the yield strain of shortening was well below 2%. A yield strain below 2% is difficult to measure with the current experimental set up, because results obtained from compression tests with strains below 2% are likely not accurate due to the variability of the height within a specimen; Kloek et al (2005) found that having test pieces lacking complete flat ends caused scatter in the values of the yield strain. The specimens used in the current research are not completely flat on the top and bottom contact surfaces causing the stress to be non-homogeneous at small strains and to lead to an increase in compliance, which is readily apparent in Figure 4.7. Due to the specimen preparation technique and the measuring instruments used, the specimen height could only be kept within 0.5 mm (3.3%) of the target height of 15 mm, and this potential variability is already bigger than 2% strain (0.3mm).

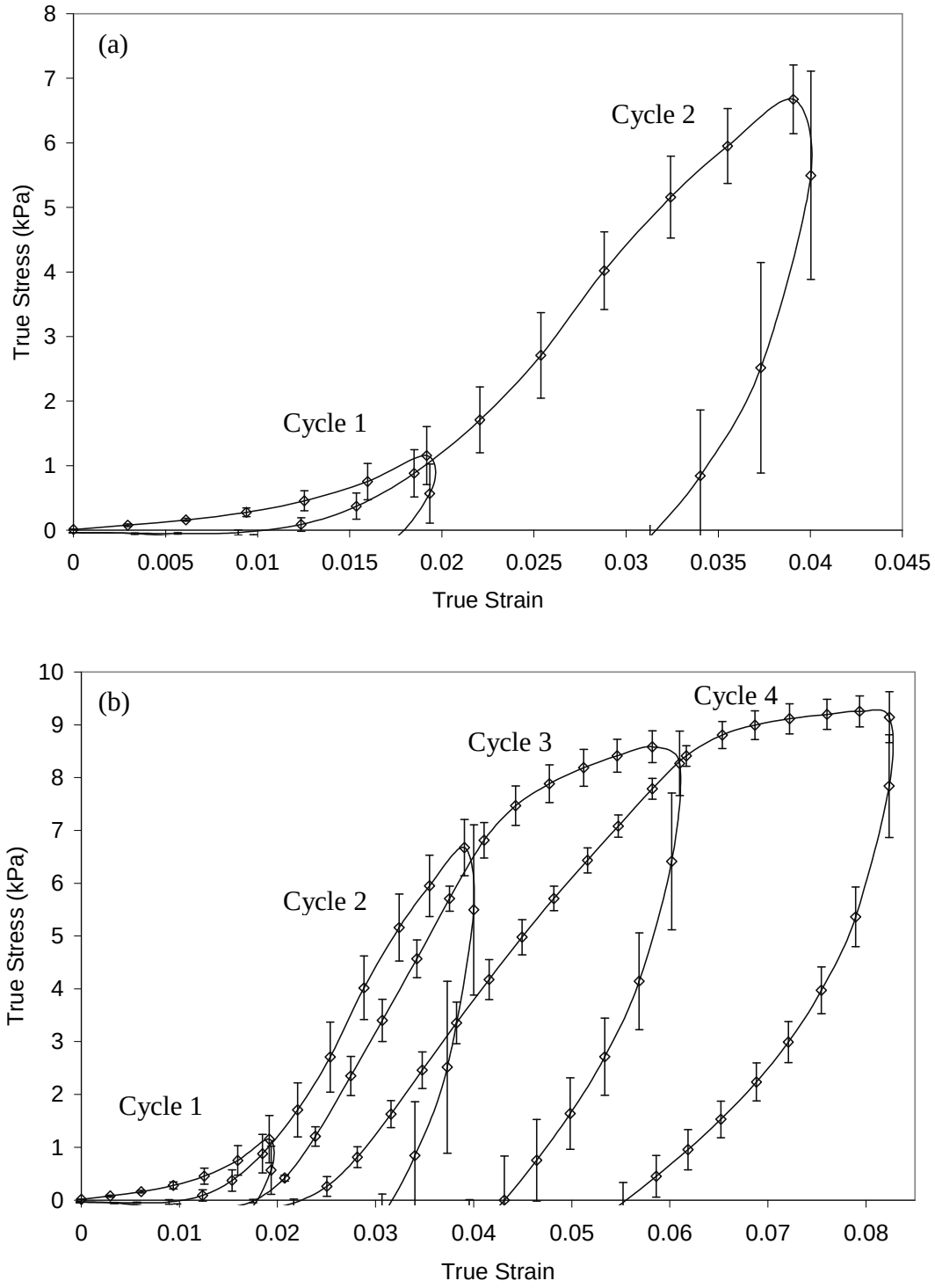

Figure 4. 7. Average cyclic uniaxial compression of vegetable shortening at 4 mm min^{-1}. (a) First two cycles up to 4% strain and (b) four cycles up to 8% strain. Error bars are one standard deviation

From Figure 4.7a it can only be concluded that the initial yield strain (ε_{y1}) is below 0.02. This upper limit for ε_{y1} should be taken into account when trying to develop a model to predict the rheological response of vegetable shortening, which is discussed later in this thesis.

4.5.2 Rate-Dependency Effect during Cyclic Compression

Similar to monotonic compression, cyclic compression exhibits the rate-dependency of vegetable shortening (Figure 4.9). The cyclic compression results are in agreement with the monotonic compression results; for vegetable shortening the true stress does not increase as the crosshead speed increases, all the curves lay within each other's error bars so that the stress peaks are not significantly different between the various crosshead speeds (Figure 4.9). However, the stress overshoot area extends over a larger strain range as the crosshead speed increases, just as it happens during uniaxial monotonic compression tests.

Also as with the monotonic compression the largest drop in stress in the overshoot region occurs at the lowest crosshead speed (4mm min^{-1}). Looking at Figure 4.8, one can see that a maximum stress of approximately 12 kPa in cycle 2 drops down to approximately 10 kPa in cycle 3 at 4 mm min^{-1}, this values correspond to stress values at equivalent strains during monotonic compression (Figure 4.8).

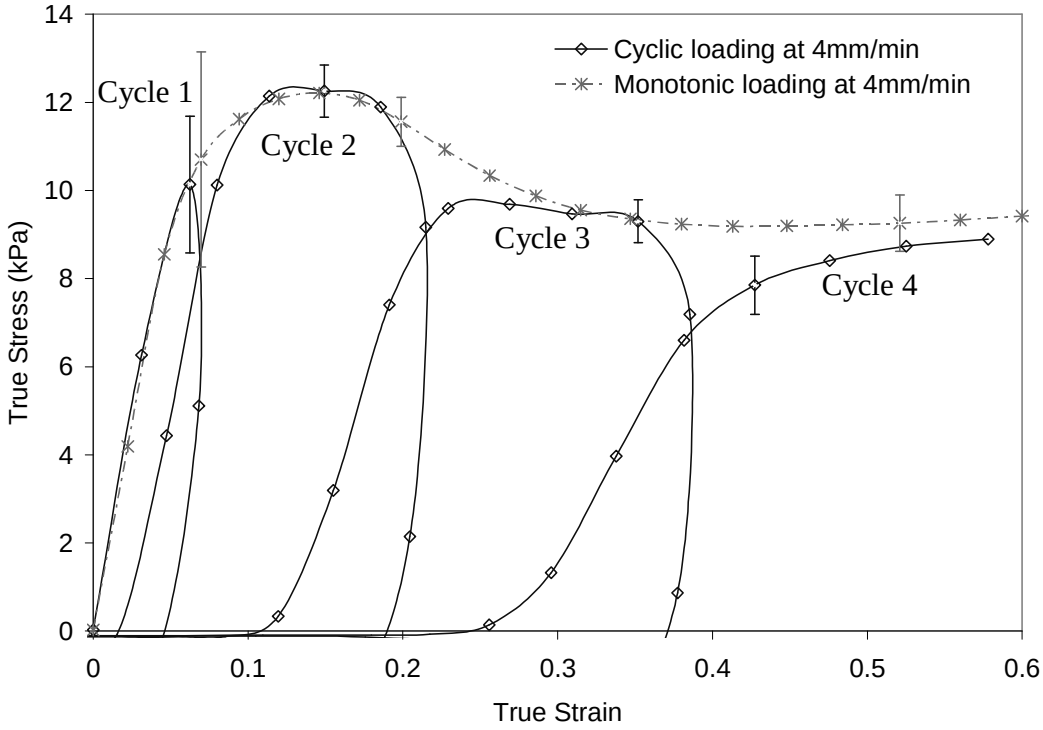

Figure 4. 8. Comparison between average cyclic and monotonic compression of vegetable shortening at 4 mm min^{-1}. Each curve is the average of 9 specimens with three different contact areas and error bars are one standard deviation

From Figure 4.9, it appears that the rate of unloading does not affects the slope of the unloading curve. From the unloading curve the unloading modulus can be calculated and be used as a measurement of the elasticity of a material. The following section describes how the unloading modulus was calculated.

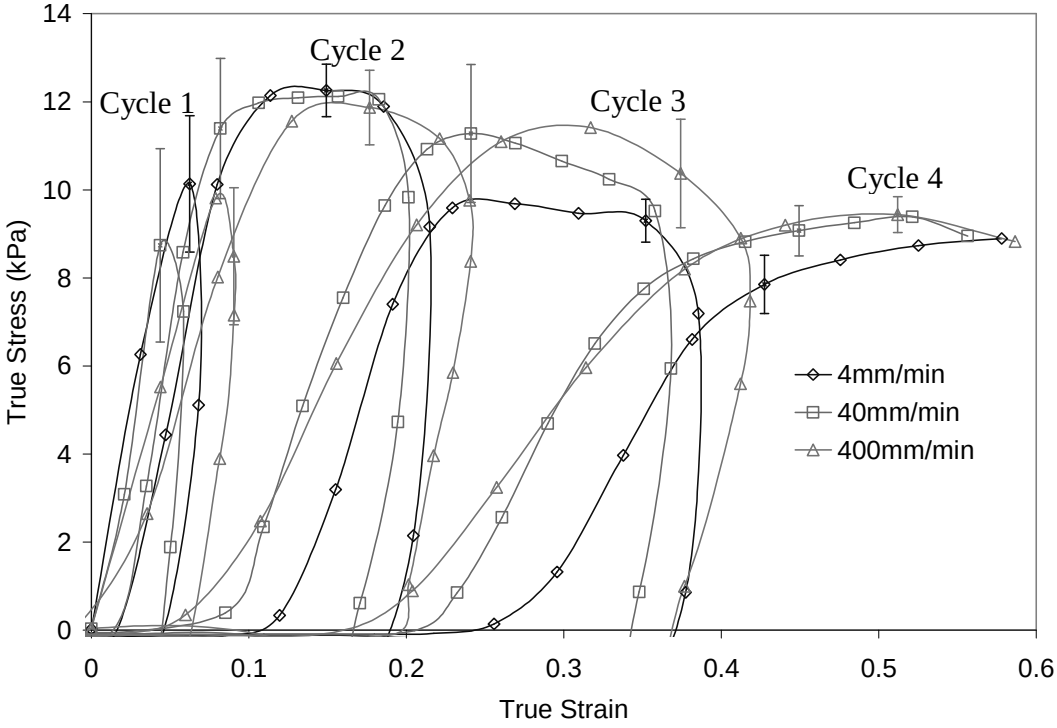

Figure 4. 9. Average cyclic uniaxial compression of vegetable shortening at three crosshead speeds. Each curve is the average of 9 specimens with three different contact areas and error bars are one standard deviation at selected strain values

4.5.3 Determination of Unloading Modulus

The unloading modulus can be used as a measure of the elasticity remaining in a material after it has been deformed. If the deformation is smaller than the yield strain then the unloading modulus and the modulus of elasticity (E) are equivalent (de With, 2006). However for large strains the loading modulus (E) has elastic and plastic components, unless the material is completely elastic, which is not the case of vegetable shortening.

The unloading modulus (E_U) is the tangent of the unloading portion of a stress-strain curve (Gunasekaran and Ak, 2003). Theoretically, the unloading process should be done in a continuous manner at constant rates, but in reality it is impossible to change the

direction of the compression-crosshead without first slowing down and stopping. Under the current experimental conditions, it was observed that at the end of each loading cycle the crosshead of the universal testing machine was starting to slow down and later stopping for a period of approximately 2 s, before unloading and starting to travel in the upward direction. Therefore a procedure to determine the unloading modulus was formulated to remove this systematic error:

1. The values of true-stress (σ) against the values of true-strain (ε) for cyclic loading at different crosshead speeds were plotted. When the crosshead is not moving the strain does not change, but the stress starts to decrease and this behaviour is shown essentially as a vertical drop in the stress-strain diagram (Figure 4.10). The lowest point of the vertical drop at the beginning of the unloading portion of the strain-stress curve was located and the corresponding time was found in the raw data given by the universal testing machine. The time period in which the strain remains constant should be less than or equal to 2.0s depending on the crosshead speed used during testing (4, 40 or 400mm min^{-1}).
2. The last data point of the vertical drop on the strain-stress curve was selected as well as the next 20, 10 or 3 data points to plot a line. The number of data points selected depended on the crosshead speeds, since less data points were collected at faster compression rates; so that at 4 mm min^{-1} 20 data points were used to plot a line, while at 40 mm min^{-1} 10 data points and at 400 mm min^{-1} 3 data points.
3. A linear trend line was fitted to the stress-strain data described in step 2 using MS Excel (Figure 4.10); the equation and the R-squared-value for the linear trend were displayed. If the R-squared-value was greater or equal to 0.99, the slope of

this equation represented the unloading modulus. If the R-squared-value was smaller than 0.99 then the data described in step 2 was shifted to the next or preceding data point (move up or down in Figure 4.10), until the R-squared-value was greater than or equal to 0.99.

4. This procedure (steps 1 to 3) was repeated for the three unloading cycles to which each 15x15 specimen was subjected and the average value over three replicates of the unloading modulus was calculated for each crosshead speed.

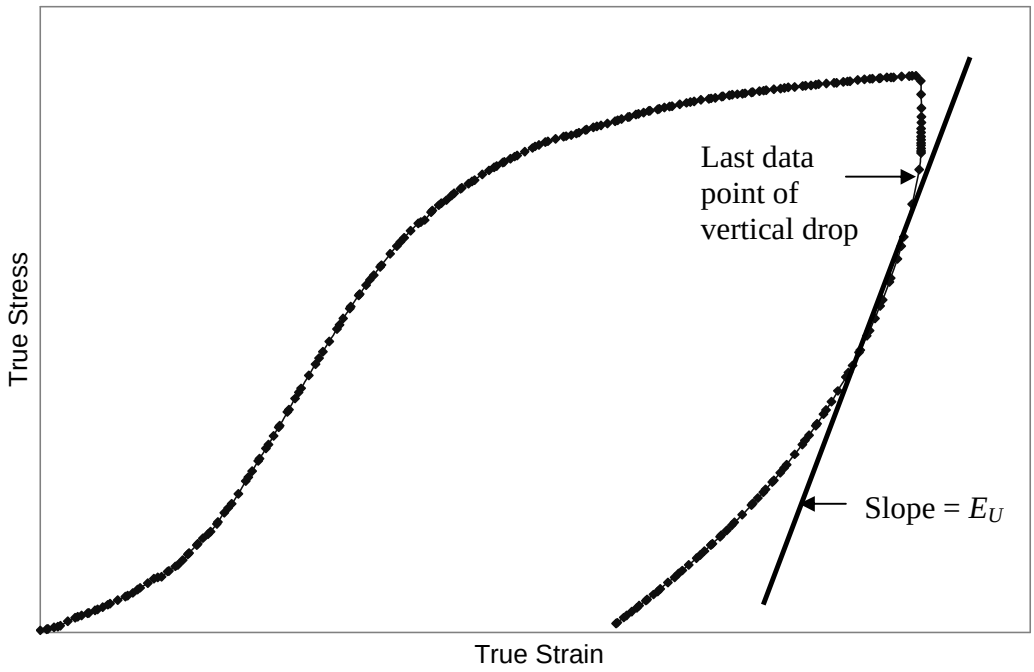

Figure 4. 10. Schematic representation of one cycle of loading-unloading curve

Using steps 1 to 4 a plot of unloading modulus against true strain was obtained (Figure 4.11). By looking at Figure 4.11, one can see that the unloading modulus of elasticity changes as the strain on the shortening increases. The maximum value for the unloading modulus (743 kPa) was found at approximately 4% true strain and after this strain the unloading modulus decays as the strain increases regardless of the crosshead speed.

Since from Figure 4.11 one can see that the unloading modulus is not rate dependent with the error bars of the unloading modulus overlapping with one another at the different crosshead speeds. The non rate dependency of the unloading modulus is expected since the unloading modulus is related to the elastic response of shortening and elasticity is a rate independent behaviour.

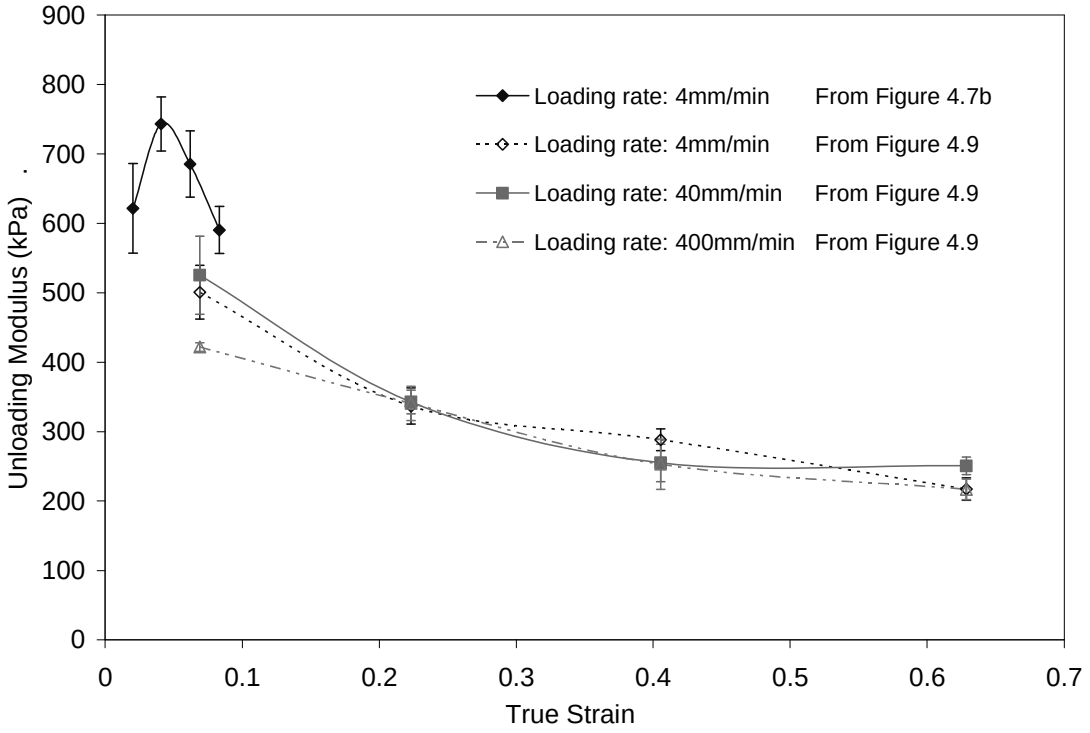

Figure 4. 11. Average unloading modulus for vegetable shortening as a function of true strain. Each curve is the average of three 15x15 shortening specimens and the error bars are one standard deviation

The unloading modulus calculated from the cyclic experimental compression cannot be used to describe the purely elastic response of vegetable shortening in its undisturbed native structure, since E_U is changing as the strain increases as a result of shortening having a plastic component. However this unloading modulus is a measurement of how elastic is the material after it has been subjected to large deformations. The values

obtained give a range of values that can be used to estimate the purely elastic modulus (Young's Modulus) of vegetable shortening. As seen in Figure 4.11, the value of the unloading modulus obtained from cyclic compression tests is between 216 and 743 kPa. This range of values was assumed to cover the range of values for the modulus of elasticity (*E*) when developing a model to simulate the rheological response of shortening (Sections 4.9.0 and 4.10.0 of the current chapter).

The change in the unloading modulus as a function of strain could be attributed to a change in the microscopic structure of vegetable shortening, similar to the structural change that occurs in metals and other crystalline solids when subject to excessive plastic deformation, such as dislocations or shear-banding (de With, 2006). The actual mechanisms occurring in vegetable shortening has not been determined yet.

4.5.4 Visual Analysis during Cyclic Compression

Photographs were taken during the unloading process of 15x15 shortening specimens, after being compressed by 6.5 mm, which is enough to cause shear failure. The results are shown in Figure 4.12. By looking at Figure 4.12 one can see that even after shortening has been compressed by 6.5 mm (Figure 4.12b), it retains a significant degree of elasticity since as soon as the compression platen starts to go up (Figure 4.12c) there is a recovery in height. If vegetable shortening did not have any elasticity left after compression, the specimen would not be able to recover any height. Approximately 31% (2/6.5 *100%) of the compressed distance is rapidly recovered after the compression

platen is removed from the vegetable shortening specimen, and this occurs after the specimen has experience shear failure (Figure 4.12d).

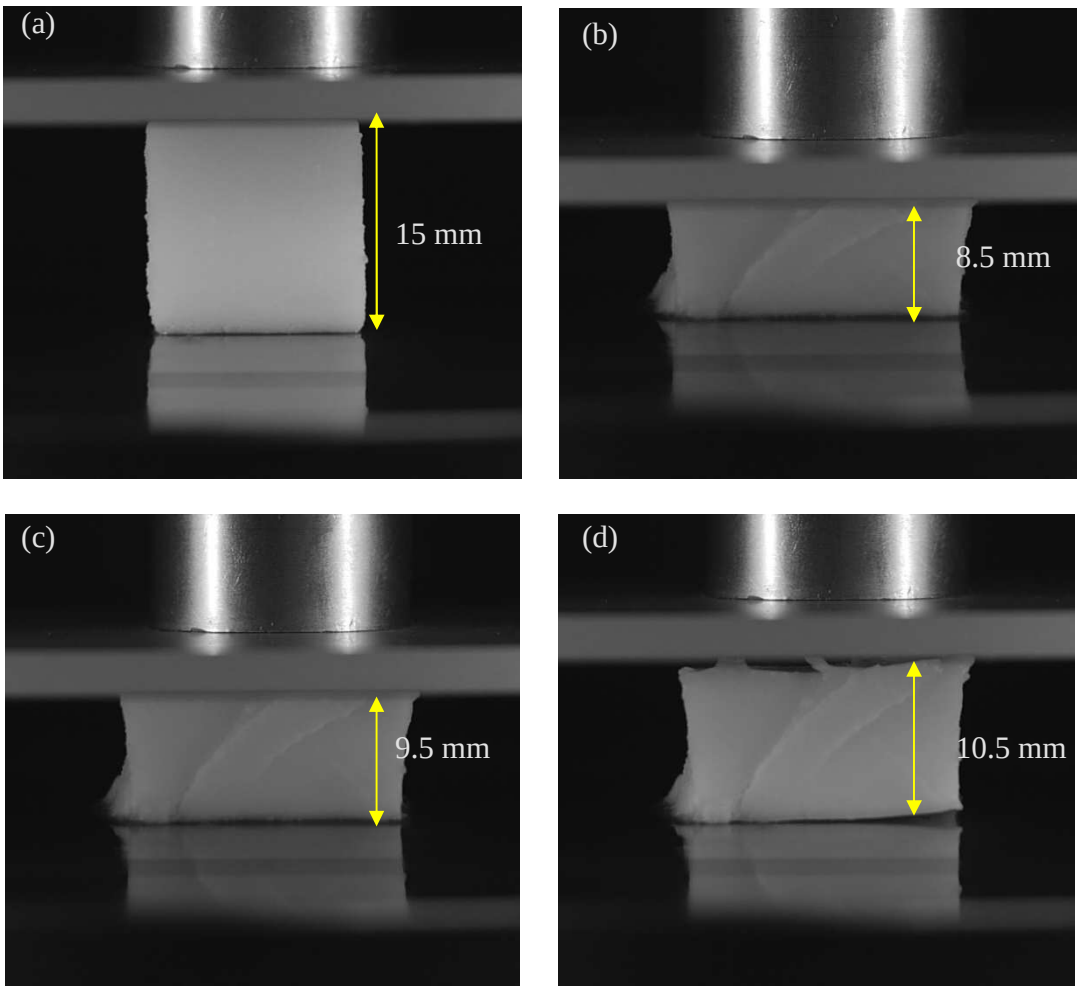

Figure 4. 12. Unloading process of a 15x15 shortening specimen. (a) Undeformed specimen, (b) specimen compressed by 6.5 mm, (c) specimen unloaded by 1 mm and (d) specimen after completely unloaded

4.5.5 Conclusions of Cyclic Compression

Cyclic compression of vegetable shortening revealed that the yield strain is below 0.02. The unloading modulus is not rate dependent and has a value between 216 and 743kPa which was dependent on the strain at which the modulus was calculated having a

maximum value at a strain of 0.04. By taking photographs during the unloading part of cyclic loading, one is able to conclude that despite the shear failure observed during larger strain compressions, vegetable shortening specimens are still very elastic.

4.6.0 Compressive Creep Test

Materials can be categorized by their creep response; a truly elastic material when subject to a constant stress would show a constant strain as time passes, a viscous material on the other hand would show a linear increase in strain as time passes (Steffe, 1996). The creep response of vegetable shortening (Figure 4.13) is something in between a truly elastic and a viscous material and for this reason vegetable shortening is sometimes classified as a viscoelastic material (Rao, 2007).

Shortening samples were subjected to different stresses by changing the applied load (0.5, 2.5 and 5.0N) and the specimen contact area (15x15, 22.5x22.5 and 30x30mm); sample results are shown in Figure 4.13. The load was applied at a rate of 400 N s^{-1}, since the load should be applied instantaneously during creep tests. The shape of the creep curves are very similar no matter what the loading conditions were as shown in Figure 4.13. The curves in Figure 4.13 show the true strain increasing with time but the rate of change becomes smaller as time passes and the strain approaches a constant value or equilibrium strain, which is a characteristic behaviour of a viscoelastic solid (Kinsella, 1987; Steffe, 1996; Rao, 2007).

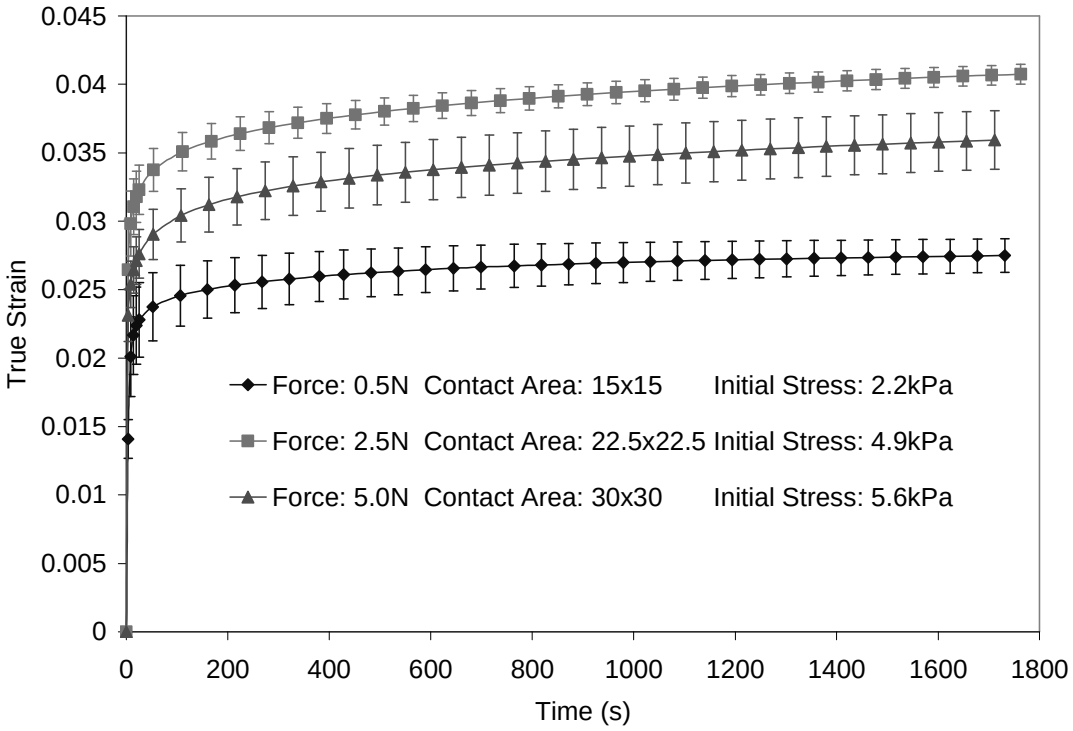

Figure 4. 13. Average compression creep test results for vegetable shortening subjected to three different stress conditions. Each curve is the average of three specimens and error bars are one standard deviation calculated from the same three specimens

The equilibrium strain was measured as the *y*-intercept of the fitted straight line to the last 200 data points of a strain-time curve obtained during creep tests. The general trend is that as the applied force increases and the size of the contact area decreases (i.e., the applied stress increases) the equilibrium true-strain increases; this was an expected result due to the direct relationship between stress and strain. The equilibrium true-strain values range from 0.02 when shortening is subjected to 0.56 kPa (0.5N applied to a 30x30 specimen) to 1.00 when subjected to 22.2 kPa (5N applied to a 15x15 specimen); the range of values for the equilibrium strain are shown in Figure 4.14.

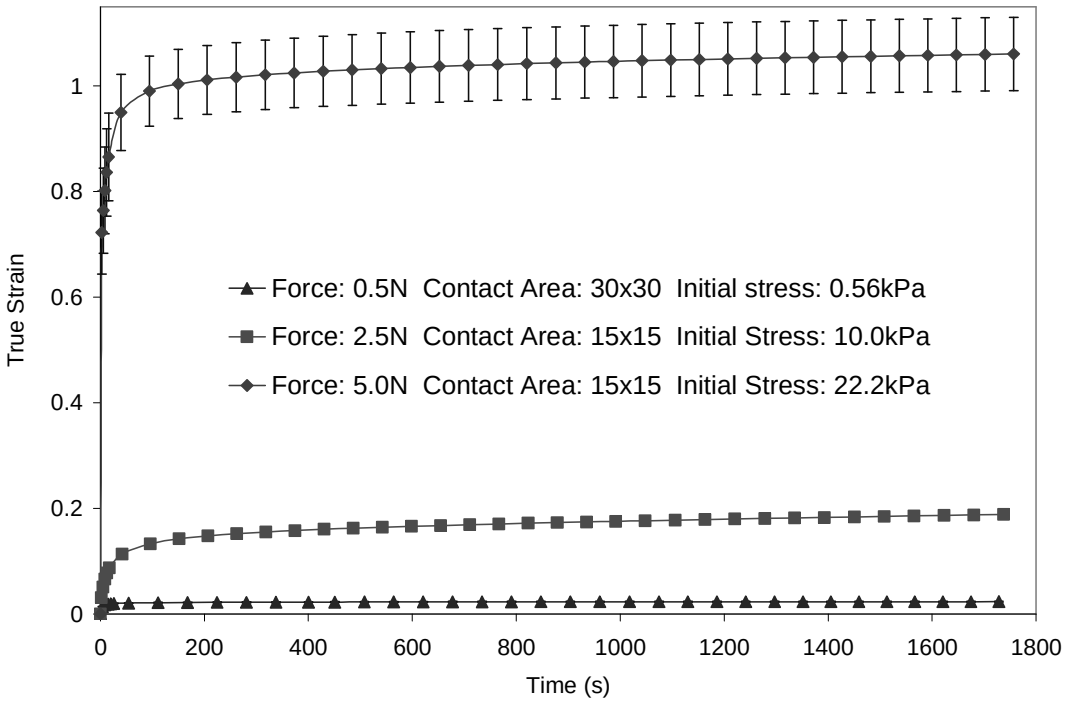

Figure 4. 14. Creep test results for vegetable shortening specimens subjected to three loading conditions, showing the maximum, intermediate and minimum equilibrium strain. Each curve is the average of three curves and error bars are one standard deviation

4.6.1 Compliance and Viscosity from Creep

Creep tests results are commonly shown in a curve of compressive creep compliance (D) as a function of time. Creep compliance is the ratio of strain as a function of time divided by the constant stress. After sufficient time has passed it can be assumed that the creep response is purely viscous and two material parameters can be obtained from the linear portion of the compliance versus time curve; these parameters are the biaxial viscosity (η_b) and the biaxial compliance (D_b) (Rao, 2007). Biaxial viscosity is the inverse of the slope of the linear portion of the compliance-time curve that is reached after a certain amount of time has passed in a creep test. For a viscoelastic solid the slope would be zero (a horizontal line) and the biaxial compliance is the y-intercept of the linear portion of the

compliance time curve (Steffe, 1996; Rao, 2007). In order to obtain the biaxial viscosity and biaxial compliance from the creep tests data, a procedure was followed that is described here:

1. The first step to find η_b and D_b was to convert the true-strain versus time curve into compliance-time curve. Compliance was calculated by dividing the strain values at a given time by the stresses at the same time. Note that the stress was not constant during creep test, since the contact area was changing with time even though the force remained constant.
2. Once the compliance was calculated for each of the replicates, the values were averaged. The last 20 seconds of the average compliance-time data (approximately 200 data points) were plotted and a linear trend line was fitted through them using MS Excel. The equation for the linear trend was displayed.
3. From the equation of the linear trend the slope and the y-intercept were extracted. The inverse of the slope was reported as the biaxial viscosity (η_b) and the *y*-intercept was reported as the biaxial compliance (D_b).

Following steps 1 to 3 the biaxial viscosity and biaxial compliance for vegetable shortening subjected to the different loading conditions were calculated; the values for η_b and D_b are shown in Figures 4.15 and 4.16 respectively.

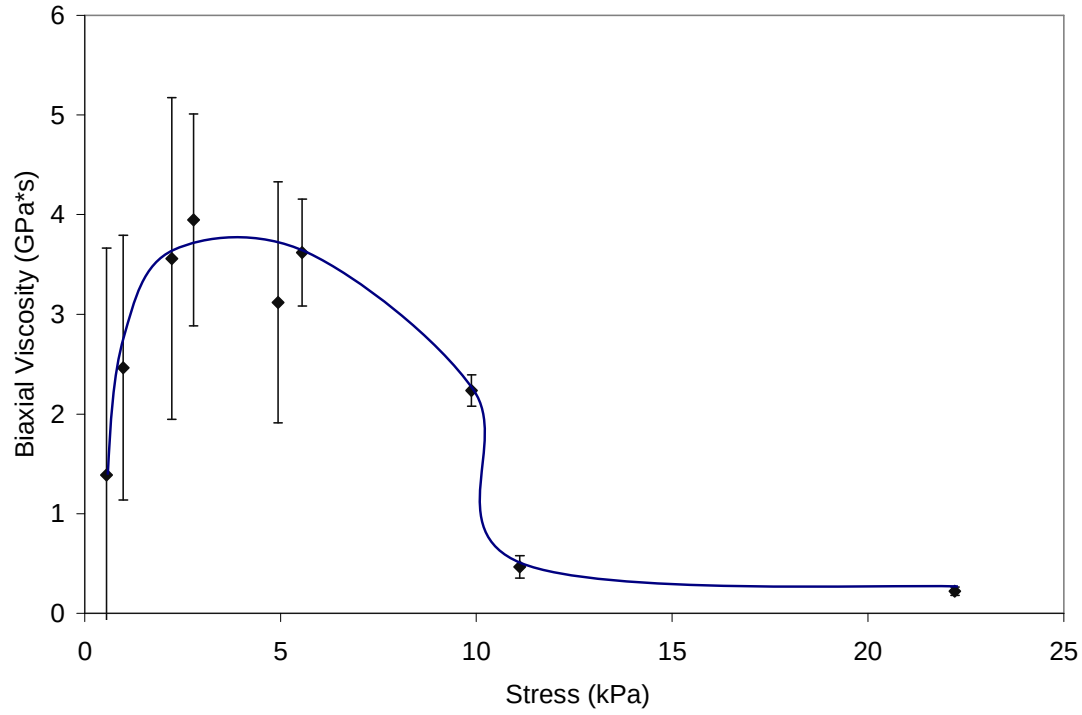

Figure 4. 15. Average biaxial viscosity of shortening as a function of engineering stress

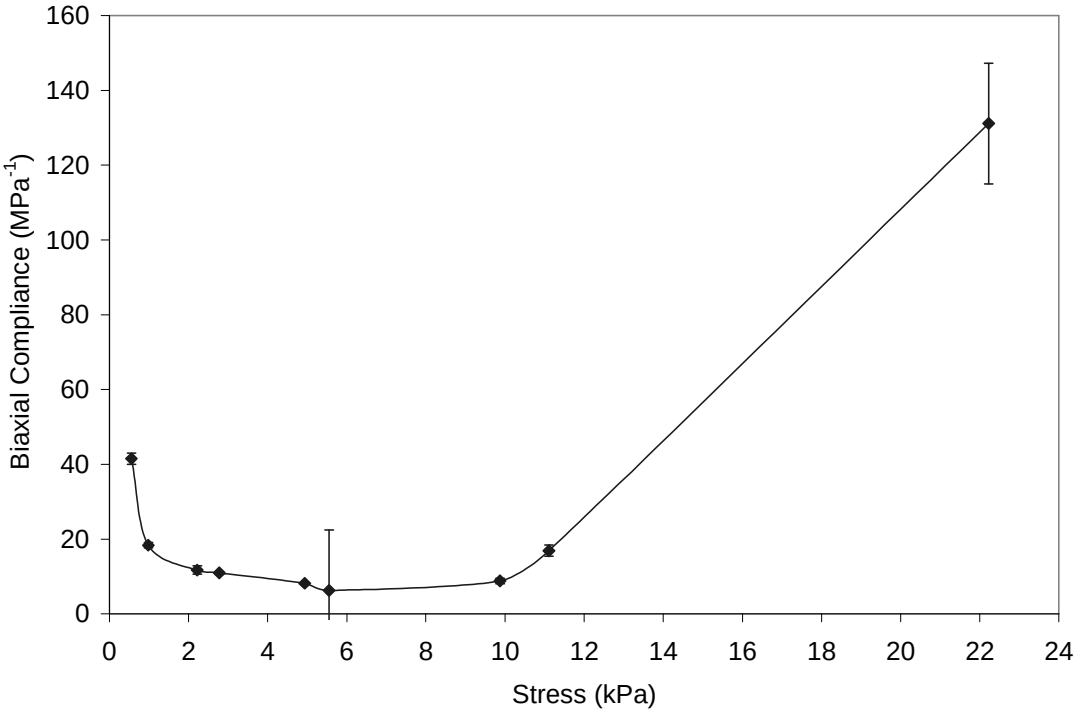

Figure 4. 16. Average biaxial compliance of shortening as a function of engineering stress

The biaxial viscosity values of vegetable shortening are dependent on the amount of stress at which they are measured. The highest value measured was at approximately 2.8 kPa. At stresses higher than 10 kPa, the viscosity appears to be approaching a constant small value, but further testing is required to be conclusive. The biaxial compliance also varies with the stress, between 0.5 and 10 kPa the compliance decays as the stress increases, beyond 10 kPa the compliance increases as the stress increases. By looking at Figure 4.15 one can see the viscous-like behaviour of vegetable shortening. Shortening is getting more resistant to flow as stress increases to a certain value (2.8 kPa), but once exceeded shortening starts to behave more like a liquid than a solid, hence the decrease in viscosity (Figure 4.15). This increase and decrease in viscosity is reminiscent of the change in elastic modulus values observed in section 4.5.3. From Figure 4.16 one can conclude that increasing the stress applied to shortening increases the compliance, and higher compliance is a characteristic of materials that can be classified as liquids (Steffe, 1996).

4.6.2 Conclusion from Compressive Creep Tests

Vegetable shortening can be classified as a viscoelastic solid, since its true strain-time curve obtained during compressive creep tests seems to be approaching an equilibrium stress in the long term, but this equilibrium stress changes with the amount of stress applied to specimens. The biaxial viscosity and the steady state compliance are not constant as the applied stress increases. Increasing the applied initial strain causes shortening to behave more like a liquid with lower viscosity and higher compliance.

4.7.0 Compressive Stress Relaxation Test

During stress relaxation tests a constant deformation or strain is held for a period of time. As time passes the stress in the material starts to decay until an equilibrium point is reached which can be zero or greater than zero, depending on whether the material being tested is liquid or solid. The stress relaxation curve is different depending on the type of material tested; a perfectly elastic material will show no relaxation, an ideal viscous material will show instantaneous relaxation, while a viscoelastic material will show a gradual decay in stress with time (Steffe, 1996).

4.7.1 Specimen Size Effect during Stress Relaxation Tests

The effect of the specimen size was also investigated during stress relaxation tests. Student t-test comparisons (95% confidence interval, 2 tail) were done between the different specimens size in order to determine if the stress after 20 minutes was significantly different between specimens of different sizes compressed to the same initial true strain. The results of the different t-test comparisons are shown in Table 4.4.

A total of 18 comparisons were made and 10 of them were not significantly different, so it was concluded that the specimen size did not affect the stress measurements during the stress relaxation tests and therefore the stress-time curves were plotted from the average of 9 specimens (3 replicates and 3 different sizes).

Table 4. 4. Student t-test comparison between stress values at 20 minutes of stress relaxation tests for specimens of different sizes.

Crosshead speed (mm min^{-1})	Initial true strain	Specimen size comparison (mm)	T-test value (95% Confidence, 2 tail)	Significantly different (Yes/No)
4.0	0.0339	15 vs. 22.5	0.00883	Yes
4.0	0.0339	15 vs. 30	0.00517	Yes
4.0	0.0339	22.5 vs. 30	0.00199	Yes
4.0	0.1431	15 vs. 22.5	0.13458	No
4.0	0.1431	15 vs. 30	0.98645	No
4.0	0.1431	22.5 vs. 30	0.12502	No
4.0	0.4055	15 vs. 22.5	0.01617	Yes
4.0	0.4055	15 vs. 30	0.00789	Yes
4.0	0.4055	22.5 vs. 30	0.08189	No
40.0	0.0339	15 vs. 22.5	0.01640	Yes
40.0	0.0339	15 vs. 30	0.08334	No
40.0	0.0339	22.5 vs. 30	0.00728	Yes
40.0	0.1431	15 vs. 22.5	0.05423	No
40.0	0.1431	15 vs. 30	0.00306	Yes
40.0	0.1431	22.5 vs. 30	0.51956	No
40.0	0.4055	15 vs. 22.5	0.59166	No
40.0	0.4055	15 vs. 30	0.29454	No
40.0	0.4055	22.5 vs. 30	0.05010	No

4.7.2 Classification of Shortening from Stress Relaxation Response

According to the stress relaxation test results obtained for vegetable shortening, shortening can be classified as a viscoelastic solid because there is a gradual decay towards an equilibrium stress which is greater than zero (Figure 4.17). Vegetable shortening specimens were subject to three different deformations (0.5, 2.0 and 5.0 mm) and the basic shape of the relaxation curve is the same for these different loading conditions, but the equilibrium stress is different depending on the loading conditions. If the applied strains were in the linear viscoelastic region of shortening the stress relaxation curves would overlap one another (Steffe, 1996), but this is not the case for the selected compressive strains.

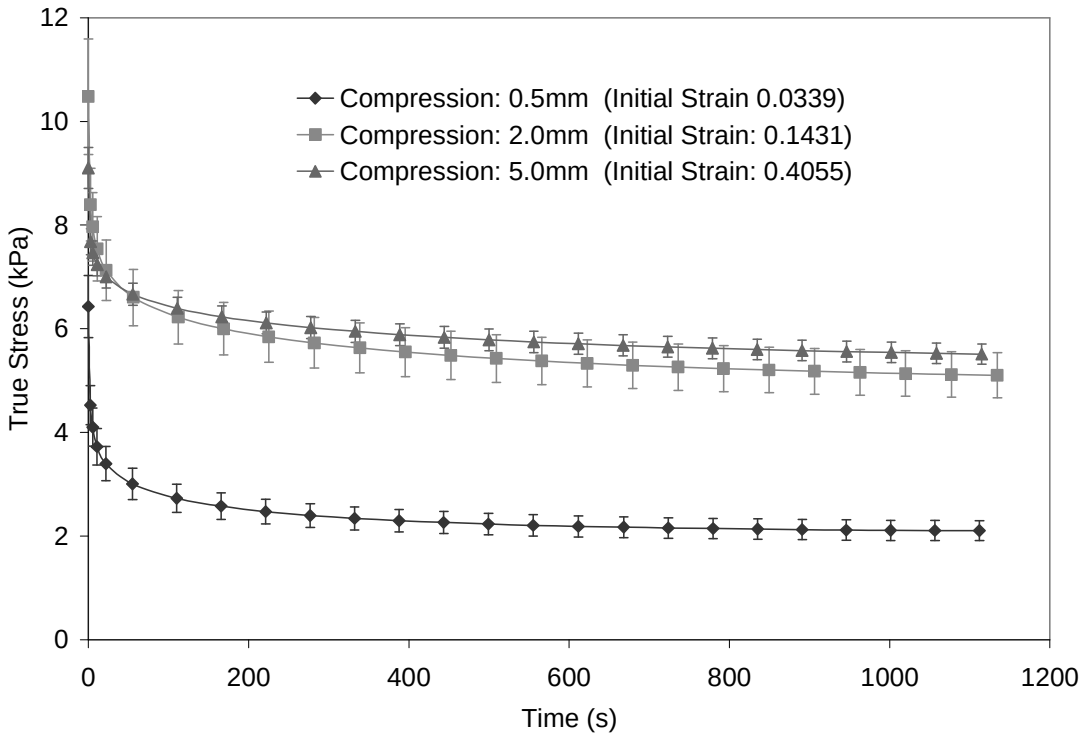

Figure 4. 17. Average stress relaxation curves for vegetable shortening after three compression distances applied at an initial rate of 40 mm min^{-1}. The curves are the average of nine specimens and error bars are one standard deviation

The equilibrium stress for the different stress relaxation treatments was calculated following the next steps:

1. The true stress-time curve was plotted for each of the 18 treatments of stress relaxation tests.
2. The last 20 seconds of the stress relaxation tests were selected and a linear trend line was fitted through these data points, using MS Excel. The equation of the line was displayed.
3. The *y*-intercept of the fitted linear trend line was reported as the equilibrium stress. The average of the three replicates per treatment was calculated and plotted against the initial applied true strain (Figure 4.18)

The equilibrium stress increases as a function of applied initial strain. By looking at Figure 4.17, one can see that when the initial applied strain increases from 3.4% to 14.3% there is a three-fold increase in the final stress value (equilibrium stress). However when the initial applied strain increases from 14.3% to 40.5% the increases is not significantly different since the two curves lie within each other's error bars. The equilibrium stress appears to remain constant after the strain increases beyond 14% (Figure 4.18). Because the equilibrium stress of vegetable shortening remains constant in a large range of stresses (14 to 41%) and is not equal to zero, this implies that vegetable shortening behaves like a viscoelastic solid even at large deformations.

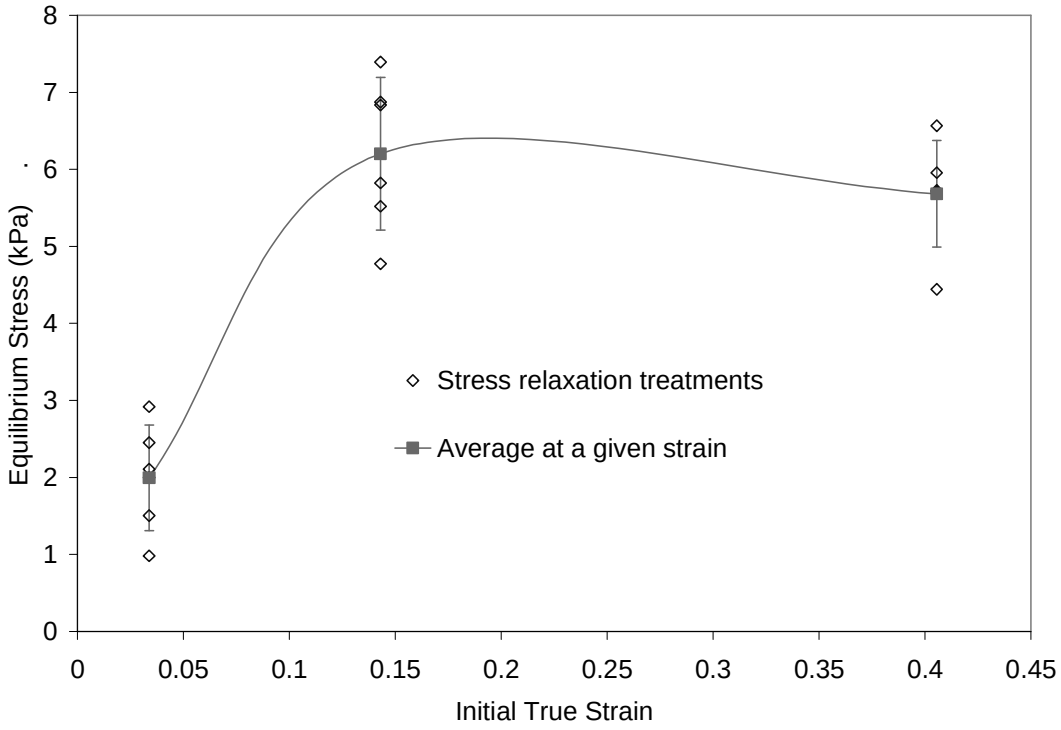

Figure 4. 18. Equilibrium stress as a function of strain; each hollow data point represents the average result of three replicate treatments. The solid data points are the average at a given applied strain and the error bars are one standard deviation

4.7.3 Rate Dependency during Stress Relaxation

During a stress relaxation test, theoretically the constant deformation should be applied instantaneously (Menard, 1999) but this is impossible in real life due to physical limitations of the universal testing machine or any other measuring device. Two initial loading rates were investigated (4 and 40 mm min^{-1}) to try to qualify the rate dependency of shortening during the stress relaxation test. Figure 4.19 shows that as the initial loading rate increases there is also an increase in the true-stress at a given time during the holding period (18 minutes) of the stress relaxation tests.

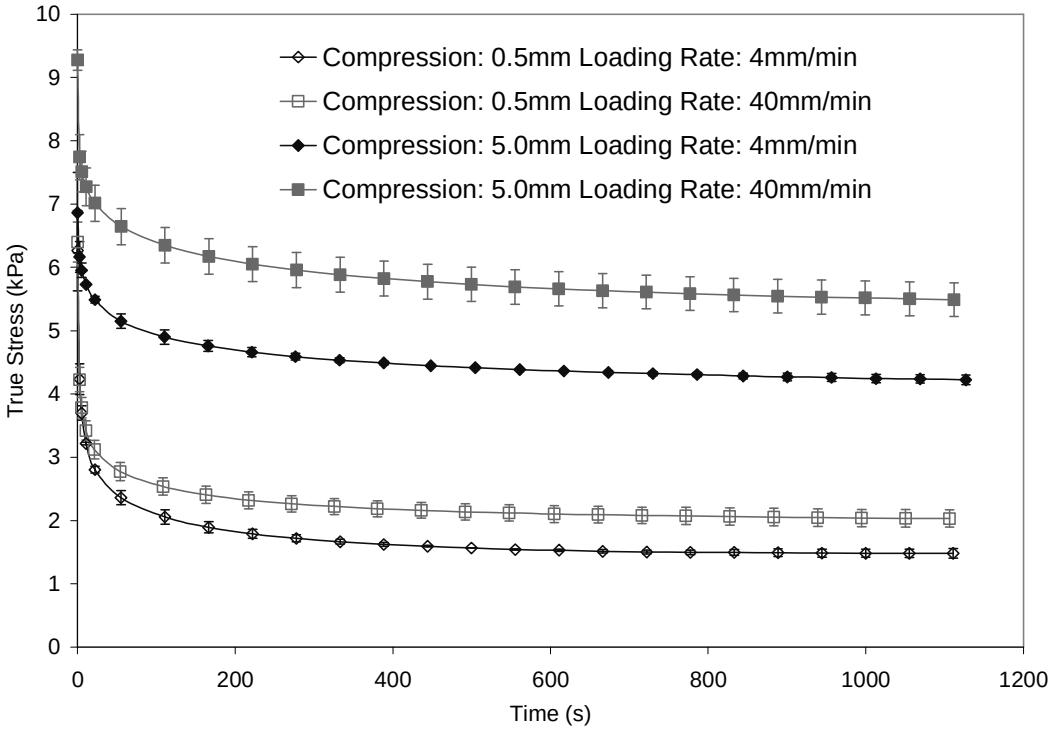

Figure 4. 19. Stress relaxation curve for vegetable shortening after compression to two distances (0.5, 5.0 mm) at two initial loading rates (4, 40 mm min^{-1}). The curves are the average of three 15x15 specimens and the error bars are one standard deviation from the same three specimens

The results of Figure 4.19 suggest that a higher loading rate (40 mm min^{-1}) can cause shortening to undergo more hardening and for this reason the stress at a given time is

higher as compared to a lower loading rate (4 mm min^{-1}). This result is not uncommon of rate-dependent materials which can show higher stresses when subjected to higher loading rates (Gunasekaran and Ak, 2003; Goh and Scanlon, 2007).

4.7.4 Stress Relaxation Time

The stress relaxation time (τ') is defined as the time (t) it takes for the stress to decay to e^{-1} of its initial value (σ_I); this definition is derived from the Maxwell model for viscoelastic materials which predicts the decay of a material from σ_0 to zero stress and is given by the following equation (Steffe, 1996):

$$\sigma(t) = \sigma_I e^{\frac{-t}{\tau'}} \qquad [4.1]$$

The stress relaxation experiments revealed that when a shortening specimen was subjected to large true strains (14 and 40%) its stress was not able to decay e^{-1} (~36.8%) in 20 minutes; therefore the stress relaxation time could not be obtained for these specimens. Only when the strain was kept at approximately 3.3% (compression by 0.5mm) were shortening specimens able to decay e^{-1} of their initial stress. During small strain experiments the overall structure of materials is less affected and it is possible for bonds to break and reform which may result in relaxation and flow (Kloek et al, 2005) in a shorter period of time. When large deformation is applied to food products such as vegetable shortening, the initial structure is irreversibly altered, bonds are permanently broken and the structural elements may rearrange in a new manner (Kloek et al, 2005); therefore the relaxation behaviour is changed due to structural changes undergone during large deformations.

The relaxation time for shortening at low strain (3.3%) is shown in Table 4.5. Table 4.5 shows that the size of the specimen affects the relaxation time. In general it can be said that increasing the contact area increased the relaxation time, except for one of the treatments (30x30 at 4mm/min). As discussed earlier, 0.5mm was the limit of accuracy during the preparation of specimens; therefore it is not advisable to derive any definite conclusions from measurements done after compressing samples by 0.5 mm. It is possible that the lack of homogeneity in dimensions can account for the variability in the relaxation time.

Table 4. 5. Parameters used to calculate relaxation time of vegetable shortening at 3.3% constant strain (0.5mm deformation)

Specimen Dimensions (mm)	Initial Loading Rate (mm min^{-1})	Average decay stress of $\sigma_i e^{-1}$ (kPa)	Average Relaxation Time (s)
15 x 15 x 15	4	2.15	117.5
22.5 x 22.5 x 15	4	3.11	552.6
30 x 30 x 15	4	1.64	31.3
15 x 15 x 15	40	2.35	132.0
22.5 x 22.5 x 15	40	2.59	438.8
30 x 30 x 15	40	2.16	530.7

4.7.5 Compressive Relaxation Modulus

The compressive relaxation modulus ($E_R(t)$) is a factor that relates the stress to the strain during stress relaxation tests (cf equation 2.23). The compressive relaxation modulus can be calculated by dividing the measured stress during the relaxation test by the applied strain, and then these values can be plotted as a function of time ($E_R(t)$ vs. t). To characterize the relaxation modulus behaviour of shortening, the *y*-intercept of this plot extrapolated from the almost horizontal portion of the curve obtained from the last 20 seconds of the stress relaxation test was taken as the long term compression relaxation modulus. The general trend for the long term compression relaxation modulus shows a

decrease in the relaxation modulus as the applied strain increased (Figure 4.20). This decay in relaxation modulus as the applied strain increases is similar to the unloading modulus decay seen during cyclic compression testing.

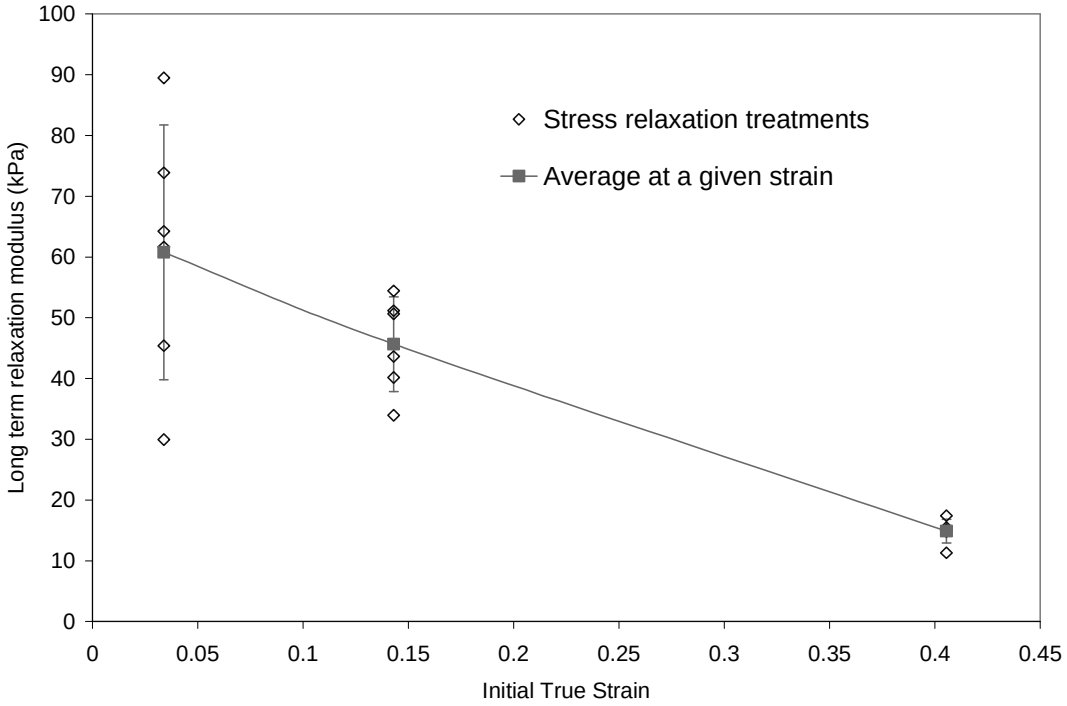

Figure 4. 20. Long term relaxation modulus as a function of initial true strain; each hollow data point represents the average result of three replicate treatments. The solid data points are the average at a given applied strain and the error bars are one standard deviation

4.7.6 Conclusions from Stress Relaxation Tests

From its stress relaxation response, vegetable shortening can be classified as a viscoelastic solid because an equilibrium stress greater than zero is reached no matter the amount of strain applied to the specimens. The equilibrium stress value is dependent on the amount of strain applied to the specimen. Rate dependency was observed during stress relaxation of shortening; the faster the initial loading the higher the value of the true stress at a given time. The long term relaxation modulus of vegetable shortening

decreases as the applied strain increases. The stress relaxation data can be used to calibrate viscoelastic models and this is the focus of section 9 of this chapter.

4.8.0 Uniaxial Monotonic Indentation

Uniaxial indentation testing has been widely used to estimate material mechanical properties (Habbab et al, 2006). Indentation tests can be done on specimens of any size even micromaterials and materials in service while compressive and tensile test require the preparation of standard specimens, and since indentation is essentially non-destructive it can be performed on very specific local areas (Jeon et al, 2006), it has a great potential to be used as a routine test for quality control of materials, including vegetable shortening.

4.8.1 Specimen Size Effects during Indentation

Results of a typical indentation test are presented as a load-depth curve, which records the continuous variation of indentation depth with load applied by an indenter of specific shape. For this particular study a self similar 45° (half angle) conical indenter was selected. The indentation was carried out on specimens of two different contact areas to observe specimen size effects. Figure 4.21 shows the load-depth curve for vegetable shortening specimens of two contact areas.

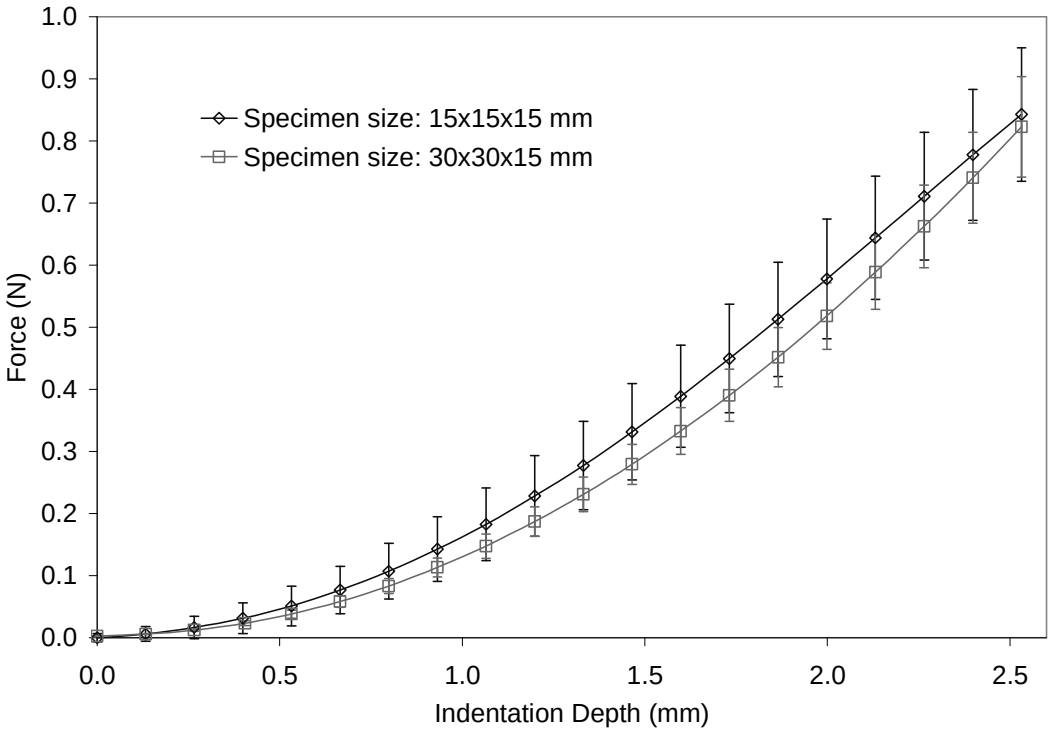

Figure 4. 21. Indentation response of vegetable shortening specimens of two different contact areas at indentation rate of 400 mm min^{-1}. Curves are the average of three replicates and error bars represent one standard deviation

According to Anand (2001) the specimen dimensions can in fact affect the indentation results, but only if the indentation depth is very large compared to the lateral dimension of the specimens. As seen in Figure 4.21, the average reaction force at indentation depths below 0.75 mm is very close between specimens of various sizes, but as the indentation depth increases beyond 0.75 mm the force of the 15x15 specimens is higher than that of the 30x30 specimens. However, the variability in the reaction force between specimens of the same size was greater for 15x15 specimens than for the 30x30 specimens, as seen by the error bars in Figure 4.21. The data points for the 15x15 specimen curve have error bars that include the values for the force response of the 30x30 specimens, and the error bars of the 30x30 specimen data points are within the error bars of the 15x15 specimen

curve; therefore it can be concluded that specimen size during the indentation of vegetable shortening does not affect the indentation response.

4.8.2 Rate Dependency during Indentation

As seen in the monotonic and cyclic uniaxial compression, vegetable shortening has a rate-dependency that affects the shape of the stress-strain curve rather than just increasing the stress values at a given strain as the loading rate increases. The rate-dependency during uniaxial monotonic indentation was also investigated during conical indentation and the results are shown in Figure 4.22.

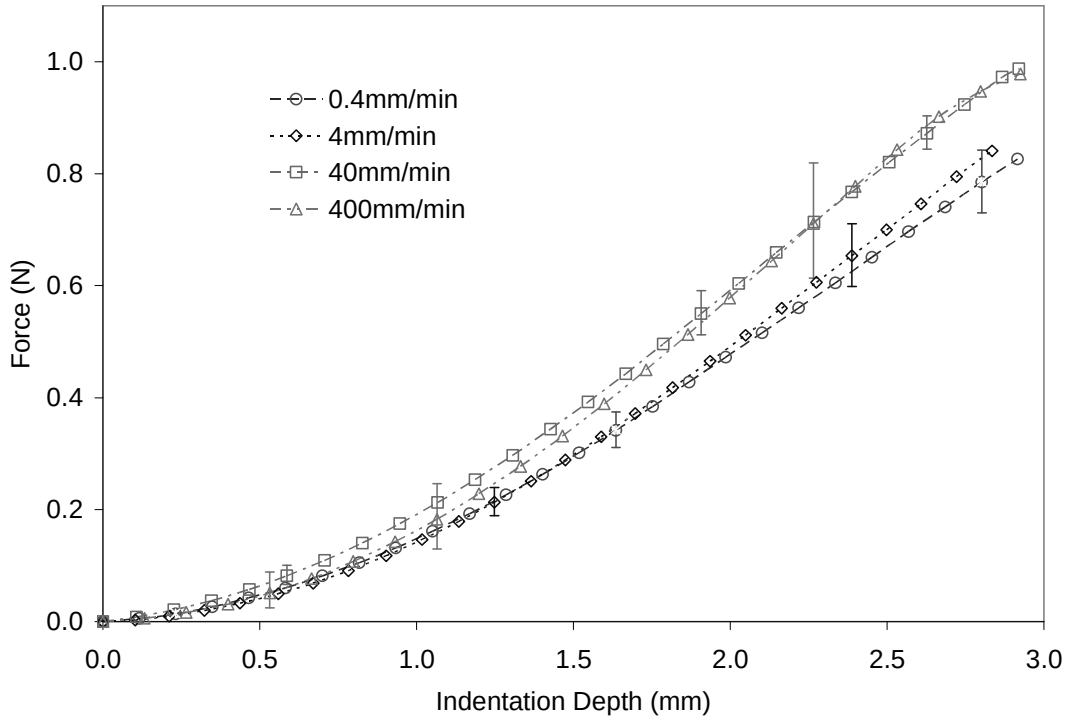

Figure 4. 22. Indentation response of vegetable shortening 15x15 cubic specimens loaded at four different crosshead speeds. Each curve is the average of three replicates and the error bars are one standard deviation

By looking at Figure 4.22, one can conclude that no rate dependency is apparent during the conical indentation of vegetable shortening, since the force error bars of each of the curves overlap at almost every given indentation depth. In order to confirm the rate independence during indentation a student t-test (2 tails, paired, 95% Confidence Interval) was done at an indentation depth of 2.5 mm between the forces measured during the indentation of vegetable shortening at different indentation rates. The results of the t-tests are shown in Table 4.6.

Table 4. 6. Student t-test comparison between force measurements obtained from indentation of cubic 15x15 vegetable shortening specimens at four indentation rates

Comparison between indentation rates (mm min^{-1})	Student T-test value (95% confidence interval, 2 tails)	Significantly Different (Yes or No)
0.4 vs. 4.0	0.609639	No
0.4 vs. 40.0	0.043913	Yes
0.4 vs. 400.0	0.129851	No
4.0 vs. 40.0	0.020304	Yes
4.0 vs. 400.0	0.142573	No
40.0 vs. 400.0	0.652971	No

Looking at Table 4.6 one can see that six comparisons were made from which four are not significantly different; therefore confirming the observations made in Figure 4.22 that no rate dependency was observed in the indentation of vegetable shortening.

4.9.0 Simulation of Vegetable Shortening as a Viscoelastic Material

It has been suggested in the literature that lipid-rich foods have viscoelastic behaviour (Shellhammer et al, 1997; Wright et al, 2001; Goh et al, 2004a; Rao, 2007), and for this reason it was decided to investigate the use of a viscoelastic model to simulate the mechanical response of all purpose vegetable shortening.

Viscoelastic behaviour can be observed in a number of tests, but most clearly when performing tests such as creep and stress relaxation. Creep and stress relaxation tests can be performed under shear, uniaxial or triaxial tension and compression. Uniaxial compression tests were used because of their simplicity to perform and the availability of a universal testing machine.

4.9.1 Abaqus Viscoelastic Model

Time-dependent viscoelastic materials, in which dissipative losses are primarily caused by internal damping or viscous effects, can be modeled using the VISCOELASTIC option in the material properties section of Abaqus. The viscoelastic material model describes isotropic rate-dependent material behaviour; it has to be used with elastic models, such as ELASTIC, HYPERELASTIC and HYPERFOAM; it can be used in large-strain problems and can be calibrated using creep test data, relaxation test data, or frequency-dependent cyclic test data (Abaqus, 2006).

For this particular study ELASTIC and VISCOELASTIC models were selected from the mechanical models available in Abaqus/CAE version 6.6. The Abaqus elastic model is just a general linear elastic model that is completely defined by two parameters, the Young's modulus or modulus of elasticity (E) and the Poisson's ratio (ν). The elastic model is visualized as a spring in which the stress (σ) is directly proportional to the strain (ε), with the proportionality constant being the modulus of elasticity, as shown in equation [2.7], which can be rewritten as: $\sigma = E\varepsilon$.

The Abaqus viscoelastic model is based on the generalized Maxwell model (Peleg and Pollak, 1982) that is generally visualized as a dashpot connected in series to a spring and is mathematically described with the following equation:

$$\sigma(t) = \sigma_e + Y(t) \qquad [4.2]$$

where t is time, σ_e is the equilibrium stress and $Y(t)$ is the relaxation function that is generally modeled as a Prony series, which has a mathematical expression of the following form (Chen, 2000):

$$\sum_{i=1}^{N'} \bar{g}_i^{\,p} e^{(t/\tau_i^G)} \qquad [4.3]$$

where $\bar{g}_i^{\,p}$ and τ_i^G are material constants in the viscoelastic model, N' is the total number of elements in the series and t is time, which is not a constant.

4.9.2 Abaqus Viscoelastic Model Input

Abaqus can be used to evaluate the behaviour of viscoelastic materials by automatically creating a response curve based on creep or stress relaxation test data. However Abaqus can only use creep and stress relaxation data from volumetric (triaxial) deformation tests or shear deformation tests or by using data from both sets of these tests.

Volumetric deformation occurs when a material specimen is subjected to uniform normal forces on all of its faces (Ferry, 1970). A schematic representation of a volumetric test is shown in Figure 4.23.

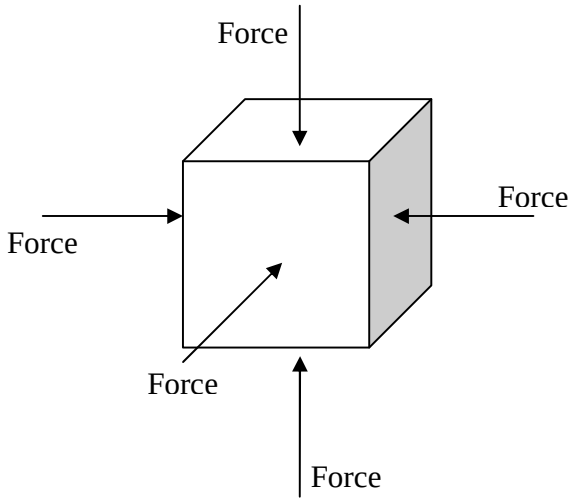

Figure 4. 23. Volumetric or triaxial compression of cubic material specimen

If a constant pressure (P_0) is suddenly applied on all of the faces of a specimen and the volume change (ΔV) is followed as a function of time (t), a bulk or volumetric creep experiment is being performed and the bulk creep compliance (B) can be calculated using the equation [2.22], repeated here for convenience (Ferry, 1970): $\frac{\Delta V}{V}(t) = -P_0 B(t)$.

The left hand side of equation [2.22] is called voluminal strain and is defined as the relative change in volume of the body. Positive change in volume is called dilatation while negative change is compression (Ferry, 1970).

One of the disadvantages of bulk tests is that they require complex measuring devices and for this reason are generally used in materials that during their applications are subjected to homogeneous forces on all of their faces simultaneously such as soils and structural components under hydrostatic pressure; the volumetric test is rarely used in food

materials because it is harder to correlate the results with textural attributes (Gunasekaran and Ak, 2003).

Simple shear deformation occurs when two opposite faces of an element are displaced by sliding (Figure 4.24a), while uniaxial compressive deformation occurs when an element is compressed by two forces of equal magnitude acting perpendicularly on two of the faces of the specimen (Figure 4.24b).

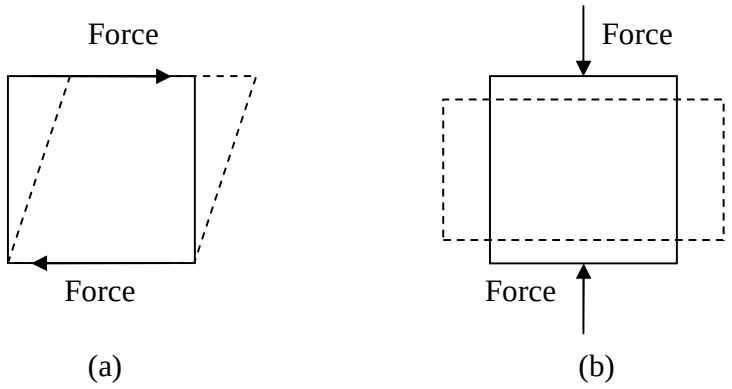

Figure 4. 24. Simple shear deformation (a) and compressive deformation (b) of a square specimen

Simple shear tests and uniaxial compressive tests can be performed with universal testing machines. According to Ferry (1970) simple compression tests, such as uniaxial compressive stress relaxation and creep tests can be related to shear stress relaxation and creep tests using equations [2.24] and [2.29] respectively, provided the material is homogeneous and incompressible:

$$G(t) = \frac{E_R(t)}{3} \qquad [2.24]$$

$$J(t) = 3D(t) \qquad [2.29]$$

where t is time, $G(t)$ is the shear stress relaxation modulus function, $E_R(t)$ is the compression stress relaxation modulus function, $J(t)$ is the shear creep compliance function and $D(t)$ is the compression creep compliance function.

Raw compressive experimental data were recorded as force and displacement, the displacement was converted into strain using the true strain [equation 2.5] and the force into stress assuming incompressibility [equation 2.6]. Then the compressive stress and the compressive strain were converted into the stress relaxation modulus ($E_R(t)$) for stress relaxation tests and into the compressive creep compliance ($D(t)$) for creep tests. The compressive modulus and compliance were converted into their shear counterparts using equations [2.24] and [2.29]. Once the test compression data were converted into shear test data, Abaqus requires the experimental data to be normalized to create dimensionless data; only then can Abaqus calculate the parameters required to simulate the viscoelastic behaviour of materials. The normalized parameters for stress relaxation test data were calculated using equation [4.4] and for creep tests using equation [4.5]

$$g_R(t) = \frac{G(t)}{G_0} \qquad [4.4]$$

$$j_s(t) = G_0 J(t) \qquad [4.5]$$

where g_R is the normalized shear modulus ($0 \leq g_R \leq 1$), j_s is the normalized shear creep compliance ($j_s \geq 1$), and G_0 is the instantaneous shear modulus. The instantaneous shear modulus (G_0) is the ratio of the stress at time zero divided by the constant strain that is applied in a stress relaxation test (Figure 4.25a) and the constant stress divided by the initial strain in a creep test (Figure 4.25b) (Abaqus, 2007). G_0 is a measurement of the elasticity of a viscoelastic material during the shear stress relaxation and creep tests (Rao,

2007). G_0 was obtained after converting the compressive data into shear data using equations [2.24] and [2.29].

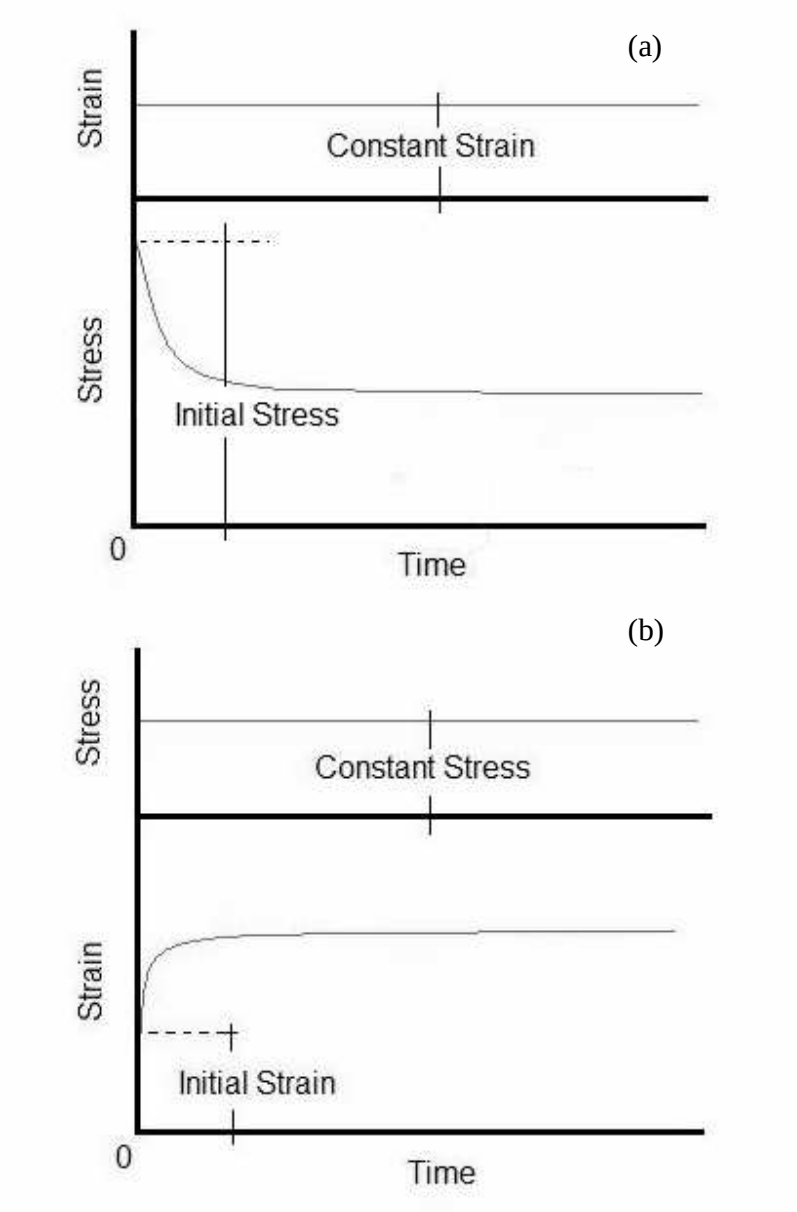

Figure 4. 25. Schematic representation of stress relaxation test (a) and creep test (b) results for a viscoelastic solid (adapted from Ferry, 1970 and Abaqus, 2007)

For stress relaxation data, Abaqus assumes that the viscoelastic material is a Maxwell solid and g_R is defined by a Prony series expansion of the following form:

$$g_R(t) = 1 - \sum_{i=1}^{N} \bar{g}_i^P (1 - e^{-t/\tau_i^G}) \qquad [4.6]$$

where N is the number of Prony elements used to get convergence, $\bar{g}_i^P$, and τ_i^G are material constants that can be directly specified or that can obtained by inputting into Abaqus the normalized shear modulus, g_R, as a function of time, t, in a tabular form. Abaqus uses a nonlinear least-square fit to obtain the parameters of the Prony series (Abaqus, 2006). Another parameter required by Abaqus is the long-term normalized shear relaxation modulus, $g_R(\infty)$. The Abaqus curve fitting procedure uses the value of $g_R(\infty)$ to constrain the numerical solution so that:

$$1 - \sum_{i=1}^{N} \bar{g}_i^P = g_R(\infty) \qquad [4.7]$$

As with the stress relaxation test data, Abaqus can calculate the Prony series parameters directly from a table of the normalized shear compliance, j_s, at a given time and using as a constraint for the fitting solution the long-term normalized compliance, $j_s(\infty)$. The normalized shear compliance and the normalized shear relaxation modulus are related by equation [4.8] (Abaqus, 2006):

$$j_s(t) = \frac{1}{g_R(t)} \qquad [4.8]$$

4.9.3 Evaluation of Abaqus Viscoelastic Model

In order to evaluate the Abaqus viscoelastic model, cyclic and simple compression tests on a 15x15 specimen were simulated in Abaqus/CAE version 6.6-5. The simulations were two-dimensional and axi-symmetrical; just like in the cyclic compression experimental data, three different crosshead speeds (4, 40, and 400 mm min^{-1}) were used

to observe the rate dependency of the material. The model was calibrated with the experimental data collected during creep and stress relaxation tests.

4.9.3.1 Calibration of Viscoelastic Model with Creep Data

During compressive creep tests a specimen is commonly subjected to a constant stress for a given amount of time. However during the current research project, creep tests were done by applying a constant force and measuring the displacement; the stress and the strain can be derived from the force and displacement at a given time and a compressive compliance, *D(t)*, can be calculated by dividing the true strain over the true stress at a given time, equation [4.9] (Rao, 2007).

$$D(t) = \frac{\varepsilon(t)}{\sigma(t)} \qquad [4.9]$$

This compressive compliance is then multiplied by the instantaneous shear modulus G_0 and a factor of three (because of incompressibility) to obtain the normalized shear compliance, j_s, as shown in equation [4.10] (Abaqus, 2006; Ferry, 1970).

$$j_s(t) = 3D(t)G_0 \quad [4.10]$$

The instantaneous shear modulus G_0 is related to the instantaneous compressive compliance, D_0, in the manner shown in equation [4.11] (Rao, 2007; Ferry 1970).

$$G_0 = \frac{1}{3D_0} \qquad [4.11]$$

The experimental data from three compressive creep tests carried out on 15x15x15 mm vegetable shortening specimens subjected to a constant load of 2.5N were averaged and used to calibrate the ABAQUS VISCOELASTIC model. These experimental data were selected because the force was high enough that the material was deformed well past its

elastic region, but low enough that the overall structure of the specimen was not completely destroyed. Theoretically, the instantaneous compressive compliance, D_0, should be calculated at the beginning of a creep test when the time is zero as shown in Figure 22b, but experimentally it was calculated at around 4 s, which was the time needed to achieve a constant load of 2.5N by the universal testing machine.

Once the normalized shear compliance, j_s, was calculated it was entered into Abaqus as a table of normalized shear compliance values against time. The ELASTIC and VISCOELASTIC models were selected. The modulus of elasticity, E, used in these models was obtained using the Excel Solver function and monotonic uniaxial compression test data (further described in Section 4.10). Vegetable shortening was assumed to be an incompressible solid following the work of Goh and Scanlon (2007); therefore, the Poisson's ratio, ν, was taken to be almost 0.5. For the VISCOELASTIC model the number of Maxwell elements needed was selected on a trial and error basis. An initial value of 1 was input into Abaqus and since there was no convergence between the input data and the solution to the Prony series, the number of Maxwell elements was incremented manually by one, until Abaqus found convergence between the input data and the solutions to the Prony series. The long term normalized shear compliance, $j_s(\infty)$, was the value of the normalized shear compliance at 30 minutes from the time the creep test was started, which was the time the load was held constant during the compressive creep tests. The following parameters were entered into the Graphic User Interface of the Property Module of Abaqus/CAE:

- Material Behaviour 1: *Elastic*

- Type: *Isotropic*
- Number of field variables: *0*
- Moduli time scale (for viscoelasticity): *Long-term*
- Young's Modulus: *593 kPa*
- Poisson's Ratio: *0.4999*

- Material Behaviour 2: *Viscoelastic*
  - Domain: *Time*
  - Time: *Creep test data*
  - Maximum number of terms in the Prony series: *6*
  - Allowable average root-mean-square error: *0.01*
  - Test Data: *Shear Test Data*
  - Long term normalized shear compliance $j_s(\infty)$: *3.05*
  - Data: j_s and *Time* entered as eleven discrete points (Table 4.7)

Table 4. 7. Normalized shear compliance as a function of time, $j_s(t)$, used to calibrate Abaqus viscoelastic model.

j_s	*Time (s)*
1.19329	8.26
1.73432	34.52
2.06826	87.38
2.13545	107
2.21074	134.26
2.36744	220.76
2.47253	311.26
2.53897	386.9
2.6191	502.58
2.78787	853.98
3.03235	1726.18

4.9.3.2 Calibration of Viscoelastic Model with Stress Relaxation Data

A stress relaxation test consists of deforming a specimen to a specific displacement and holding this displacement for a given amount of time, while recording the force. From the force and the displacement the true stress and strain can be derived so that a compressive stress relaxation modulus, $E_R(t)$ can be calculated by using equation [2.23] (Rao, 2007), which can be rewritten as: $E_R(t) = \frac{\sigma(t)}{\varepsilon_0}$.

The compressive stress relaxation modulus, $E_R(t)$, needs to be converted into a normalized shear relaxation modulus, $g_R(t)$, by using equation [4.12], so that the value of $g_R(t)$ should be greater or equal to zero and smaller or equal to one (Abaqus, 2006; Ferry, 1970):

$$g_R(t) = \frac{E_R(t)}{3G_0} \qquad [4.12]$$

where G_0 is the instantaneous shear relaxation modulus. The instantaneous shear modulus, G_0, is related to the instantaneous compressive relaxation modulus, E_0, as given by equation [4.13] (Ferry, 1970):

$$G_0 = \frac{E_0}{3} \qquad [4.13]$$

The instantaneous compressive relaxation modulus (E_0) was taken to be the compressive relaxation modulus at time zero ($E_R(0)$) obtained from the data collected during compressive stress relaxation tests.

The experimental compressive stress relaxation data from three 15x15x15 mm vegetable shortening specimens subjected to a constant deformation of 0.5mm imposed by means of an initial loading rate of 4mm min^{-1} were converted into shear data and normalized to obtain g_R, and these values were averaged. Once the normalized shear relaxation modulus, g_R, was calculated it was input into Abaqus as a table of shear relaxation modulus values as a function of time. The ELASTIC and VISCOELASTIC material behaviours were selected from the list of mechanical models available in Abaqus. The elastic parameters were the same as the parameters used when the VISCOELASTIC model was calibrated with creep test data. As with the creep test data the maximum number of terms in the Prony series was determined in a trial and error basis until Abaqus provided an output without error messages. The long term normalized shear modulus, $g_R(\infty)$, was the value of normalized shear modulus at 20 minutes after the relaxation test had started, which was the maximum time that the deformation was held during the compressive stress relaxation tests. The following parameters were input into the Graphic User Interface of the Abaqus property module:

- Material Behaviour 1: *Elastic*
    - Type: *Isotropic*
    - Number of field variables: *0*
    - Moduli time scale: *Long-term*
    - Young's Modulus: *593 kPa*
    - Poisson's Ratio: *0.4999*
- Material Behaviour 2: *Viscoelastic*
    - Domain: *Time*

- Time: *Relaxation test data*
- Maximum number of terms in the Prony series: *3*
- Allowable average root-mean-square error: *0.01*
- Test Data: *Shear Test Data*
- Long –term normalized shear relaxation modulus $g_R(\infty)$: *0.224*
- Data: g_R and *Time* entered as eleven discrete points (Table 4.8)

Table 4. 8. Normalized shear modulus as a function of time, $g_R(t)$, used to calibrate the Abaqus viscoelastic model

$g_R(t)$	*Time (s)*
0.991	0.02
0.871	0.4
0.556	5.02
0.471	10.14
0.4	20.24
0.339	41.46
0.294	82.26
0.25	187.26
0.243	227.38
0.225	467.36
0.225	1134.7

4.9.4 Results from the AbaqusViscoelastic Model

The Abaqus viscoelastic model predicts perfect elastic recovery when the load is removed from the sample, or in other words, there is no permanent or plastic deformation. However this elastic recovery is not instantaneous after the sample is subject to large strains, so if a loading cycle starts immediately after unloading has been completed, it may look like there is some permanent deformation; this behaviour is shown in Figure 4.26 using a constitutive model which was derived from creep test experimental data, where a cyclic compression test at a crosshead speed of 40 mm min^{-1} was simulated. The specimen was subjected to a 1 mm compression, then unloaded to 0 mm, subject to 3 mm

compression, unloaded and compressed by 5mm, followed by a final unload to 0 mm. The stress in loading cycle #3 shows zero value until approximately 0.03 strain and the loading curve of this cycle runs parallel to the previous loading cycles. In reality, if a new loading cycle does not start immediately after unloading to 0mm, but starts after some resting time has passed, then this permanent deformation is not observed and all the loading curves overlap as shown in Figure 4.27. This is classic viscoelastic behaviour in which the stress relaxation is time dependent.

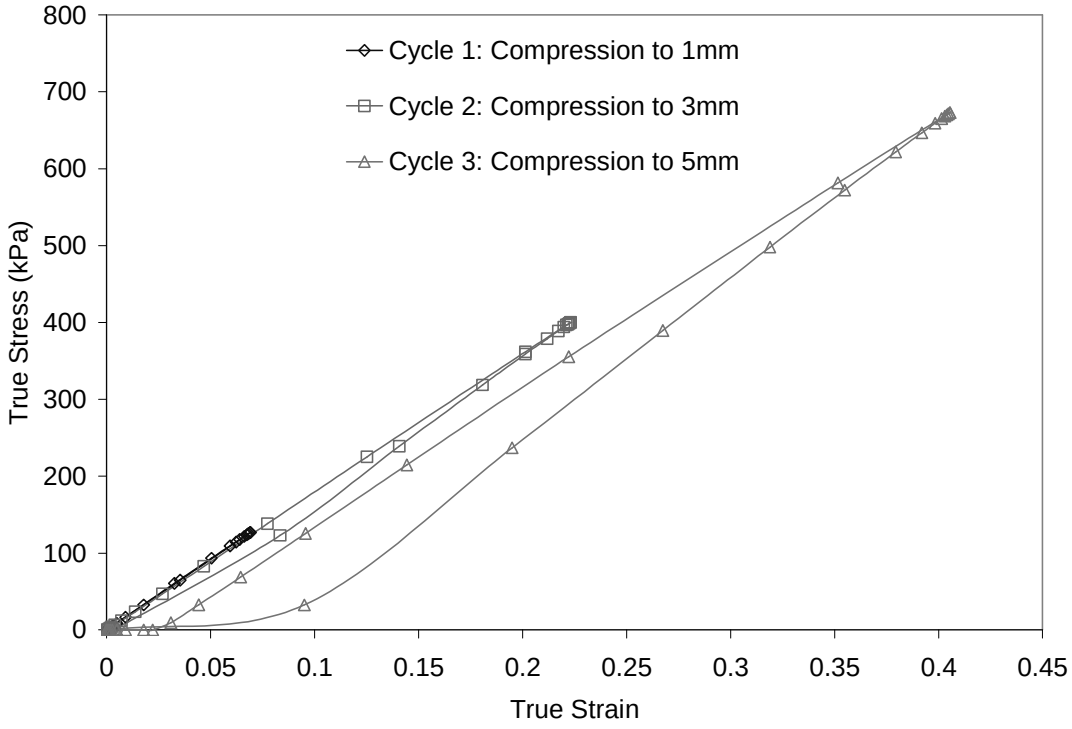

Figure 4. 26. Cyclic compression at 40 mm min^{-1} without resting time between loading cycles of viscoelastic material modeled by Abaqus using creep test data

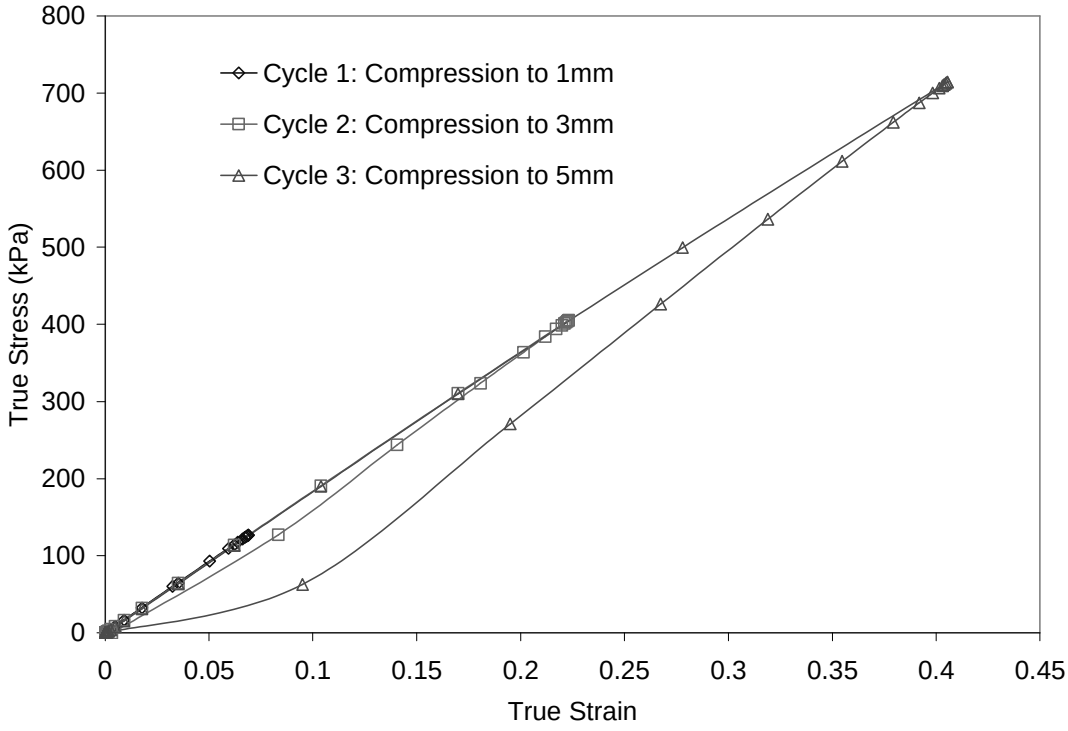

Figure 4. 27. Cyclic compression as in Figure 4.26, but with resting time of 2000s between loading cycles of viscoelastic material modeled by Abaqus using creep test data

Additionally, it can be seen that since the elastic recovery is not instantaneous after the load is removed, the stress-strain curve obtained from the viscoelastic simulations shows hysteresis during the unloading part of the cyclic compression. The hysteresis is more visible as the strain increases and this is related to the viscous component of the Abaqus model, which becomes more dominant at larger strains (Peleg and Pollak, 1982; Abaqus, 2006).

Complete recovery after deformation cannot be seen during the cyclic loading of real vegetable shortening; even at compressions smaller than 1mm real vegetable shortening specimens show permanent deformation (Figure 4.28). The viscoelastic model on the other hand shows complete elastic recovery after unloading from 1mm (0.07 strain) and

hysteresis is barely visible at these low strains. Basically at strains between 0 and 0.07 the viscoelastic material simulated by Abaqus behaves pretty close to a linear-elastic material. The viscoelastic model also overpredicts the experimental stress values by at least one order of magnitude as seen in Figure 4.28.

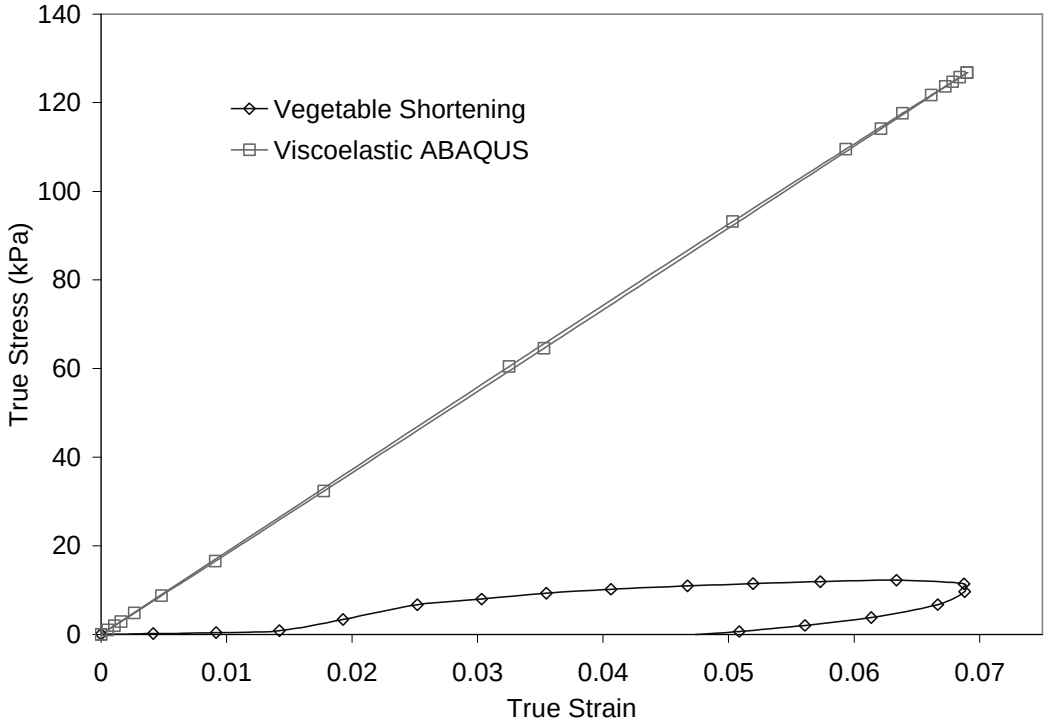

Figure 4. 28. Loading-unloading curve obtained from compression at 40 mm min^{-1} of a 15x15x15 vegetable shortening and simulation using Abaqus viscoelastic model calibrated with creep test data

4.9.5 Comparison between Creep and Relaxation Data Calibration

Similar results were obtained regardless of whether creep or stress relaxation data were used to calibrate the Abaqus viscoelastic model (Figure 4.29): stresses at a given strain have similar values especially in the loading part of the cycle, and the overall shape of the stress-strain curve for cyclic compression is very similar. However, when running Abaqus with the viscoelastic model calibrated by creep test data at least six Prony

elements had to be used in order to get convergence in the simulation. On the other hand, when calibrating the viscoelastic model with stress relaxation test data only three Prony elements had to be used. Tables 4.9 and 4.10 show the values of the material constants, $\bar{g}_i^P$ and τ_i^G calculated by Abaqus from the stress relaxation and creep test data respectively.

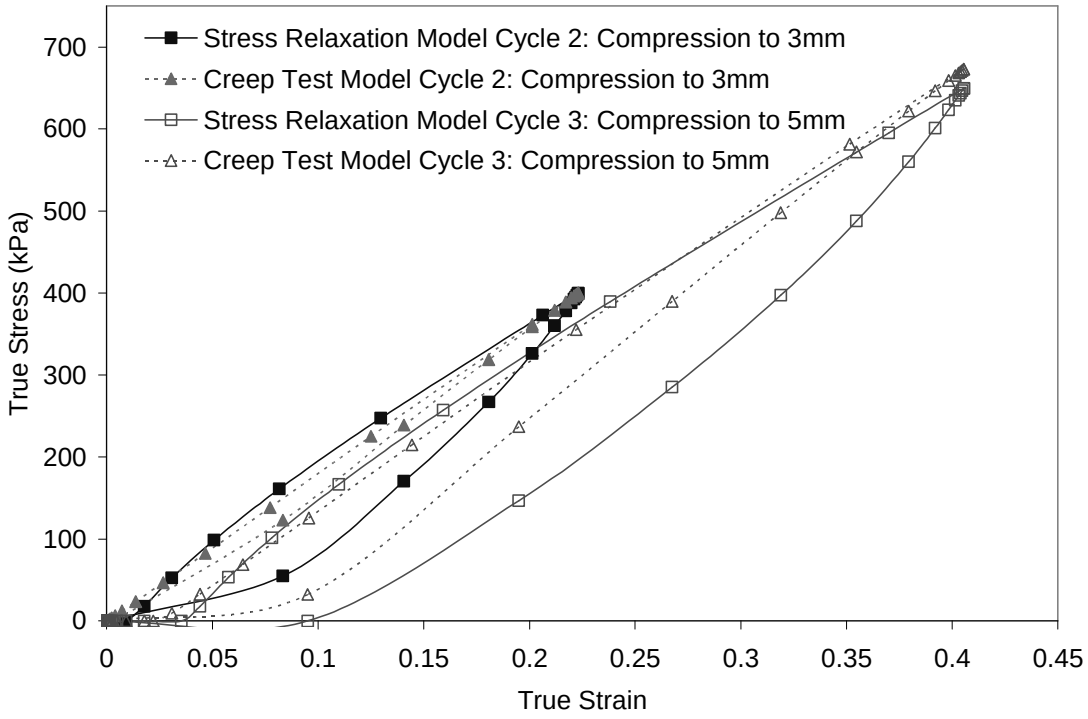

Figure 4. 29. Cyclic compression at 40 mm min^{-1} comparing viscoelastic materials simulated by Abaqus viscoelastic model calibrated with stress relaxation or creep test data. Cyclic simulation was done as described for Figure 4.26 but the first cycle is not shown for clarity

Table 4. 9. Prony series constant values calculated by Abaqus from stress relaxation data

I	1	2	3
$\bar{g}_i^P$	0.32107	0.28416	0.17077
τ_i^G (s)	0.88734	9.451	97.255

Table 4. 10. Prony series constant values calculated by Abaqus from creep test data

I	1	2	3	4	5	6
$\bar{g}_i^P$	-0.13453	4.02160	-5.83480	2.53510	0.51040	-0.42566
τ_i^G (s)	1.6966	28.548	38.621	50.288	1862.1	2447.7

It is important to notice that the dimensionless constants $\bar{g}_i^P$ can take the value of any real number since they don't have a direct physical meaning like the modulus of elasticity and the Poisson's ratio, and are just constants that give the desired curve shape when used in a Prony series which is part of the Maxwell or Kelvin models that can be used to mathematically describe the viscoelastic behaviour of materials.

Using the values shown in Tables 4.9 and 4.10, the normalized data entered into Abaqus to calibrate the VISCOELASTIC model can be back calculated, and these results are shown in Figures 4.30 and 4.31. By looking at Figure 4.30 one can see that when the viscoleastic model is calibrated with stress relaxation test data, the Abaqus input and the values predicted using equation [4.6] and the Prony constants from Table 4.9, almost completely overlap with one another (Figure 4.30), but when the model is calibrated with creep test data and the constants from Table 4.10, the prediction is not as good, but still acceptable (Figure 4.31). When using the stress relaxation data, the root-mean-square error for the fit was 0.23%. On the other hand, when using the creep test data the root-mean-square error was 0.46%.

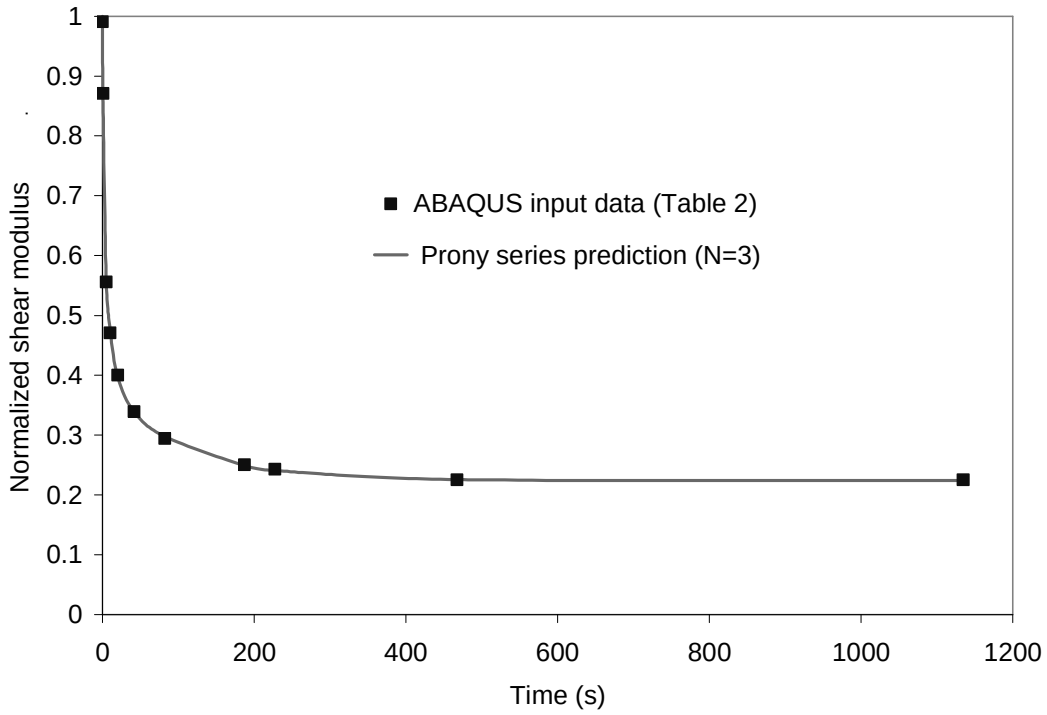

Figure 4. 30. Comparison between input stress relaxation test data (experimental) and prediction of input data with Prony constants calculated by Abaqus

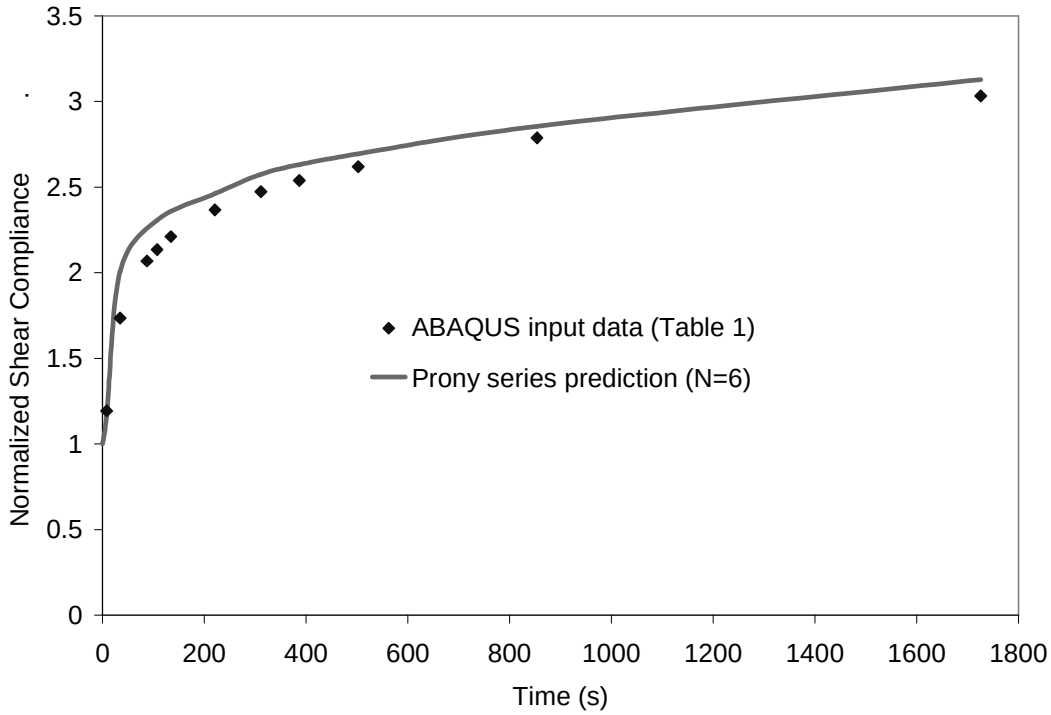

Figure 4. 31. Comparison between input creep test data (experimental) and prediction of input data with Prony constants calculated by Abaqus

Another difference between the model calibrated with stress relaxation and creep test data was that the model calibrated with stress relaxation test data shows a slower recovery after deformation; this can be seen in Figure 4.29 as a larger hysteresis during unloading and a larger 'apparent' permanent deformation following 5mm of compression. This is to be expected based on an inspection of the time constants in Table 4.9 compared to Table 4.10. The larger time constants in the creep test calibration make the stress decay faster than when the time constants are small (Abaqus, 2006). It is important to notice that the deformation only appears to be permanent but in reality the model predicts a very slow but total recovery. If not enough time is allowed to pass then one might think that the deformation is permanent, when in reality the viscoelastic model does not predict any permanent deformation (Abaqus, 2006).

Abaqus provides a visual representation of the results that shows the viscoelastic model calibrated with stress relaxation data has an 'apparent' permanent deformation after compression to 3mm (Figure 4.32b), but after the load is removed there is a rapid partial recovery of 2.3 mm (Figure 4.32c) and then a complete recovery after 870s of waiting time.

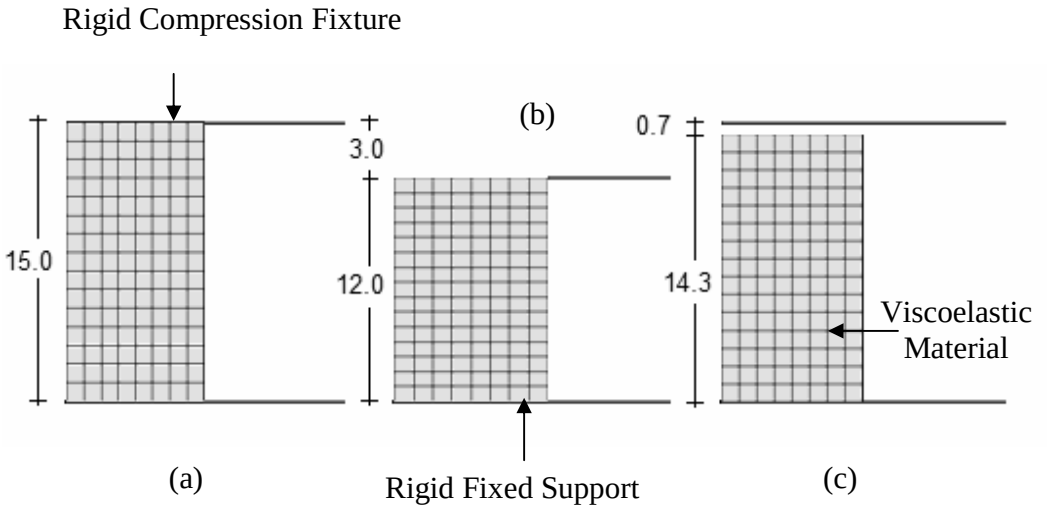

Figure 4. 32. Cyclic compression at 40mm min^{-1} simulated by Abaqus viscoelastic model calibrated with stress relaxation data: (a) undeformed specimen 15.0mm in height, (b) specimen being compressed to 3.0mm, and (c) specimen after load is removed showing a rapid recovery of 2.3mm

In contrast, the model calibrated with creep test data shows a rapid partial recovery after 3mm compression to 2.6 mm (Figure 4.33c) and a complete recovery after 420 s. The rapid recovery is attributed to the elastic component of the model, while the time-dependent recovery is due to the time dependent component of the model which is related to the Prony series of the mathematical model. Therefore it can be stated that the viscoelastic model calibrated with creep test data appears to have more elasticity than the model calibrated with stress relaxation test data because of the larger time constants in Prony series and the model calibrated with stress relaxation test data requires more time to flow (i.e. more viscous) than the model calibrated with creep test data because of the smaller time constants in its Prony series.

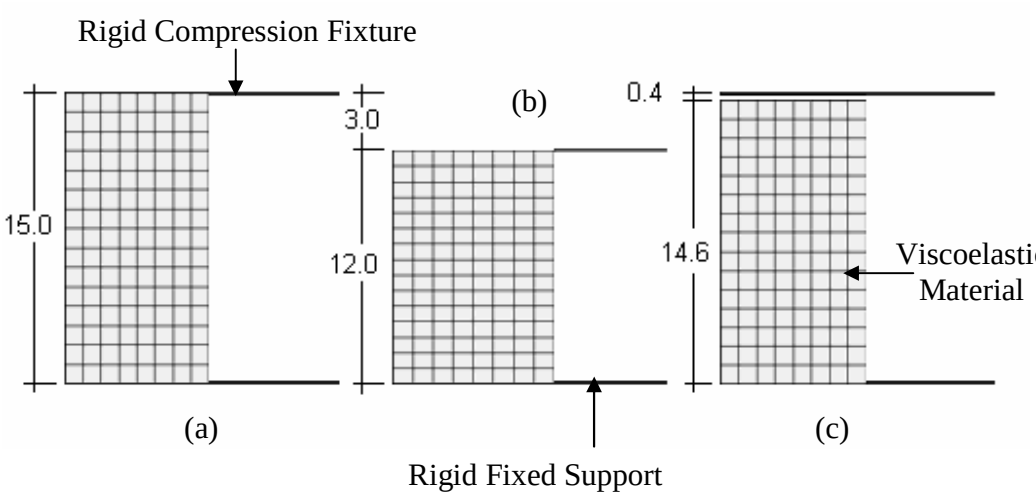

Figure 4. 33. Cyclic compression at 40mm min^{-1} simulated by Abaqus viscoelastic model calibrated with creep test data: (a) undeformed specimen 15.0mm in height, (b) specimen being compressed to 3.0mm, and (c) specimen after load is removed showing a rapid recovery of 2.6 mm

The viscoelastic model calibrated with stress relaxation test data is more robust at larger deformations than when calibrated with creep test data, since it is able to handle compression up to 7 mm without aborting the results due to excessive deformation of the elements in the mesh. This behaviour appears to be rate-dependent because at 4 mm min^{-1} even the model calibrated with relaxation data is unable to handle the unloading after being compressed to 7 mm, but at 40 and 400 mm min^{-1} the model is capable of simulating unloading after 7 mm of compression. The Abaqus viscoelastic model cannot deal with excessive distortion at slow rates because it requires very small iteration times which cannot be handled by its current version (Abaqus, 2006).

4.9.6 Rate Dependency of Abaqus Viscoelastic Model

The literature review showed that vegetable shortening is a rate dependent material, since its stress-strain curve varies depending on the rate of compression (Goh and Scanlon, 2007). An appropriate mechanical model for vegetable shortening should predict rate dependency during compression testing. The Abaqus viscoelastic model is a rate dependent model (Abaqus, 2006). In order to make visible the rate dependent behaviour of the Abaqus viscoelastic model, simulations of cyclic compression at different crosshead speeds (4, 40 and 400 mm min^{-1}) were done. An example of the results is shown in Figure 4.34. By looking at Figure 4.34, one can see an increase in the predicted stress at a given strain as the crosshead speed increases. During the current research project, rate dependent behaviour can also be observed during experimental cyclic compression of the chosen vegetable shortening, but the effect is not an increase in the stress as the crosshead speed increases but rather a change in the shape of the curve with a larger stress overshoot range (Figure 4.9); in other words the onset of what can be considered as perfect plasticity occurs at larger strains as the crosshead speed increases. Therefore, one can say that some modifications need to be done to the Abaqus viscoelastic model in order to properly predict the rate dependency of the vegetable shortening used in the current research.

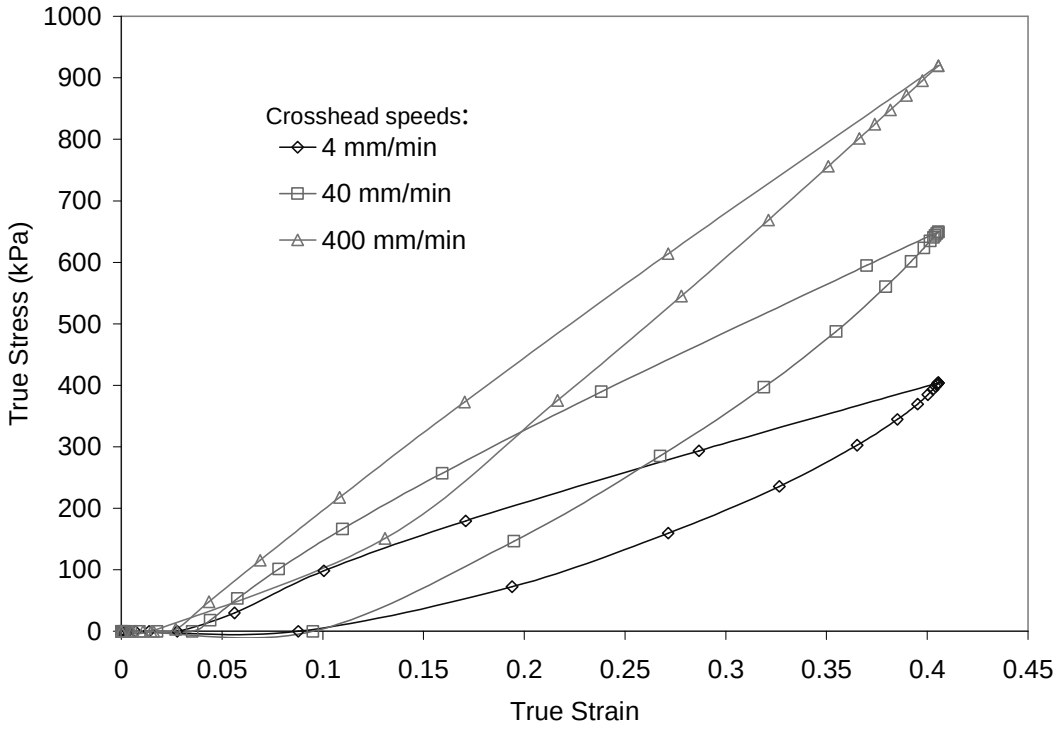

Figure 4. 34. Loading-unloading curve after compression to 5 mm, showing the rate-dependency of the Abaqus viscoelastic model calibrated with stress relaxation test data

4.9.7 Comparison between Abaqus Viscoelastic Model and Experimental Results

The viscoelastic constitutive model calibrated from creep and stress relaxation data was applied to predict the compression test. During the simple compression simulation the Abaqus viscoelastic model predicts a fast increase in the stress at low strains just as seen in the experimental results (Figure 4.35). However the Abaqus viscoelastic model overpredicts the stress values by two orders of magnitude (note logarithmic scale on *y*-axis of Figure 4.35). Also, the Abaqus viscoelastic model shows the stress increasing in an exponential manner as the strain increases, something that does not occur in vegetable shortening in which the stress seems to be reaching a maximum stress at approximately

0.05 strain that later decays until it reaches a constant stress beyond the 0.2 true-strain mark (see Figure 4.35 and experimental compression results in section 4.4.0).

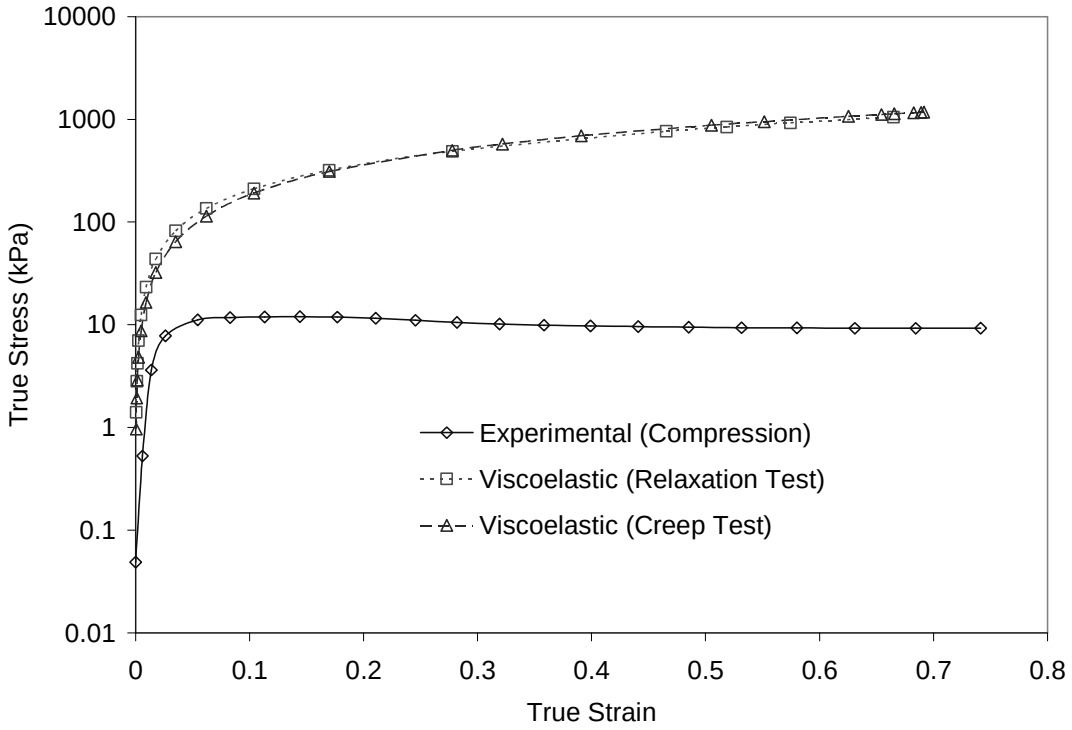

Figure 4. 35. Simple compression of 15x15x15 specimen of vegetable shortening at 40 mm min^{-1} and Abaqus simulation as a viscoelastic material calibrated with creep and stress relaxation test data

Figure 4.28 shows a linear stress-strain loading response with barely visible hysteresis and perfect deformation recovery during unloading of an Abaqus viscoelastic simulated material, while the linear elastic region for vegetable shortening is almost not visible. The lack of hysteresis of the viscoelastic prediction shown in Figure 4.28 implies that the Abaqus viscoelastic material remains perfectly elastic for only small strains (up to approximately 7×10^{-2}). On the other hand it has been estimated that vegetable shortening has a linear elastic region up to a strain of only 7.19×10^{-4} (Goh and Scanlon, 2007) which is two orders of magnitude smaller than the viscoelastic prediction by

Abaqus. This delay in the onset of permanent deformation may contribute to the overprediction of the stress values by the Abaqus viscoelastic model.

Comparing the results of the Abaqus viscoelastic model with the experimental results, one can say that the Abaqus viscoelastic model retains a higher level of elasticity even after larger deformations; the highly elastic behaviour of the viscoelastic model can be seen in the rapid partial recovery during unloading as shown in Figures 4.32 and 4.33. In order to quantify the amount of height rapidly recovered during the viscoelastic simulations, the 'rapid recovery percentage' was calculated (Table 4.11). The 'rapid recovery percentage' was calculated by dividing the rapidly recovered height over the initial compression distance and then multiplied by 100. As the compression distance in the viscoelastic simulations increases the rapid recovery percentage decreases, as shown in Table 4.11.

Table 4. 11. Percentage of rapidly recovered height after cycling compression as predicted by the Abaqus viscoelastic model calibrated with stress relaxation data.

Compression Distance (mm)	Initial Specimen Height (mm)	Rapidly Recovered Height (mm)	Rapid Recovery Percentage (%)
3.0	15	2.3	77
5.0	15	3.8	76
7.0	15	5.0	71

Continuous photographs were taken during the unloading process of vegetable shortening (Figure 4.36). In the continuous photographs of vegetable shortening, the rapid partial recovery in height is also visible, although not to the same extent as the predictions obtained by the Abaqus viscoelastic model. Figure 4.36 shows vegetable shortening before being compressed by 6.5 mm (a) and after it has gone through rapid recovery (b).

The initial height of the cubic vegetable shortening specimen was 15 mm and the rapidly recovered height was measured to be 10.5 mm which gives a recovery percentage of 31% (2/6.5*100%) which is significantly lower than the predicted viscoelastic value of 71% (5/7*100%).

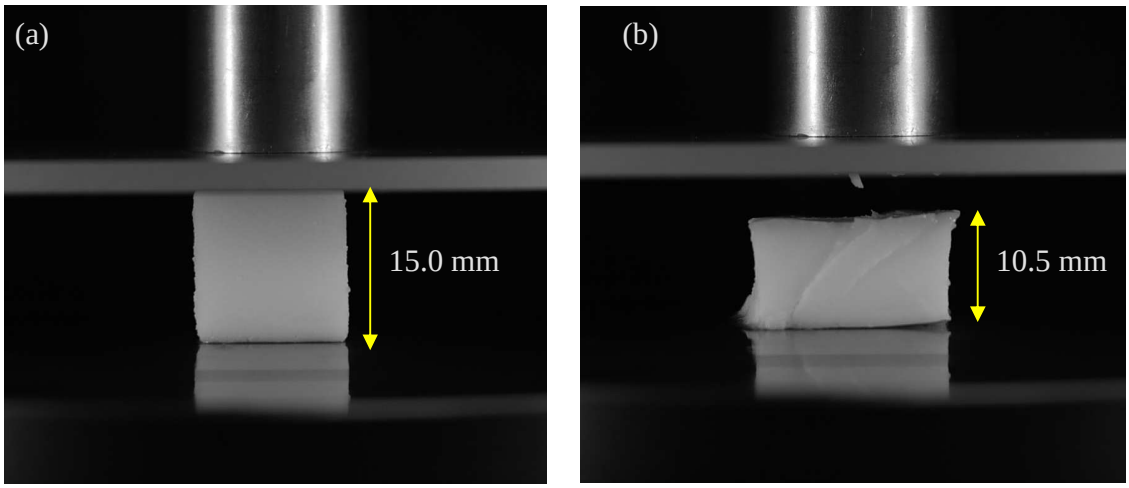

Figure 4. 36. Cubic vegetable shortening specimen before compression (a) and vegetable shortening specimen after being compressed to 6.5 mm (b)

4.9.8 Conclusion for Viscoelastic Simulation of Shortening

The Abaqus viscoelastic model can be calibrated by using compressive stress relaxation and creep test data, after they have been converted into shear test data and normalized to obtain dimensionless parameters. This model can be used to simulate the rheological behaviour of materials that show hysteresis during unloading and rate dependency. Using stress relaxation data gives the ability to predict the stresses at higher strains than when using creep test data. The viscoelastic model predicts elastic recoil even at the large strain of 46%, and it was observed that the recoil was greater when using the creep test data.

When compared to the vegetable shortening experimental data, the Abaqus viscoelastic model greatly overpredicts the stress at a given strain, and does not show permanent deformation even at greater strains, as well as greater increase in stress values as the speed of compression increases. Elastic recoil is also observed during experimental unloading of vegetable shortening but it is also overpredicted by the viscoelastic model used here. The Abaqus viscoelastic mode is incapable of predicting a behaviour that resembles a perfectly plastic deformation, which consists of reaching a constant stress after passing a given strain value. The Abaqus viscoelastic model needs to be modified in order to include perfect plasticity behaviour in order to better predict the rheological response of vegetable shortening. The information shown here supports the idea that vegetable shortening could be better described as an elastic-viscoplastic material (Goh and Scanlon, 2007) rather than just a viscoelastic material.

4.10.0 Development of Mechanical Model for Vegetable Shortening

Goh and Scanlon (2007) developed a rate independent model to describe the static rheological response of vegetable shortening. This model had three distinct regions: a linear elastic region, a strain hardening plastic deformation region and a region of perfect plasticity. The model can be summarized with the following equations:

$$\text{if } \varepsilon \le \varepsilon_{y1},\ \sigma_{st} = E\varepsilon,$$

$$\text{if } \varepsilon_{y1} \le \varepsilon \le \varepsilon_{y2},\ \sigma_{st} = E\varepsilon_{y1}\left(\frac{\varepsilon}{\varepsilon_{y1}}\right)^{z}, \qquad [4.14]$$

$$\text{if } \varepsilon \ge \varepsilon_{y2},\ \sigma_{st} = E\varepsilon_{y1}\left(\frac{\varepsilon_{y2}}{\varepsilon_{y1}}\right)^{z},$$

where σ_{st} is the static stress, E is the modulus of elasticity, ε_{y1} is the true strain at first yield, ε_{y2} is the strain which marks the onset of perfect plasticity, and z is the power law strain hardening constant. The basic shape of the compression stress-strain diagram for the static Goh and Scanlon (2007) model is shown in Figure 4.37. When one compares the Goh and Scanlon (2007) model to the experimental compression data obtained at 0.4 mm min^{-1} (which is the closest experimental trial to being static), one can see that the model does not accurately predict the middle section of the diagram, because the experimental data shows a region with hardening followed by a region of softening before reaching perfect plasticity. Therefore some modifications to the model shown in equation [4.14] are needed to take into account the stress overshoot shown by all experimental results.

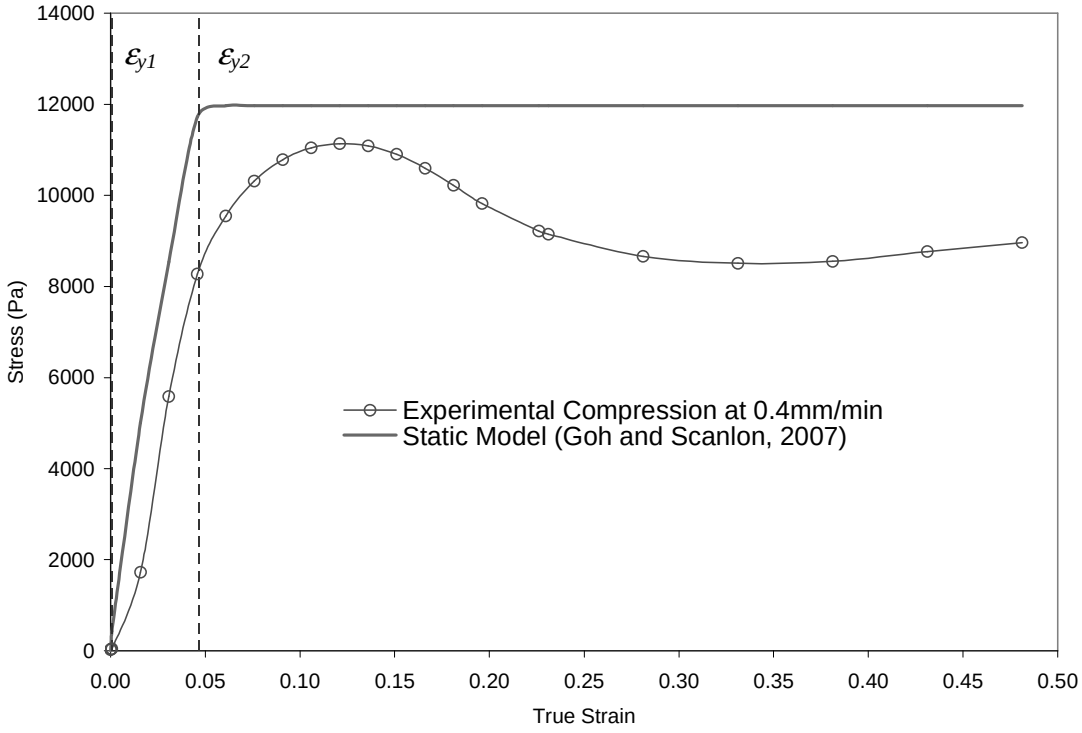

Figure 4. 37. Compression stress-strain curve for vegetable shortening as obtained during compression at 0.4 mm/min and as predicted by static model formulated by Goh and Scanlon (2007)

In order to take into account the stress overshoot region seen in the experimental data, equation [4.14] was modified to include a function that will increase and decrease the stress value as the strain increases in the middle section of the model; an exponential function similar to that present in a Prony series was added to the Goh and Scanlon (2007) model, since the exponential function provided the rapid decay in stress observed in the experimental compression data. The raising part of stress overshoot region seen in the experimental results is related to the strain hardening process caused by the movement of defects in crystalline solids after the onset of plasticity (Gottstein, 2004; de With, 2006), while the descending part of the stress overshoot is related to the shear failure that occurs at large compressive strains due to the presence of macroscopic defects in the solid

matrix (Dowling, 2007), such as nitrogen bubbles in vegetable shortening. In order to take into account strain hardening and shear failure equation [4.14] can be modified as follows:

$$\text{if } \varepsilon \le \varepsilon_{y1},\ \sigma = E\varepsilon,$$

$$\text{if } \varepsilon_{y1} \le \varepsilon \le \varepsilon_{y2},\ \sigma = E\varepsilon_{y1}\left(\frac{\varepsilon}{\varepsilon_{y1}}\right)^{z} e^{-(\varepsilon-\varepsilon_{y1})/\omega}, \qquad [4.15]$$

$$\text{if } \varepsilon \ge \varepsilon_{y2},\ \sigma = E\varepsilon_{y1}\left(\frac{\varepsilon_{y2}}{\varepsilon_{y1}}\right)^{z} e^{-(\varepsilon_{y2}-\varepsilon_{y1})/\omega},$$

where ω is a stress decaying factor (a material constant), and all other variables are as previously defined. The elastic region of the model was kept unchanged, but an exponential function was added to the other two sections. The added exponential function is analogous to the exponential function used in the Maxwell model to describe viscoelastic behaviour of materials and therefore ω is a strain dependent analogy to the relaxation time in the Maxwell model. Therefore it can be said that the modified model has elastic, viscous and plastic components.

Equation [4.15] was calibrated using the material constants obtained during monotonic and cyclic compression test in an Excel spread sheet following the procedure described by Goh and Scanlon (2007). The value for *E* was restricted to be a numbers in the range of results obtained during monotonic and cyclic compression (185kPa≤*E*≤743kPa). The value for ε_{y1} was limited to be a number greater than zero and smaller than 0.02, which was the smallest strain measured during cyclic compression at which permanent

deformation was already visible. The initial values for E and ε_{y1} were the values given by Goh and Scanlon (2007) (E = 315 kPa and ε_{y1} =1.53x10^{-4}), since they were within the ranges of values obtained during compression tests. The initial value of ε_{y2} was taken directly from the average stress-strain curve from monotonic compression tests at a given loading rate (ε_{y2} = 0.22, 0.32, 0.36 and 0.46 at 0.4, 4, 40 and 400 mm/min respectively) and it was the largest strain in the stress overshoot, just before the onset of perfect plasticity. The initial value of z was the value found by Goh and Scanlon in 2007 (z = 0.468) and ω was just limited to be a number smaller than one and larger than zero ($0<\omega<1$) in order to create an exponential decay before reaching ε_{y2} (initial value was guessed to be ω = 0.1). The predictions of the model using the initial values for the parameters in equation [4.15] were matched to the experimental compressive data in a least square error method via the Excel Solver function. After several iterations of the Solver function the following numerical values for the constitutive parameters at four loading rates were obtained (Table 4.12):

Table 4. 12. Numerical values of constitutive parameters of shortening model shown in Equation [4.15]

Loading Rate (mm min^{-1})	0.4	4.0	40.0	400.0
E (kPa)	593.2	593.2	593.2	593.2
ε_{y1}	7.19 x 10^{-4}	7.19 x 10^{-4}	7.19 x 10^{-4}	7.19 x 10^{-4}
ε_{y2}	0.226	0.300	0.350	0.436
Z	0.798	0.784	0.751	0.721
ω	0.146	0.180	0.234	0.302

The numerical values of Table 4.12 were inputted into equation [4.15] and plotted in order to verify the accuracy of the modified Goh and Scanlon model, these results are shown in Figure 4.38.

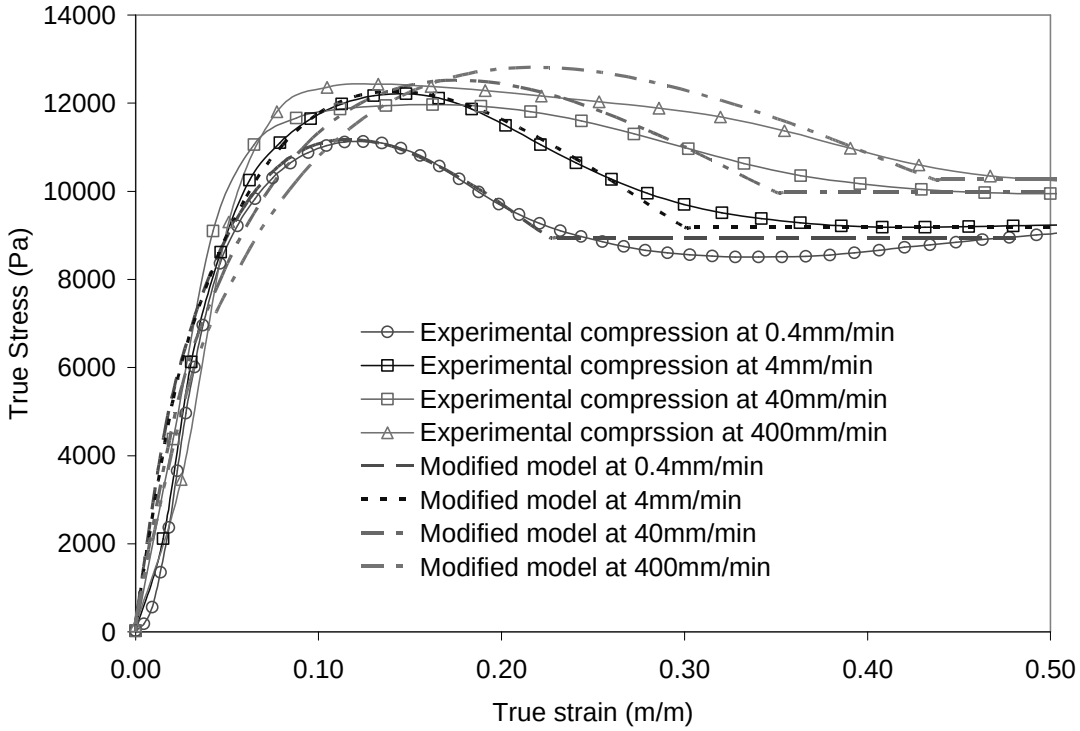

Figure 4. 38. Comparison between experimental compression data and results from the modified constitutive model

By looking at Figure 4.38, one can see that the modified Goh and Scanlon model (equation [4.15]), closely predicts the experimental data using the values obtained from the Solver function. However as the crosshead speed increases the accuracy of the model decreases, especially in the hardening section of the model.

The model formulated by Goh and Scanlon (2007), equation [4.14], provided adequate prediction of the compression response of shortening, margarine and butter up to a true strain of 0.3. However, Goh and Scanlon did not take into account the stress overshoot that is particularly visible in their experimental results for margarine and butter and did not try to fit the model past the 0.3 true strain mark. The modified model, equation [4.15], is capable of simulating the stress overshoot that is more visible in the shortening used in

the current research project and adequately predicts the compression response of vegetable shortening up to a true strain of 0.5.

4.10.1 Testing Constitutive Model with Indentation

In order to check the robustness of equation [4.15] in predicting the rheological response of vegetable shortening, conical indentation simulations were set up in Abaqus/CAE. As previously stated in the methodology section of this thesis, indentation was simulated with a two dimensional axisymmetrical model in order to save on computational time. Figure 4.39 shows the schematic representation of the conical indentation simulation set up in Abaqus/CAE.

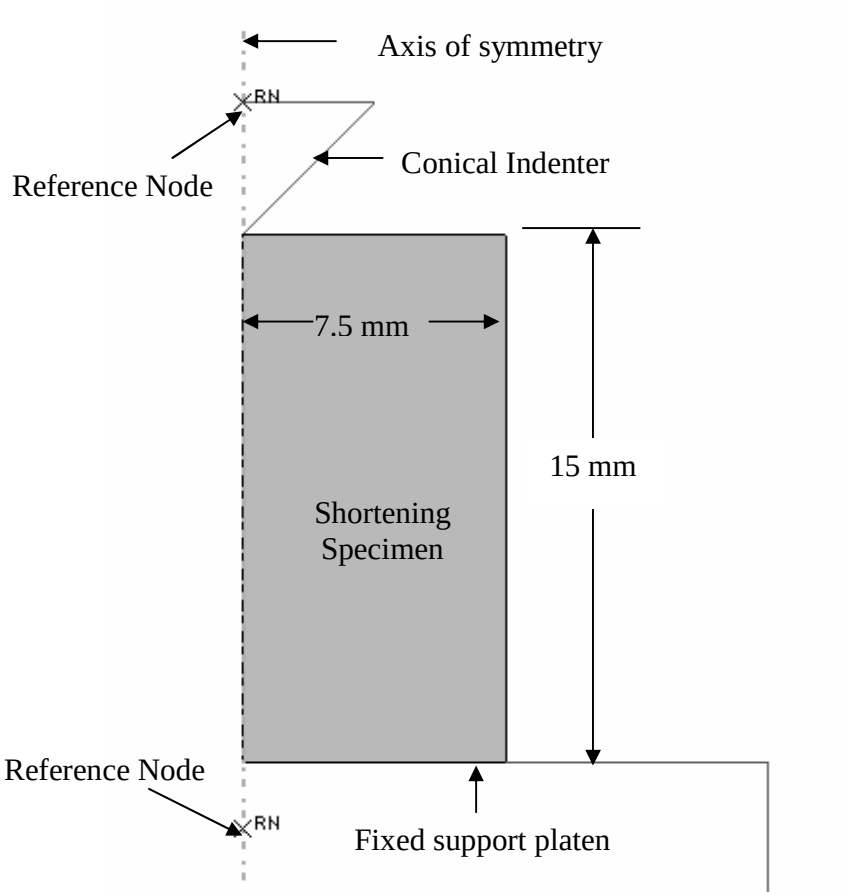

Figure 4. 39. Conical indentation (45° half angle) set-up in Abaqus/CAE

The visual representation during indentation provided by Abaqus is shown in Figure 4.40. By looking at Figure 4.40, one can see that the deformation under the indenter is extremely large and a concentration of stresses occurs around the indentation area.

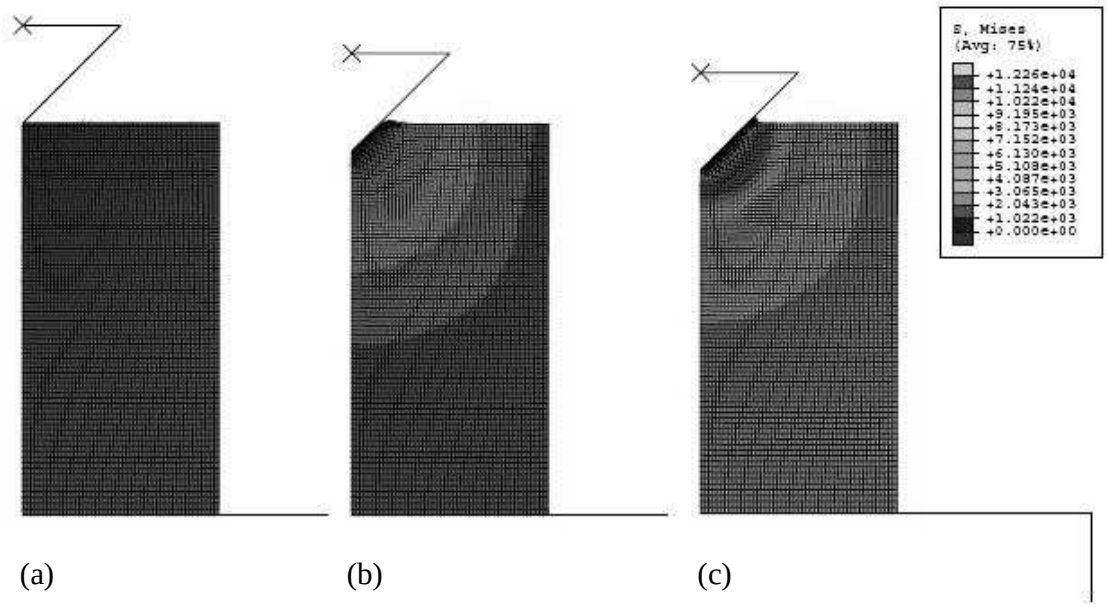

Figure 4. 40. Visual representation of indentation response of vegetable shortening simulated using Abaqus with model shown in equation [4.15]. (a) Undeformed specimen, (b) indentation to 1.2 mm, and (c) indentation to 2.5 mm

4.10.1.1 Material Properties Used during Virtual Indentation

During the simulations in Abaqus it was assumed that vegetable shortening is an isotropic, homogeneous, and incompressible solid just as Goh and Scanlon did in 2007. The ELASTIC and PLASTIC models were selected in the Properties Module of Abaqus. For the ELASTIC Abaqus model two parameters are required: the modulus of elasticity (E) and the Poisson's ration (ν); these two parameters are used to describe the purely elastic behaviour shown by shortening at strains below ε_{y1} (first part of equation [4.15]). For the Abaqus PLASTIC model the yield stress and the non-elastic strain (ε_p) are required; in order to take into account the material's hardening and softening shown by shortening at

strains between ε_{y1} and ε_{y2} (middle part of equation [4.15]), the yield stress as a function of non-elastic strain (plastic and viscous strain) was entered as 15 discrete points in a tabular form. The non-elastic strain (ε_p) is defined as the total strain (ε) minus the elastic strain (ε_e) and the elastic strain is the strain prior to the first yield strain (ε_{y1}), which is equal to the yield stress (σ_y) divided by the modulus of elasticity (E):

$$\varepsilon_p = \varepsilon - \varepsilon_e = \varepsilon - \frac{\sigma_y}{E} = \varepsilon - \varepsilon_{y1} \qquad [4.16]$$

It is important to notice that the non-elastic strain at the yield stress is equal to zero and that the 15th data point is the stress at ε_{y2}; ε_{y2} marks the onset of perfect plasticity predicted by the third part of equation [4.15]. Different values of yield stress as a function of non-elastic strain were used at different indentation rates (Figure 4.41), since ε_{y2} was rate dependent. The parameters entered in the Abaqus Graphic User Interface can be summarized as follows:

- Material Behaviour 1: *Elastic*
    - Type: *Isotropic*
    - Number of field variables: *0*
    - Moduli time scale (for viscoelasticity): *Long-term*
    - Young's Modulus: *593 kPa*
    - Poisson's Ratio: *0.4999*
- Material Behaviour 2: *Plastic*
    - Hardening: *Isotropic*
    - Number of field variables: *0*
    - Data: Yield stress as function of non-elastic strain as shown in Figure 4.41

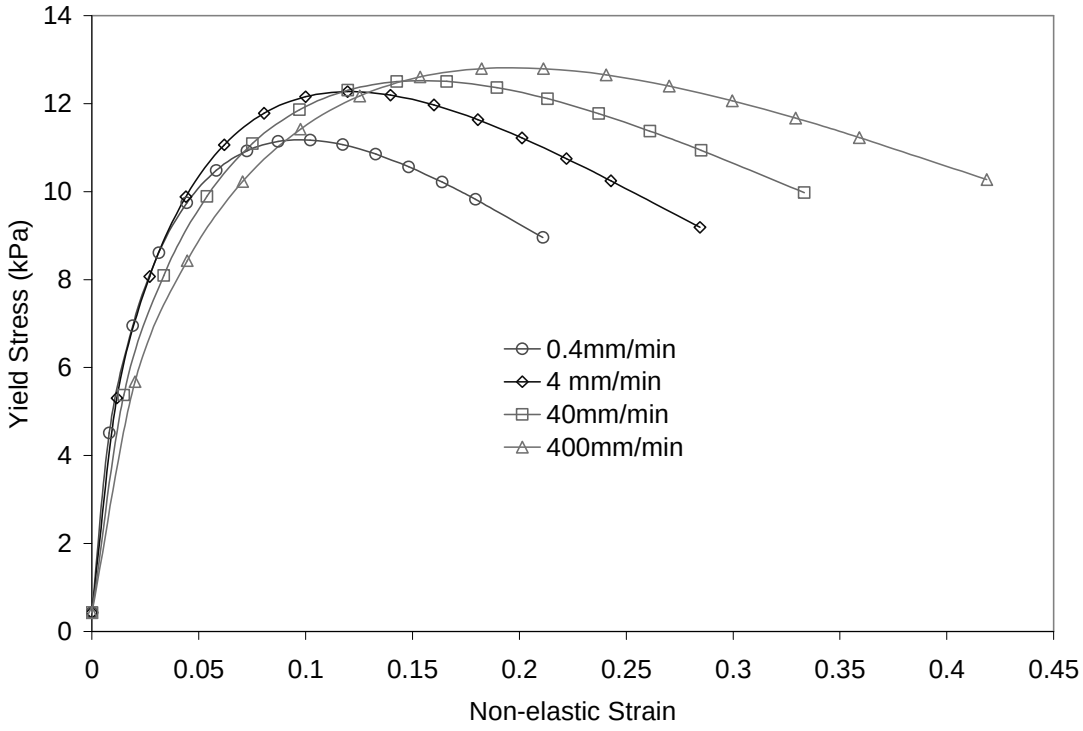

Figure 4. 41. Yield stress as a function of non-elastic strain; data used to calibrate strain hardening/softening part of the constitutive model for shortening

4.10.1.2 Comparison between Abaqus Indentation and Experimental Data

After the virtual indentation at different crosshead speeds (0.4, 4, 40 and 400 mm min^{-1}) was set-up in Abaqus/CAE with the modified Goh and Scanlon (2007) model as the constitutive model (equation [4.15]), the forces and the displacements were plotted and compared with the experimental data (Figure 4.42). As seen in Figure 4.42, the model shown in equation [4.15] can be used to predict the indentation response of vegetable shortening. The prediction is best at the lower crosshead speed of 0.4 mm min^{-1} (Figure 4.42a). As the crosshead speed increases the model increasingly under predicts the reaction force from indentation (Figure 4.42b) and in addition as the indentation depth increases the Abaqus results deviate more from the experimental results.

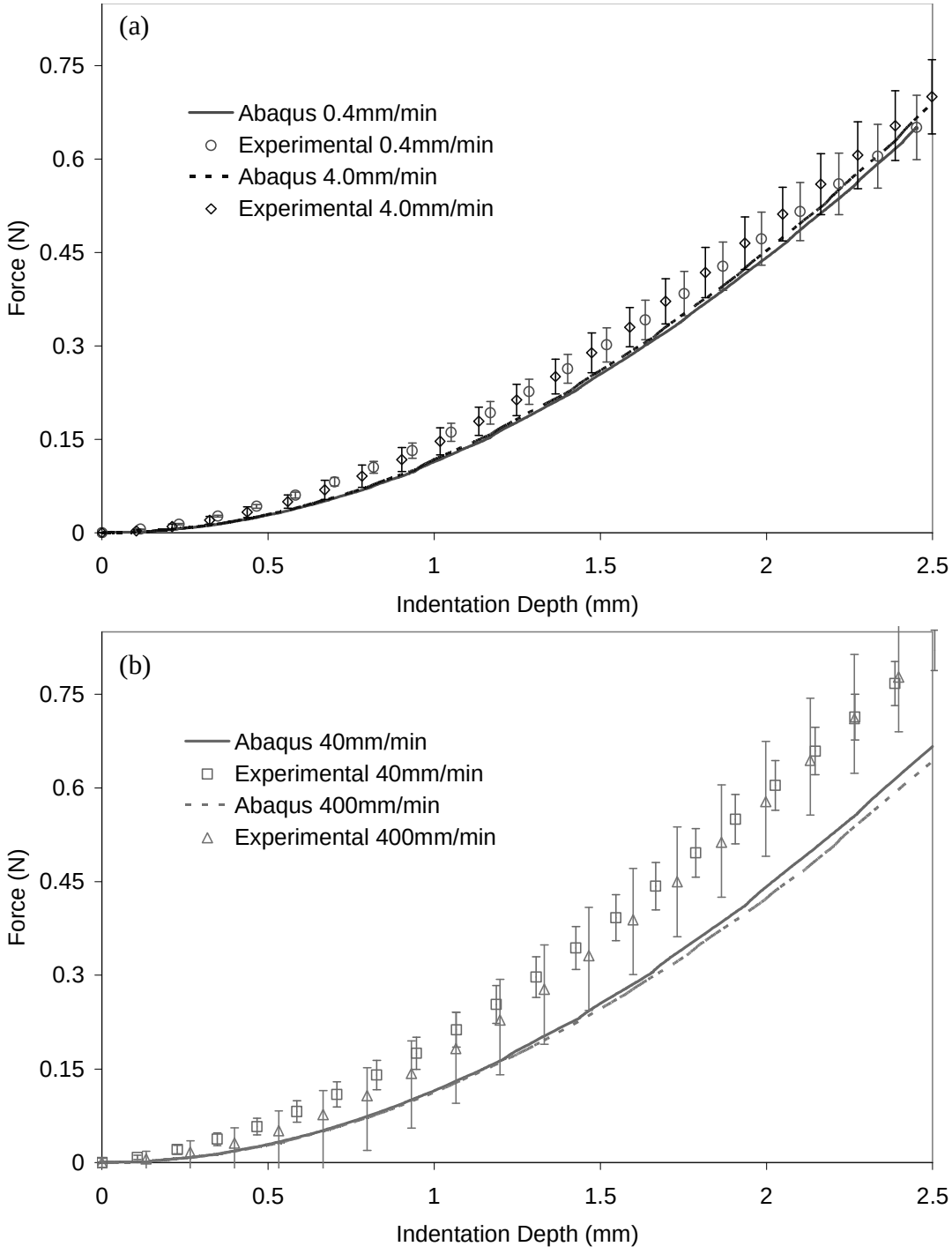

Figure 4. 42. Average indentation response of vegetable shortening at (a) two slower and (b) two faster speeds and simulated results from Abaqus calibrated using equation [4.15]. Error bars on experimental data are one standard deviation

4.10.2. Manipulating Abaqus Simulation Parameters

The force predicted by the Abaqus indentation becomes smaller as the crosshead speed increases; this is the opposite of what occurs in indentation of vegetable shortening experimentally. In order to understand what factors were responsible for the inability of the constitutive model to accurately predict the indentation response, Abaqus experimental simulations were manipulated to bring the predicted indentation response closer to the experimental data. The conditions that were manipulated were the following:

1. Increase the value of the modulus of elasticity of the material, and adjust other material constants accordingly so that equation [4.15] still provides an adequate fit to the experimental monotonic compression (Figure 4.38).
2. Simulate the effect of friction between the conical indenter and the shortening specimen in the simulation.
3. Change the geometry of the specimen, so that the top of the specimen is not completely horizontal. This permits us to simulate the experimental conditions in which the ±0.5 mm variation in specimen height cannot be controlled.

4.10.2.1 Effect of Increasing the Modulus of Elasticity in Model

Increasing the value of the modulus of elasticity (E) can increase the value of the predicted stress (Goh and Scanlon, 2007), since the modulus of elasticity is multiplying all other parameters in equation [4.15]. However, the increase must still be limited by the values obtained during experimental monotonic and cyclic compression tests ($E \leq$ 743kPa). In order to maintain an adequate fit between the predicted curve and the experimental data, all other parameters in equation [4.15] have to be adjusted if the value

of the modulus of elasticity is increased. The new parameters obtained from the Solver function are shown in Table 4.13.

Table 4. 13. Numerical values of constitutive parameters of shortening model shown in Equation [4.15] after modulus of elasticity was deliberately increased to 732 kPa

Loading Rate (mm min^{-1})	0.4	4.0	40.0	400.0
E (kPa)	732.2	732.2	732.2	732.2
ε_{y1}	7.50×10^{-4}	7.50×10^{-4}	7.50×10^{-4}	7.50×10^{-4}
ε_{y2}	0.208	0.286	0.397	0.433
Z	0.752	0.740	0.674	0.669
ω	0.145	0.181	0.299	0.326

Using the values in Table 4.13 into equation [4.15] and running indentation simulations at an indentation rate of 0.4mm min^{-1} with Abaqus, Figure 4.43 was obtained.

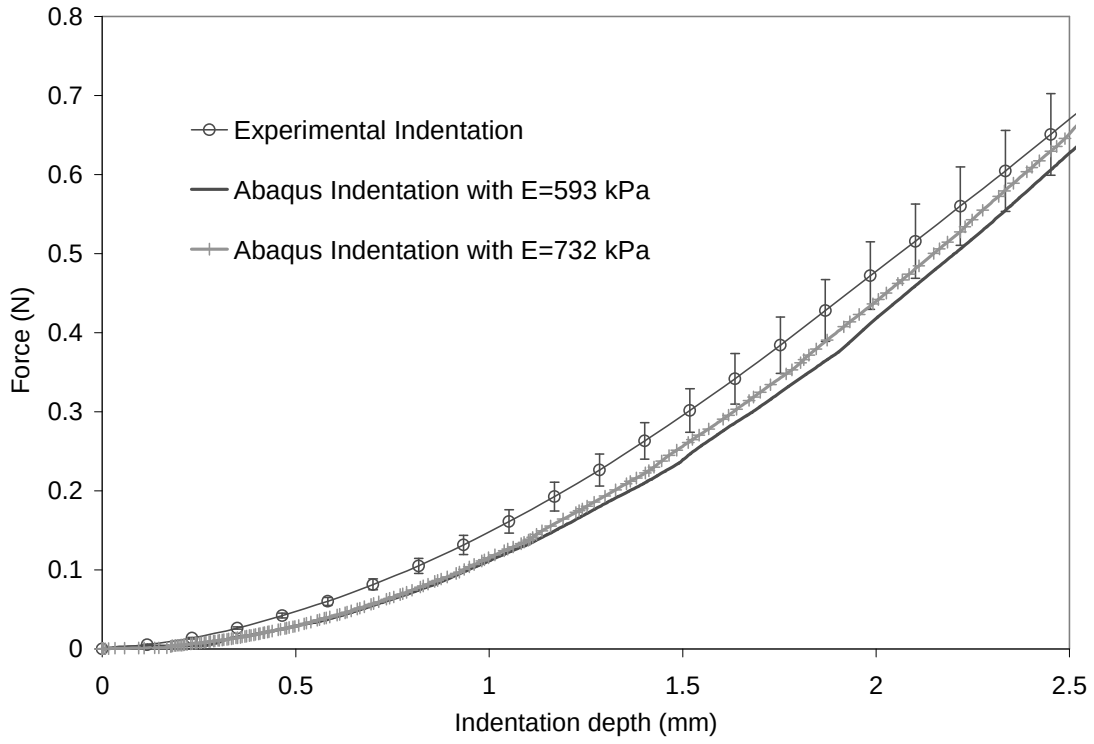

Figure 4. 43. Comparison between experimental indentation at 0.4mm min^{-1} and simulated indentations with different values of the material properties used in equation [4.15]. Error bars on experimental data are one standard deviation

By looking at Figure 4.43 one can see that increasing the modulus of elasticity from 593 to 732 kPa slightly increased the predicted reaction force. The increase in predicted reaction force is more apparent after the indentation depth of 1.25 mm, but in all cases the increased modulus does not improve the match between experimental and simulation; therefore, it can be concluded that increasing the value of the modulus of elasticity within the experimental values does not significantly improve the simulation indentation response.

4.10.2.2 Effect of Increasing Friction during Simulations

Friction increases the force recorded during compression testing (Gunasekaran and Ak, 20003). Therefore, it is necessary to investigate the effects of friction on the indentation simulations. In order to investigate the frictional effects during indentation, conical indentation simulations were performed in Abaqus using equation 4.15 as the constitutive model with the parameter values shown in Table 4.13, and the ROUGH option as the friction condition between the indenter and the specimen. In Abaqus, the ROUGH option assigns a coefficient of friction of 10,000 (Abaqus, 2006). The results of the indentation simulations with friction are shown in Figure 4.44. Adding friction to the indentation simulation causes the indentation curve to be jagged due to the slip and stop effect (Abaqus, 2006) caused by the excessive resistance (Figure 4.44). Also adding friction to the indentation simulations, the force is even more under-predicted than when frictionless conditions are used (Figure 4.44). Therefore one can say that the experimental indentation occurred in frictionless conditions, since the indentation curve is smooth, and

the presence of friction is not the factor that causes the force under-prediction of the model shown in equation [4.15].

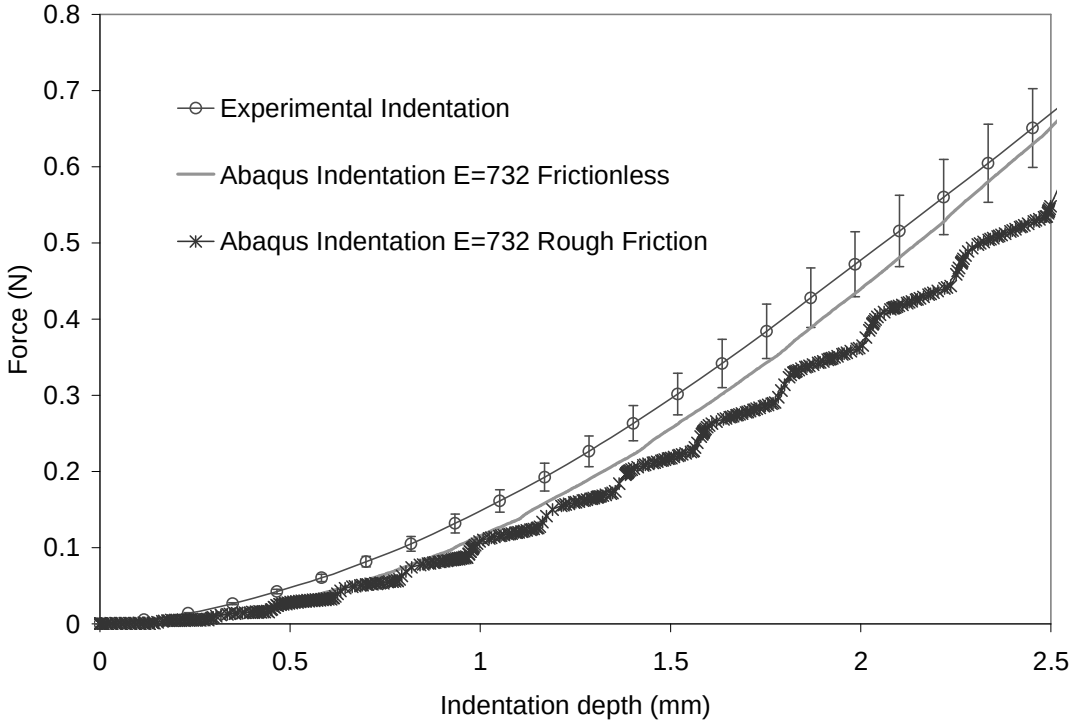

Figure 4. 44. Comparison between experimental indentation curve at 0.4 mm min^{-1} and simulated indentation with rough friction and frictionless conditions. Error bars on experimental data are one standard deviation

4.10.2.3 Effect of Changing the Geometry of Simulated Specimen

The geometry of the contact area of the specimen can affect the results of mechanical tests, particularly during compression testing (Gunasekaran an Ak, 2003). It has been reported that indentation is less susceptible to the change in geometry of specimens, but is not completely exempt from its effects (Anand, 2001). Indentation simulations were set up in Abaqus in which the top part of the specimen was not completely horizontal but rather had a triangular shape with an excess height of 0.25 mm (Figure 4.45a), which is

within the maximum permissible height variation (±0.5 mm) in experimental shortening specimens.

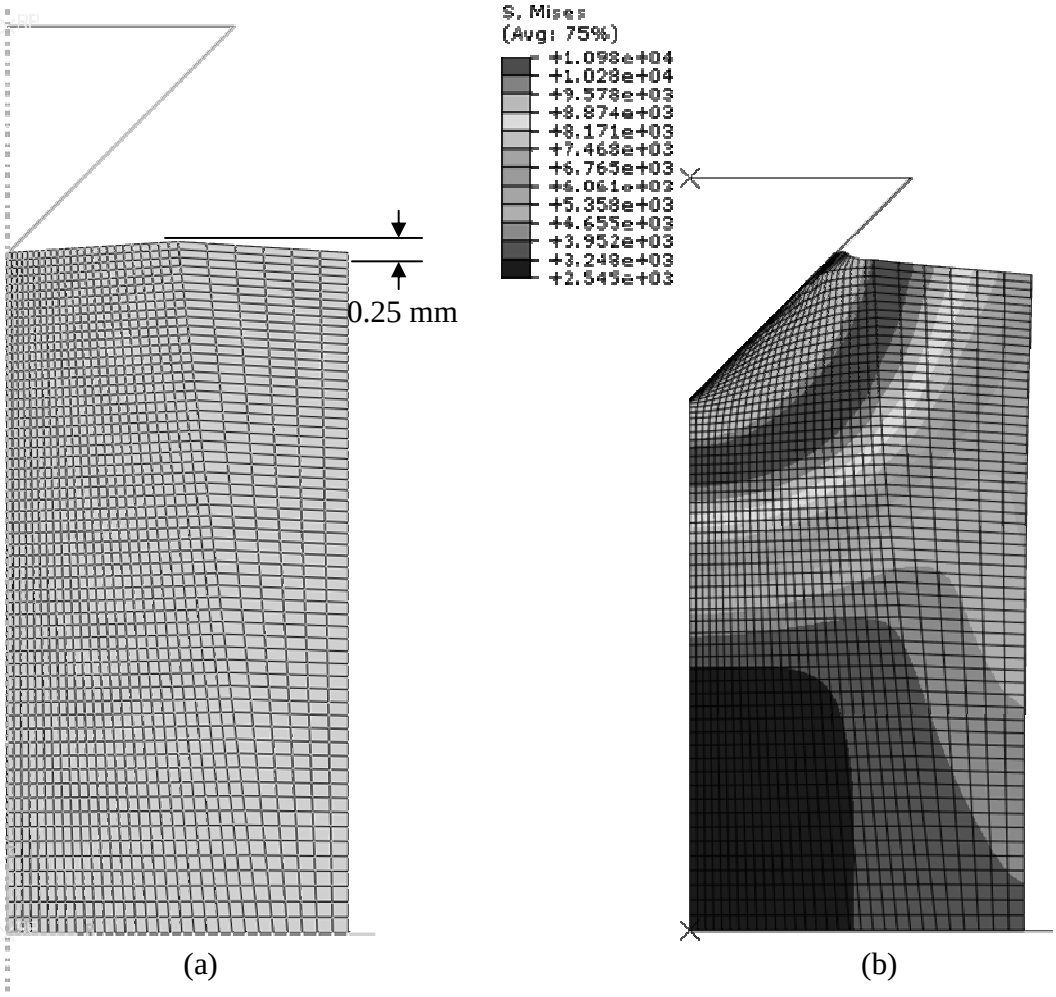

Figure 4. 45. Conical indentation setup in Abaqus/CAE with non-flat contact specimen surface (a) and stress contour of indented specimen to 2.9 mm (b). The stress values are in Pascals

Having a specimen with a triangular top part caused the predicted force to be closer to the experimental indentation results (Figure 4.46). The triangular top specimen has excess material that accumulates on the sides of the indenter and this accumulation of the excess material is what produces higher forces at a given indentation depth when compared to a

simulated specimen with a perfectly horizontal top contact surface. Therefore one can conclude that a change in geometry of the specimen can in fact affect the indentation results, and the deviation of the predicted curve from the experimental curve can be attributed to the unevenness of the shortening specimens during experimental indentation.

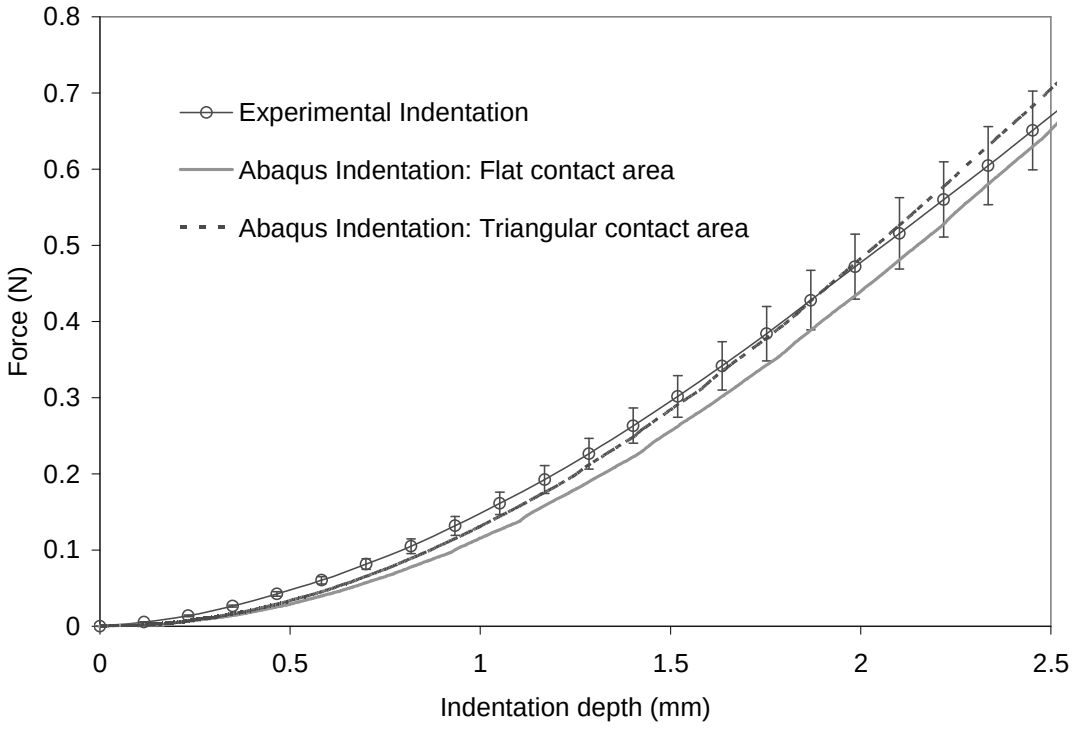

Figure 4. 46. Comparison between experimental indentation of shortening at 0.4 mm min^{-1} and simulated results with equation [4.15] on specimens with different geometry. Error bars on experimental data are one standard deviation

Looking at Figure 4.45b, one can see that after indentation to 2.9 mm the edge of the specimen is not undisturbed since the stress is no longer dark blue (2.5 to 3.2 kPa) but rather green (6.1 to 8.2 kPa). This stress change at the edge indicates that 'edge effects' are increasing the overall value of the measured force and can make indentation measurements on specimens with different lateral dimensions vary, as discussed by Anand (2001).

CHAPTER 5: GENERAL CONCLUSIONS & RECOMMENDATIONS

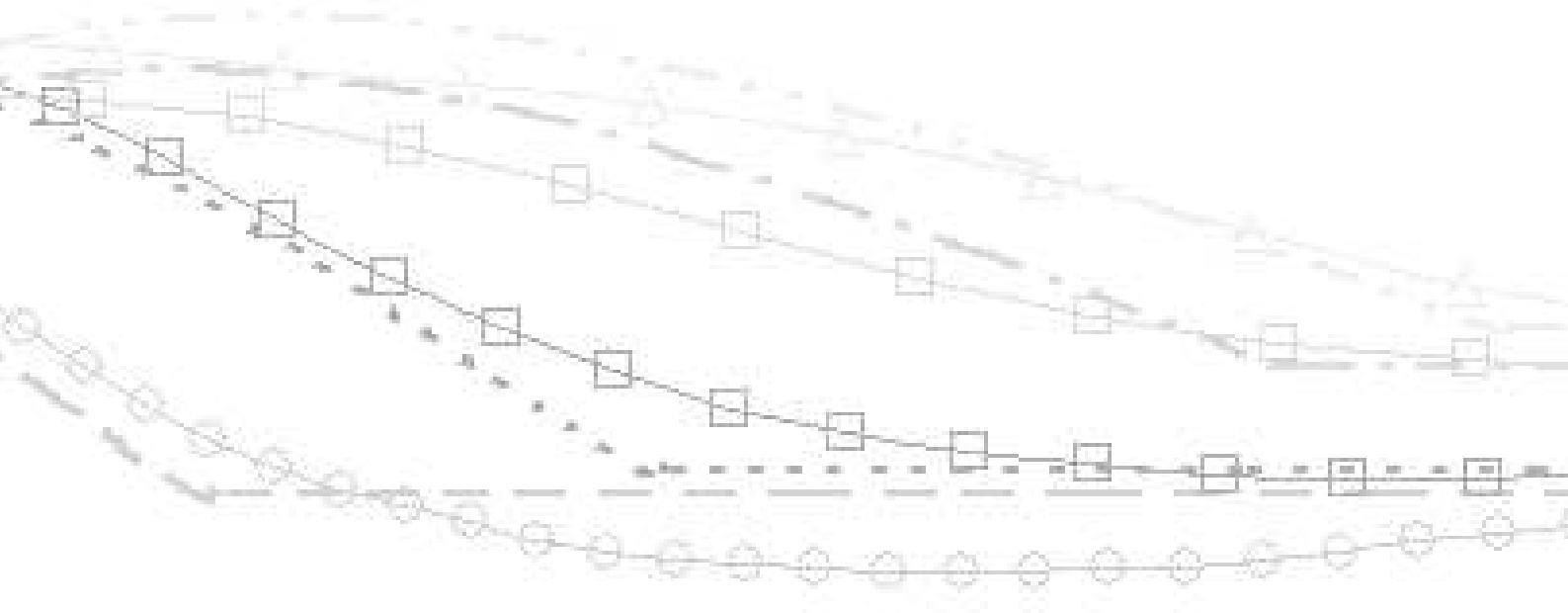

5.1.0. Conclusion and Recommendations

Vegetable shortening shows a complex rheological response between that of a solid and a liquid. However, from uniaxial compression tests it was seen that plastic or permanent deformation in vegetable shortening occurred even at very low strains. As the strain increases during compression the plastic response of vegetable shortening can be characterized by a section undergoing strain hardening followed by a section where failure in shear mode occurs before finally reaching a section where shortening displays perfect plasticity. This rheological behaviour can be attributed to shortening's composition which consists of weakly bonded solid fat particles comprised of highly crystalline material surrounded by fluid oil (Rzepiela et al, 2002; Goh and Scanlon, 2007). Using uniaxial compression stress relaxation and creep tests, it was shown that the complex rheological response of vegetable shortening cannot be described only by a viscoelastic model based on the generalized Maxwell model (Peleg and Pollak, 1982). The generalized Maxwell model is able to predict liquid and solid behaviour of materials but it greatly overpredicts the stress at any given strain for vegetable shortening and it lacks the ability to predict the extensive permanent deformation of shortening.

The rheological response of shortening can be better described as elasto-visco-plastic with rate dependency. Modifying a model proposed by Goh and Scanlon (2007), an elasto-visco-plastic constitutive model was developed and calibrated using the data from uniaxial compression tests (equation [4.15]). The viscous component can be described by an exponential function just like in the Maxwell or Kelvin-Voigt models (Steffe, 1996). The rate dependency cannot be described by a simple power law as previously proposed

by Goh and Scanlon, 2007. The model proposed in this thesis was capable of predicting with reasonable accuracy the uniaxial compression and indentation of vegetable shortening. However, the model accuracy declined as the rate of deformation increased. Further research is required to further refine the elasto-visco-plastic model to better predict the rate dependency of vegetable shortening observed during compression and indentation tests. Taking into account microstructural changes occurring during the plastic deformation responsible for strain hardening and understanding the shear failure mechanisms in vegetable shortening could be used to improve the accuracy of a rheological model for vegetable shortening.

The constitutive model developed from compression tests was then used to predict the indentation response of shortening. The indentation force was underpredicted at all indentation depths for all indentation speeds. A number of numerical simulations were performed to determine potential mechanisms for the discrepancy. Slight modification of geometry at the top plane of the specimen allowed good correspondence between experimental and model results to be obtained.

It has been suggested that indentation is less susceptible to specimen shape variation than compression (Menčik, 2007) is, and as it has been shown using finite element simulations the indentation response is indeed sensitive to slight variations in the geometry of the specimen. Having specimens with an uneven contact surface between the indenter and the specimen can produce higher force values at a given indentation depth due to pile-up of this excess material at the sides of the indenter. Therefore it is important that the

specimen preparation method be improved. Different cutting techniques besides wire cutting should be investigated, such as core cutters with plungers and mechanized blade cutters, to reduce unevenness in horizontal and vertical surfaces of the specimen.

References

Abaqus, Inc. 2008. Unified FEA: Abaqus FEA. Accessed on April 18, 2008. http://www.simulia.com/products/Abaqus_fea.html

Abaqus, Inc., 2007. Abaqus/CAE User's Manual version 6.7. Abaqus Inc., and Dassault Systemes SIMULIA, Providence, RI, USA

Abaqus, Inc., 2006. Abaqus/CAE User's Manual Version 6.6. Abaqus Inc.., and Dassault Systemes-SIMULIA, Providence, RI, USA

Adams, M.J., Briscoe, B.J., and Sinha, S.K. 1996. An indentation study of an elastoviscoplastic material. Philosophical Magazine A 74 (5): 1225-1233

Afoakwa, E.O., Paterson, A., and Fowler, M. 2008. Effect of particle size distribution and composition on rheological properties of dark chocolate. European Food Research and Technology 226: 1259-1268

Alonso, L., Fraga, M.J., Juarez, M., and Carmona, P. 2002. Fatty acid composition of Spanish shortenings with special emphasis on trans unsaturation content as determined by Fourier transform infrared spectroscopy and gas chromatography. Journal of the American Oil Chemists' Society 79(1): 1-6

Anand, A. 2001. A fundamental approach using theories of elasticity to study texture-related mechanical properties of foods. A thesis submitted to the Faculty of Graduate Studies in partial fulfillment of the requirement for a degree of Master of Science. Department of Food Science, University of Manitoba, Winnipeg, Manitoba, Canada.

Anderson, D. 2005. A primer on oils processing technologies. In Shahidi, F. 2005. *Bailey's Industrial Oil and Fat Products.* Sixth Edition. Hoboken, NJ, USA: John Wiley & Sons, Inc. Volume 5: 1-56

Andrikopoulos, N.K. 2002. Triglyceride species composition of common edible vegetable oils and methods used for their identification and quantification. Food Reviews International 18(1): 71-102

Argyris, J.H. 1954. Energy theorems and structural analysis. Aircraft Engineering 26: 347-356, 383-387, 394

Awad, T.S., Rogers, M.A., and Marangoni, A.G. 2004. Scaling behaviour of the elastic modulus in colloidal networks of fat crystals. Journal of Physical Chemistry B 108: 171-179

Bae, W.C., Lewis, C.W., Levenston, M.E., and Sah, R.L. 2006. Inentation testing of human articular cartilage: Effect of probe tip geometry an indentation depth on intra-tissue strain. Journal of Biomechanics 39: 1039-1047

Baran, N.M. 1988. *Finite Element Analysis on Microcomputers.* Toronto, ON, Canada. McGraw-Hill Inc. 256 pp

Basturk, A., Javidipour, I., and Boyaci, I.H. 2007. Oxidative stability of natural and chemically interesterified cottonseed, palm and soybean oils. Journal of Food Lipids 14: 170-188

Beghini, M., Bertini, L., and Fontanari, V. 2006. Evaluation of the stress-strain curve of metallic materials by spherical indentation. International Journal of Solids and Structures 43: 2441-2459

Bermudez, A., Gomez, D., Muñiz, M.C., and Salgado, P. 2007. A FEM/BEM for axisymmetric electromagnetic and thermal modelling and induction furnaces. International Journal for Numerical Methods in Engineering 71(7): 856-878

Betten, J. 2005. *Creep Mechanics.* New York, NY, USA: Springer. 345 pp.

Böhme, G. 1987. *Non-Newtonian Fluid Mechanics.* New York, NY, USA: Elsevier Science Publishing Company, Inc. 351 pp.

Bourne, M. 2002. *Food Texture and Viscosity: Concepts and Measurements.* San Diego, CA, USA: Academic Press, 427pp

Brummer, R. 2006. *Rheology Essentials of Cosmetics and Food Emulsions.* Berlin, Germany. Springer-Verlag, 180pp

Bucaille, J.L., and Felder, E. 2002. Finite-element analysis of deformation during indentation and scratch tests on elastic-perfectly plastic materials. Philosophical Magazine A 82(10): 2003-2012

Bulatov, V.V., Hsiung, L.L., Tang, M., Arsenlis, A., Bartelt, M.C., Cai, W., Florando, J.N., Hiratani, M., Rhee, M., Hommes, G., Pierce, T.G., and Diaz de la Rubia, T. 2006. Dislocation multi-junctions and strain hardening. Nature 440: 1174-1178

Carden, L.A., and Basilio, L.K. 2004. Fats: Vegetable shortening. In Smith, J.S., and Hui, Y.H. *Food Processing: Principles and Applications.* Ames, IA, USA Blackwell Publishing Professional: 343- 351

Cardenas-Weber, M., Stroshine, R.L., Haghighi, K., and Edan, Y. 1991. Melon material properties and finite element analysis of melon compression with application to robot gripping. Transactions of the ASAE 34(3): 920-929

Casiraghi, E.M., Bagley, E.B., and Christianson, D.D. 1985. Behaviour of Mozzarella, cheddar and processed cheese spread in lubricated and bonded uniaxial compression. Journal of Texture Studies 16: 281-301

Cenkowski, S., Zhang, Q., Bielewicz, J., and Britton, M.G. 1992. Effect of maturity stage on mechanical properties of canola seeds. Transactions of the ASAE 35(4): 1243-1248

Charalambides, M.N., Williams, J.G., and Chakrabarti, S. 1995. A study of the influence of ageing on the mechanical properties of Cheddar cheese. Journal of Material Science 30: 3959-3957

Charalambides, M.N., Goh, S.M., Lim, S.L., and Williams, J.G. 2001. The analysis of frictional effect on stress-strain data from uniaxial compression of cheese. Journal of Material Science 36: 2313-2321

Charalambides, M.N., Wanigasooriya, L., Williams, J.G., Goh, S.M., and Chakrabarti, S. 2006. Large deformation extensional rheology of bread dough. Rheologica Acta 46: 239-248

Chen, T. 2000. Determining a Prony series for a viscoelastic material from time varying strain data. NASA Technical Documentation: NASA/TM-2000-210123 ARL-TR-2206

Choe, E., and Min, D.B. 2007. Chemistry of deep-fat frying oils. Journal of Food Science 72 (5): R77-R86

Choi, J.B., and Lakes, R.S. 1992. Non-linear properties of polymer cellular materials with a negative Poisson's ratio. Journal of Material Science 27: 4678-4684

Clough, R.W., and Wilson, E.L. 1999. Early finite element research at Berkeley. Presented at the Fifth U.S. National Conference on Computational Mechanics, August 4-6. 1999. Accessed on January 8, 2008 http://www.edwilson.org/History/fe-history.pdf

Cooke, J.R., De Baerdemaeker, J.G., Rand, R.H., and Mang, H.A. 1976. Finite element shell analysis of guard cell deformations. Transactions of the ASAE 19: 1107-1121

Cowie, J.M.G. 1991. *Polymers: Chemistry and Physics of Modern Materials.* Cheltenham, Glos, U.K. Nelson Thornes Ltd. 436 pp.

Dasgupta, A., and Hu, J.M. 1992. Failure mechanism models for plastic deformation. IEEE Transactions on Reliability 41(2): 168-174

Del Nobile, M.A., Chillo, S., Mentana, A., and Baiano, A. 2007. Use of the generalized Maxwell model for describing the stress relaxation behaviour of solid-like foods. Journal of Food Engineering 78: 978-983

deMan, L., deMan, J.M., and Blackman, B. 1991. Physical and textural characteristics of some North American shortenings. Journal of the American Oil Chemists' Society 68(2): 63-69

deMan, L., D'Souza, V., deMan, J.M., and Blackman, B. 1992. Polymorphic stability of some shortenings as influenced by fatty acid and glyceride composition of the solid phase. Journal of the American Oil Chemists' Society 69(3): 246-250

de With, G. 2006. *Structure, Deformation, and Integrity of Materials.* Weinheim, Germany. Wiley-VCH Verlag GmbH & Co. 454 pp.

Dian, N.L.H.M., Sundram, K., and Idris, N.A. 2006. DSC study on the melting properties of palm oil, sunflower oil, and palm kernel olein blends before and after chemical interesterification. Journal of the American Oil Chemist' Society 83(8): 739-745

Di Monaco, R., Cavella, S., and Masi, P. 2008. Predicting sensory cohesiveness, hardness and springiness of solid foods from instrumental measurements. Journal of Texture Studies 39: 129-149

Do, T.L., Hargreaves, J.M., Wolf, B., and Mitchell, J.R. 2007. Impact of particle size distribution on rheological and textural properties of chocolate models with reduced fat content. Journal of Food Science 72(9): E541-E552

Dogan, I.S., Javidipour, I., and Akan, T. 2007. Effects of interesterified palm and cottonseed oil blends on cake quality. International Journal of Food Science and Technology 42: 157-164

Dowling, N.E. 2007. *Mechanical Behavior of Materials: Engineering Methods for Deformation, Fracture and Fatigue.* Third Edition. Upper Saddle River, NJ, USA. Pearson Education, Inc. 912 pp.

Duval, F.P., van Duynhoven, J.P.M., and Bot, A. 2006. Practical implications of the phase-compositional assessment of lipid-based food products by time-domain NMR. Journal of the American Oil Chemists' Society 83 (11): 905-912

Faber, T.E. 1996. *Fluid Dynamics for Physicists.* New York, NY, USA: Cambridge University Press. 440pp.

Farhloul, M., and Zine, A.M. 2008. A posteriori error estimation for a dual mixed finite element approximation of non-Newtonian fluid flow problems. International Journal of Numerical Analysis and Modeling 5(2): 320-330

Ferry, J.D. 1970. *Viscoelastic Properties of Polymers.* Toronto, ON, Canada: John Wiley and Sons, Inc. 671 pp

Findley, W.N., Lai, J.S., and Onaran, K., 1989. *Creep and Relaxation of Nonlinear Viscoelastic Materials: with an Introduction to Linear Viscoelasticity.* New York, NY, USA. Dover Publications, Inc. 371 pp.

Friis, E.A., Lakes, R.S., and Park, J.B. 1988. Negative Poisson's ratio polymeric and metallic foams. Journal of Material Science 23: 4406-4414

Fung, Y.C. 1969. *A First Course in Continuum Mechanics.* Englewood Cliffs, NJ, USA. Prentice-Hall, Inc. 301 pp.

Ghotra, B.S., Dyal, S.D. and Narine, S.S. 2002. Lipid shortenings: a review. Food Research International 35: 1015-1048

Goh, S.M., Charalambides, M.N., and Williams, J.G. 2004. Characterisation of non-linear viscoelastic foods by the indentation technique. Rheologica Acta 44:47-54

Goh, S.M., Charalambides, M.N., and Williams, J.G. 2004b. Determination of the constitutive constants of non-linear viscoelastic materials. Mechanics of Time-Dependent Materials 8: 255-268

Goh, S.M., Charalambides, M.N., and Williams, J.G. 2005. On the mechanics of wire cutting of cheese. Engineering Fracture Mechanics 72: 931-946

Goh, S.M., and Scanlon, M.G. 2007. Indentation of lipid-based particle gels: An experimental, theoretical and numerical study. Acta Materialia 55: 3857-3866

Gottstein, G. 2004. *Physical Foundations of Material Science.* Berlin, Germany. Springer-Verlag Berlin Heidelberg. 502 pp.

Grün, I.U. 2004. Fats: Edible fat and oil processing. In Smith, J.S., and Hui, Y.H. *Food Processing: Principles and Applications*. Ames, IA, USA Blackwell Publishing Professional: 353-360

Gunasekaran, S., and Ak, M.M. 2003. *Cheese Rheology and Texture.* Boca Raton, FL, USA: CRC Press LLC. 512 pp

Habbab, H., Mellor, B.G., and Syngellakis, S. 2006. Post-yield characterisation of metal with significant pile-up through spherical indentation. Acta Materialia 54: 1965-1973

Hakamada, M., Kuromura, T., Chino, Y., Yamada, Y., Chen, Y., Kusuda, H., and Mabuchi, M. 2007. Monotonic and cyclic compressive properties of porous aluminum fabricated by spacer method. Material Science and Engineering A 459: 286-293

Han, S.N., Leka, L.S., Lichtenstein, A.H., Ausman, L.M., Schaefer, E.J., and Meydani, S.N. 2002. Effect of hydrogenated and saturated, relative to polyunsaturated, fat on immune and inflammatory response of adults with moderate hypercholesterolemia. Journal of Lipid Research 43: 445-542

Hassan, B.H., Alhamdan, A.M., and Elansari, A.M. 2005. Stress relaxation of dates at khalal and rutab stages of maturity. Journal of Food Engineering 66: 439-445

Hatzikiriakos, S.G., and Migler, K.B. 2004. *Polymer Processing Instabilities: Control and Understanding.* New York, NY, USA, Marcel Dekker 488pp.

Heertje, I., and Leunis, M. 1997. Measurement of shape and size of fat crystals by electron microscopy. Lebensmittel Wissenschaft und Technologie 30(2): 141-146

Hiemenz, P.C. 1984. *Polymer Chemistry: The Basic Concepts*. New York, NY, USA. Mercel Dekker, Inc. 738 pp

Higaki, K., Koyano, T., Hachiya, I., Sato, K., and Suzuki, K. 2004. Rheological properties of b-fat gel made of binary mixtures of high-melting and low-melting fats. Food Research International 37: 799-804

Hjelmstad, K.D. 2005. *Fundamentals of Structural Mechanics*. Second edition. New York, NY, USA: Springer 480 pp

Huang, Z., Lucas, M., and Adams, M.J. 2002. A numerical and experimental study of the indentation mechanics of plasticine. Journal of Strain Analysis 37 (2): 141-150

Illston, J.M., and Domone, P.L.J. 2001. *Construction Materials: Their Nature and Behaviour*. Third edition. New York, NY, USA. Spon Press., 566pp.

Jeon, E.C., Kim, J.Y., Baik, M.K., Kim, S.H., Park, J.S., and Kwon, D. 2006. Optimum definition of true strain beneath a spherical indenter for deriving indentation flow curves. Materials Science and Engineering A 419: 196-201

Kajberg, J., and Wikman, B. 2007. Viscoplastic parameter estimation by high strain-rate experiments and inverse modelling – Speckle measurements and high-speed photography. International Journal of Solids and Structures 44 (1): 145-164

Kinsella, J.E. 1987. Physical properties of food and milk components: Research needs to expand uses. Journal of Dairy Science 70: 2419-2428

Kloek, W., van Vliet, T., and Walstra, P. 2005. Large deformation behaviour of fat crystal networks. Journal of Texture Studies 36: 516-543

Körstgens, V., Flemming, H.C., Wingender, J., and Borchard, W. 2001. Uniaxial compression measurement device for investigation of the mechanical stability of biofilms. Journal of Microbiological Methods 46: 9-17

Kummerow, F.A., Zhou, Q., Mahfouz, M.M., Smiricky, M.R., Grieshop, C.M., and Schaeffer, D.J. 2004. Trans fatty acids in hydrogenated fat inhibited the synthesis of the polyunsaturated fatty acids in the phospholipids of arterial cells. Life Sciences 74 (22): 2707-2723

Lakes, R.S. 1987. Foam structures with a negative Poisson's ratio, Science 235: 1038-1040

LaBell, F. 1997. Cottonseed oil for frying and baking. Prepared Foods, February 1997. Online April 7, 2008 http://findarticles.com/p/articles/mi_m3289/is_/ai_19242501

Ledux, M., Juaneda, P., and Sebedio, J.L. 2007. Trans fatty acids: Definition and occurrence in foods. European Journal of Lipid Science and Technology 109 (9): 891-900

Lee, T., and Lakes, R.S. 1997. Anisotropic polyurethane foam with Poisson's ratio greater than 1. Journal of Material Science 32: 2397-2401

Linton P.F., McVay, M.C., and Bloomquist, D. 1988. Measurement of deformations in standard triaxial environment with a comparison of local versus global measurements on fine, fully drained sand. In Donaghe, R., Charney, R., and Silver, M. *Advanced Triaxial Testing of Soil and Rock.* Baltimore, MD, USA, American Society for Testing and Materials: 202- 215

Litwinenko, J.W., Rojas, A.M., Gerschenson, L.N., and Marangoni, A.G. 2002. Relationship between crystallization behaviour, microstructure, and mechanical properties in a palm oil-based shortening. Journal of the American Oil Chemist Society 79(7): 647-654

Liu, A.F. 2005. *Mechanics and Mechanisms of Fracture: An Introduction.* Materials Park, OH, USA. ASM International. 458 pp

Liu, Z., and Scanlon, M.G. 2003. Modelling indentation of bread crumb by finite element analysis. Biosystems Engineering 85 (4): 477-484

Lucey, J.A. 2002. Formation and physical properties of milk protein gels. Journal of Dairy Science 85: 281-294

Ma, X., Yoshida, F., and Shinbata, K. 2003. On the loading curve in microindentation of viscoplastic solder alloy. Material Science and Engineering A 344: 296-299

Madenci, E., and Guven, I. 2006. *The Finite Element Method and Applications in Engineering Using ANSYS®*. New York, NY, USA. Springer Science + Business Media, LLC 686 pp

Marangoni, A.G., and Lencki, R. W. 1998. Ternary phase behaviour of milk fat fractions. Journal of Agricultural and Food Chemistry 46: 3879-3884

Marangoni, A.G., and Narine, S.S. 2002. Identifying key structural indicators of mechanical strength in networks of fat crystals. Food Research International 35: 957-969

Marangoni, A.G., and Rogers, M.A. 2003. Structural basis for the yield stress in plastic disperse systems. Applied Physics Letters 82 (19): 3239-3241

Martini, S., and Herrera, M.L. 2008. Physical properties of shortening with low-trans fatty acids as affected by emulsifiers and storage conditions. European Journal of Lipid Science and Technology 110: 172-182

McClements, D.J. 2003. The rheology of emulsion-based food products. In McKenna, B.M. *Texture in Food, Volume 1: Semi-solid Foods.* Boca Raton, FL, USA. CRC Press LLC: 3-32

Menard, K.P. 1999. *Dynamic Mechanical Analysis: A Practical Introduction.* Boca Raton, FL, USA. CRC Press LLC. 208 pp

Menčik, J. 2007. Determination of mechanical properties by instrumented indentation. Meccanica 42: 19-29

Mensink, R.P., and Katan, M.B. 1990. Effect on dietary trans fatty acids on high-density and low-density lipoprotein cholesterol levels in healthy subjects. New England Journal of Medicine 323: 439-445

Metzroth, D.J. 2005. Shortenings: Science and technology. In Shahidi, F. 2005. *Bailey's Industrial Oil and Fat Products.* Sixth Edition. Hoboken, NJ, USA: John Wiley & Sons, Inc. Volume 4: 83- 123

Meyers, A., and Chawla, K.K. 1999. *Mechanical Behaviour of Materials.* Englewood Cliffs, NJ, USA: Prentice Hall, 544 pp

Mura, T., and Koya, T. 1992. *Variational Methods in Mechanics.* New York, NY, USA. Oxford University Press, Inc. 244 pp.

Narine, S.S., and Marangoni, A.G. 2000. Elastic modulus as an indicator of macroscopic hardness of fat crystal networks. Lebensmittel Wissenschaft und Technologie 34: 33-40

Narine, S.S., and Humphrey, K.L. 2004. A comparison of lipid shortening functionality as a function of molecular ensemble and shear: microstructure, polymorphism, solid fat content and texture. Food Research International 37: 28-38

Nussinovitch, A., Peleg, M., and Normand, M.D. 1989. A modified Maxwell and a nonexponetial model for characterization of the stress relaxation of agar and alginate gels. Journal of Food Science 54(4): 1013-1016

O'Brien, R.D. 1998. *Fats and Oils: Formulating and Processing for Applications.* Lancaster, PA, USA: Technomic Publishing Company

O'Brien, R.D. 2005. Shortenings: Types and formulations. Shahidi, F. 2005. *Bailey's Industrial Oil and Fat Products.* Sixth Edition. Hoboken, NJ, USA: John Wiley & Sons, Inc. Volume 4: 125-157

Ouriev, B., and Windhab, E.J. 2002. Rheological study of concentrated suspensions in pressure-driven shear flow using a novel in-line ultrasound Doppler method. Experiments in Fluids 32: 204-211

Parteder, E., and Bünten, R. 1998. Determination of flow curves by means of a compression test under sticking friction conditions using an iterative finite-element procedure. Journal of Materials Processing Technology 74(1): 227-233

Peleg, M., and Pollak, N. 1982. The problem of equilibrium conditions in stress relaxation analyses of solid foods. Journal of Texture Studies 13: 1-11

Pepper, D.W., and Heinrich, J.C. 1992. *The Finite Element Method: Basic Concepts and Applications.* Bristol, London, UK. Hemisphere Publishing 256 pp

Perzyna, P. 1963. The constitutive equations for rate sensitive plastic materials. Quarterly of Applied Mathematics 20: 321-332

Podmore, J. 2002. Bakery fats. In Rajah, K.K. *Fats in Food Technology.* Boca Raton, FL, USA. CRC Press LLC: 30-68

Prager, W. 1955. The theory of plasticity: A survey of recent achievements. Proceedings of the Institution of Mechanical Engineers (London) 169: 41-57

Puri, V.M., and Anantheswaran, R.C., 1993. The finite element method in food processing: A review. Journal of Food Engineering 19: 247-274

Rao, S.S. 1982. *The Finite Element Method in Engineering.* Willowdale, ON, Canada. Pergamon Press Canada Ltd. 625 pp

Rao, M.A. 2007. *Rheology of Fluid and Semisolid Foods: Principles & Applications*. New York, NY, USA, Springer 481 pp

Rao, M.V.N., and Quintero, X. 2003. Solid food rheology. In Heldman, D.R. *Encyclopedia of Agriculture, Food, and Biological Engineering*. New York, NY, USA. Marcel Dekker Inc: 920-923

Reigel, G.W., and McMichael, C.E. 1966. The production of quick-tempered shortenings. Journal of the American Oil Chemists' Society 43(12): 687-689

Ressing, H., Ressing, M., and Durance, T. 2007. Modeling the mechanisms of dough puffing during vacuum microwave drying using the finite element method. Journal of Food Engineering 82: 498-508

Ribeiro, K.O., Rodrigues, M.I., Sabadini, E., and Cunha, R.L. 2004. Mechanical properties of acid sodium caseinate-k-carrageenan gel: effect of co-solute addition. Food Hydrocolloids 18: 71-79

Riviere, J.P., and Castaing, J. 1997. Compression test and plastic strain of α-Al_2O_3 single crystals. Journal of the American Ceramic Society 80 (7): 1711-1714

Roduit, B., Borgeat, C.H., Cavin, S., Fragniere, C., and Dudler, V. 2005. Application of finite element analysis (FEA) for the simulation of release of additives from multilayer polymeric packaging structures. Food Additives and Contaminants 22(10): 945-955

Roylance, D. 1996. *Mechanics of Materials*. Toronto, ON, Canada. John Wiley & Sons, Inc. 315 pp

Rumsey, T.R., and Fridley, R.B. 1977. Analysis of viscoelastic contact stresses in agricultural products using a finite element method. Transactions of the ASAE 20: 162-167 and 171

Rzepiela, A.A., van Opheusden, J.H.J., and van Vliet, T. 2002. Large shear deformation of particle gels studied by Brownian dynamic simulations. Computer Physics Communications 147: 303-306

Schaink, H.M., van Malssen, K.F., Morgado-Alves, S., Kalnin, D., and van der Linden, E. 2007. Crystal network for edible oil organogels: Possibilities and limitations of the fatty acid and fatty alcohol system. Food Research International 40: 1185-1193

Senanayake, N.S.P.J., and Shahidi, F. 2005. Modification of fats and oils via chemical and enzymatic methods. In Shahidi, F. 2005. *Bailey's Industrial Oil and Fat*

Products. Sixth Edition. Hoboken, NJ, USA: John Wiley & Sons, Inc. Volume 3: 555-584

Shahidi, F. 2005. *Bailey's Industrial Oil and Fat Products.* Sixth Edition. Hoboken, NJ, USA: John Wiley & Sons, Inc.

Shellhammer, T.H., Rumsey, T.R., and Krochta, J.M. 1997. Viscoelastic properties of edible lipids. Journal of Food Engineering 33: 305-320

Shukla, A., and Rizvi, S.S.H. 1995. Viscoelastic properties of butter. Journal of Food Science 60(5): 902-905

Steffe, J.F. 1996. *Rheological Methods in Food Process Engineering*. Second Edition. East Lansing, MI, USA: Freeman Press 430 pp.

Tang, D., and Marangoni, A.G. 2006. Microstructure and fractal analysis of fat crystal networks. Journal of the American Oil Chemist's Society 83(5): 377-388

Tang, D., and Marangoni, A.G. 2007. Modeling the rheological properties and structure of colloidal fat crystal networks. Trends in Food Science and Technology 18: 474-483

Taylor, R.L., Pister, K.S., and Goudreau, G.L. 1970. Thermomechanical analysis of viscoelastic solids. International Journal of Numerical Methods in Engineering 2: 45-59

Tecstra Systems, 2007. Vegetable shortening. Retrieved from the internet November 17, 2007. http://www.recipetips.com/glossary-term/t--34959/vegetable-shortening.asp

Thomas, A.E. 1978. Shortening formulation and control. Journal of the American Oil Chemists' Society 55(11): 830-833

Trigg, G.L., Vera, E.S., and Greulich, W. 1999. *Encyclopedia of Applied Physics*. New York, Wiley-VCH: 616 pp.

Tong, X., and Tuan, C.Y. 2007. Viscoplastic cap model for soils under high strain rate loading. Journal of Geotechnical and Geoenvironmental Engineering 113 (2): 206-214

Turner, M.J., Clough, R.W., Martin, H.C., and Topp, L.J. 1956. Stiffness and deflection analysis of complex structures. Journal of Aeronautical Sciences 23: 805-823

Ubachs, R.L.J.M., Schreurs P.J.G., and Geers M.G.D. 2007. Elasto-viscoplastic nonlocal damage modelling of thermal fatigue in anisotropic lead-free solder. Mechanics of Materials 39 (7): 685-701

Vandamme, M., and Ulm, F.J. 2006. Viscoelastic solutions for conical indentation. International Journal of Solis and Structures 43: 3142-3165

Wassell, P., and Young, N.W.G. 2007. Food applications of trans fatty acid substitutes. International Journal of Food Science and Technology 42: 503-517

White, M.A. 1999. *Properties of Materials.* New York, NY, USA: Oxford University Press Inc. 334 pp.

Wright, A.J., Scanlon, M.G., Hartel, R.W., and Marangoni, A.G. 2001. Rheological properties of milkfat and butter. Journal of Food Science 66 (8): 1056-1071

Xiong, Y., Aguilera, J.M., and Kinsella, J.E. 1991. Emulsified milkfat effects on rheology of acid-induced milk gels. Journal of Food Science 56 (4): 920-

Yanez, J.A., Laarz, E., and Berstrom, L. 1999. Viscoelastic properties of particle gels. Journal of Colloid and Interface Science 209: 162-172

Yu, M.H., Ma, G.W., Qiang, H.F., and Zhang Y.Q. 2006. *Generalized Plasticity.* Berlin, Germany: Springer Berlin Heidelberg. 447 pp.